Aspects on Structural Assessment of a Bulk Carrier Using First Principles

A Thesis Submitted for the
Degree of Master of Science
in the Faculty of Engineering
of the University of Glasgow

By

Iason Papageorgiou Lambos, B.Eng.

Department of Naval Architecture and Ocean Engineering
University of Glasgow

October 98

DECLARATION

Except where reference is made to the work of others,
This thesis is accepted to be original.

Abstract

In the last twenty years a significant number of Bulk Carriers sank or suffered serious casualties, many of them involving loss of lives. This Study is reviewing certain aspects which either separately, as duly dealt with in each Chapter of the Study, or interrelated and combined can be the cause and the origin of possible structural weaknesses on a Bulk Carrier structure. All the calculations performed are based on the M/V Victor, which is a single skin Panamax Bulk Carrier built 1976 with typical structural configuration.

Throughout the Study an attempt is made to compare calculations of loads, stresses and fatigue lives based on Classification Society rules, idealised structural models of the ship structure and finite element models.

The accuracy of the results from simple first principles methods when applied to complicated problems are subject to the assumptions and simplifications used. However the ability to make rough checks on computer generated results may become even more important as nowadays sophisticated methods are incorporated into computer programs which allow limited access to the assumptions and the procedures used.

Acknowledgements

The author wishes to thank Professor N. Barltrop for his care and guidance.

Mr. E. Tzanetatos and Mr D. Zakakis of Endeavor Shipping Co S.A. (Piraeus) for providing the technical drawings of the Panamax Bulk Carrier M/V *Victor*.

Mr. David Cooper for his advice on the use of Hydro computer package by Kockums. Dr. Andy Bell for the information and explanations he provided for the use of Lusas computer package by FEA.

Mr David Buck and H. Jin of IACS London office for the regulatory information provided regarding the Bulk Carrier structure. Mr. Nick Paleokrassas of Lloyds Register of Shipping London, for the Classification's recommendations regarding structural analysis. Mr Kenneth Lilley of ABS London for the information regarding the application of IACS Unified requirements S22 and S19. Dr. W. Fricke of Germanischer Lloyd Hamburg for the information provided in respect of rule based and from first principles fatigue.

Finally the author wishes to thank Ioannis Tsarouchas for the mutual assistance regarding aspects of fatigue assessment and further Andre Maerli, Trim Tveitnes and Iannis Tsarouchas for their valuable friendship.

Table of Contents

List of Figures

List of Tables

Notation

k_S: Rule coefficient for still water sagging moment
k_H: Rule coefficient for still water hogging moment
C_1: Rule coefficient for still water moment
Lpp: Length between perpendiculars
B: Breadth of the vessel
Cb: Block coefficient
Mss: Still water sagging moment
Msh: Still water hogging moment
f(h,t): The long-term joint probability density of wave heights and periods
Hs: Significant wave height
T: Mean zero crossing period
Cs: Skewness parameter
ω:: Wave frequency
T: Mean zero crossing period
Ta : Average wave period
$G(\theta)$: Directional spectrum
$S(\omega)$: Wave spectrum
$P(x_1>x)$: Probability of exceedance of the value x by the value x_1
m_o: Variance (volume under the response spectrum)
x_1: any amplitude chosen randomly
k_1: Rule coefficient for wave sagging moment
k_H: Rule coefficient for wave hogging moment
C_1: Rule coefficient for wave moment
Mws: Wave sagging moment
Mwh: Wave hogging moment
P_i: The pressure fluctuation at point I
f_d: A function of ship breadth and wave characteristics to include the diffraction of waves
H : Wave height
L : Wave length
B : Breadth of the ship taken into consideration
f_h: A function of ship heading
θ : Heading of the vessel with respect to the waves
$P_{(R+M)i}$ Pressure fluctuation at point i including the effect that point I will move according the vessel's motion
ω_e: Frequency of encounter
l : Distance from centre of motion which for simplicity was assumed to be the midship section. In reality it depends on the fore and aft underwater shape and lies near the midship section.
γ_v: Vertical acceleration
γ_h: Horizontal acceleration

VBM : Vertical Bending moment
y : Distance from neutral axis of the point at which the stress is calculated.
I_{yy} : Inertia of section from the neutral axis
σ_{VBM} : Resultant stress due to VBM

HBM : Horizontal Bending moment
x : Distance from centre-line of the point at which the stress is calculated
I_{xx} : Inertia of section from the centre-line
σ_{HBM} : Resultant stress due to HBM
VSF : Vertical Shear force
q_v : Vertical shear flow per unit of vertical shear force at the point of interest
t : Thickness at point of interest
τ_{VSF} : Resultant vertical shear stress
HSF ; Horizontal Shear stress
q_h : Horizontal shear flow per unit horizontal shear force at the point of interest
τ_{HSF} : Resultant horizontal shear stress
TM : Torsion moment
q_t : Shear flow per unit torque
ϕ_o : The curvature of the hull girder at which the first panel collapses

Np: Number of panels

i: Panel considered

$\varepsilon_{\alpha,\upsilon}$: Ultimate strain

ε_y Average elastic hull girder bending strain

y_i: The distance from the elastic neutral axis of the panel's cross section

σ_x : global bending stress

σ_p : stress due to water pressure

τ : global shear stress

SCF: Stress concentration factor

A_{fb}: Fictitious area of bar
a: Frame spacing
b: Longitudinal spacing
t: Plate thickness
t : Thickness of steel
k_{cor} : Corrosion rate
T: Time
$S_{cor}(t)$: Corrosion factor
D : Fatigue damage
n : Number of stress cycles
K: Constant depending on welding class

σ : Random variable denoting fatigue stress occurring for n cycles
fi : Zero crossing rate
$\Gamma(\ )$: Gamma function
UF : Usage factor
$\varpi_{\alpha\tau}$: Factor to account for the effect of welding class change

Glossary

ABS:	American Bureau of Shipping
BIMCO:	The Baltic and International Maritime Council
DNV:	Det Norske Veritas
EPS:	Enhanced Survey Program
f.e.:	Finite element (method)
f.p.:	First principles (method) (hand calculations)
IACS:	International Association of Classification Societies
ILLC:	International Load-Line Convention
IMO:	International Maritime Organisation
ISSC:	International Ship Structures Congress
ISM Code:	International Safety Management Code
M/V:	Motor Vessel
MSC:	Maritime Safety Council
NKK:	Nippon Kaiji Kyokai
P&I:	Protection & Indemnity
RINA:	The Royal Institution of Naval Architects
RS:	Response Spectrum
SNAME:	The Society of Naval Architects and Marine Engineers
SOLAS:	Safety of Life at Sea
SSC:	Ship Structure Committee
UR:	Unified Requirement
VLCC:	Very Large Crude Carrier

Chapter 1

Historical Perspective of Structural Failures of Bulk Carriers

1.1 Bulk Carrier Evolution

Dry Bulk Carriers carry out the essential transport of commodities without which our modern society would be unable to function. The Bulk Carrier evolved from the closed shelter-deck cargo vessel (the "tramp"), and the ore carrier, in the mid-1950s and thereafter developed rapidly in both size and number. Whilst in 1960 only about a quarter of bulk cargoes were carried in single deck Bulk Carriers, the situation had been transformed by 1980 at which time almost all bulk cargoes were transported by bulkers. Changes to international rules, such as the 1966 Load Line Convention and the IMO Grain Rules, enabled designers to take advantage of the inherent stability of the Bulk Carrier, and develop its self-stowing characteristics. In 1990 world seaborne trade in both iron ore and coal was about 350 million tonnes, with 190 million tones of grain being shipped [1].

In the same year (1990) an alarming number of Bulk Carriers sank or suffered serious accidents. Six of these resulted in the loss of 125 lives. In 1991 nine losses accounted for 156 lives. The 1991 IMO General Assembly adopted an unprecedented resolution on bulker safety measures. As a result, in 1992 and 1993 there was a substantial drop in casualties. The P&I clubs, the insurance underwriters and the shipowners were understandably requesting action from the classification societies from 1990 leading to the adaptation of the Enhanced Survey System (ESP) which began in 1993. However in 1994 there were fourteen serious losses or accidents of which four involved the loss of 113 lives. It was evident that the problem was far from solved [2].

1.2 Casualty Causation Review

A research effort was launched because it was realised just how little was actually known about the reasons for the accidents. A statistical analysis of the characteristics of the ships involved in accidents showed some common features and helped establish the nature of the problem.

Each ship undergoes a special survey every five years; this coincides with the expiration of its Safety Construction Certificate. The statistical analysis (Fig. 1.2.1) demonstrates that there is an increase in the number of casualties before the special

survey and a decline afterwards. The analysis is for the years 1980-1996, the ships have not passed an Enhanced Special Survey, and it is based on data printed by Lloyds Register [2].

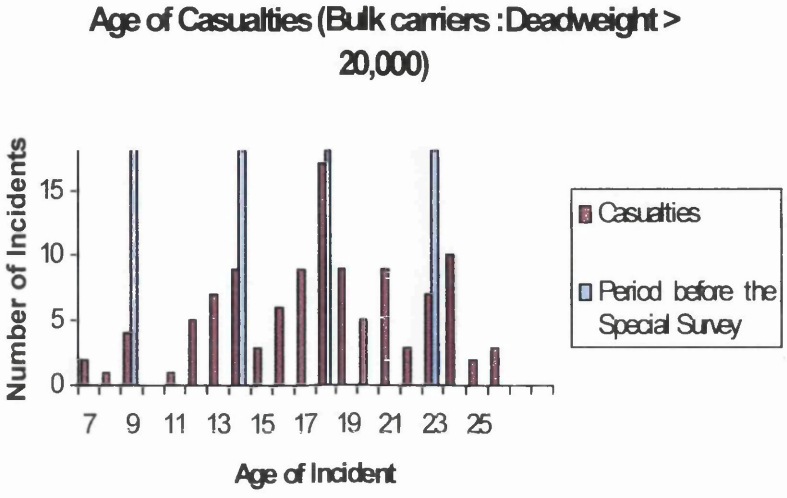

Figure 1.2.1 Graphical representations of the number and age of ships with respect to casualties and special survey

We can therefore conclude that a lack of maintenance / inspection exacerbates the problem. Moreover, an analysis performed by ABS regarding Bulk Carrier losses from an economic perspective has shown that fluctuations in the freight market are directly connected to Bulk Carrier losses [3]. The probable reason is that ship management companies in their efforts to reduce operating costs minimise their expenditure upon maintenance of their vessels, underestimating the effect that this decision may have upon safety.

Weather conditions are also a factor. As we can see in table 2.1, out of the 29 Bulk Carriers that were lost or suffered serious structural damage between January 1991 and August 1995, 21 occurred during heavy weather conditions. The remaining 8 accidents occurred in winter zones or stormy seasons, perhaps also an indication of heavy weather conditions [2].

Weather conditions when the incidents occurred. (data from IMO)

Weather	Beaufort 10+	Beaufort 8	unspecified
# of incidents	5	16	8

Table 1.2-1 Weather conditions and number of incidents

The loading characteristics of the vessels that were lost or suffered damages can be seen in table 1.2.1 [2]. Ships carrying heavy cargo apparently constitute the majority of those involved in accidents. However the data shows that ships loaded in alternate holds are almost arithmetically equal to those loaded homogeneously.

Loading data of the 42 ships lost

Loading	Alternate	homogeneous	unknown
# of ships	17	20	5

Cargo carried	heavy	Probably heavy
# of ships	26	13

Loading data of the 40 ships that were serious casualties.

Loading	Alternate	homogeneous	unknown
# of ships	14	23	3

Cargo carried	Heavy	Probably heavy
# of ships	28	4

Table 1.2-2 Loading characteristics of Bulk Carriers that were lost or suffered damages.

(Data from MSC 67/4/3 – 1 Oct. 1996 submission by IACS)

Loading and unloading procedures in ports may also contribute to the problem. In the last ten years the machinery used in ports for loading has a very fast rate of tdw/hr due to time restraints. The grabs have also become bigger so that the structure of the ship has to withstand higher stresses and bending moments every time she is loaded and unloaded.

A study by N.K.K with respect to corrosion was initiated in August 1991 and published its findings in January 1992 [4]. The connection between cargo transported and corrosion rates was emphasised with coal being the most corrosive cargo. The effectiveness of oil paint based coating materials was questioned against epoxy based with respect, of course, to the coatings' specifications. The corrosion rates for the reasons

mentioned above varied greatly adding more complexity to the situation. If we take into consideration that stresses, fatigue and corrosion interact; the wear and tear of the structure increases significantly.

We can therefore conclude that the problem involves the wear and tear of the vessel's structure. According to IACS casualty data, analysis has shown that around 40% of bulker accidents and losses are known to have involved water entry into number 1 hold (Fig. 1.2.2) [5]. The true figure cannot, of course, be established with certainty. Investigations have shown that the vulnerability of the transverse watertight bulkhead at the aft end of number 1 hold requires a greater margin of safety to withstand flooding loads. Without such safety margins the probable course of an accident is believed to be as follows:

- As a result of water ingress, the forward draught increases. The pressure on the corrugated bulkhead between # 1 and # 2 holds will then be relatively high when the ship is in a fully loaded condition.
- The bulkhead between #1 and # 2 holds may collapse, causing flooding of # 2 hold.
- The ship is subsequently likely to sink due to loss of buoyancy or collapse due to excessive hogging.
- There are reasons to believe that such an accident scenario could progress rapidly due to loss of longitudinal stability, leaving the crew very little time to abandon the ship with consequent high risk of loss of life.

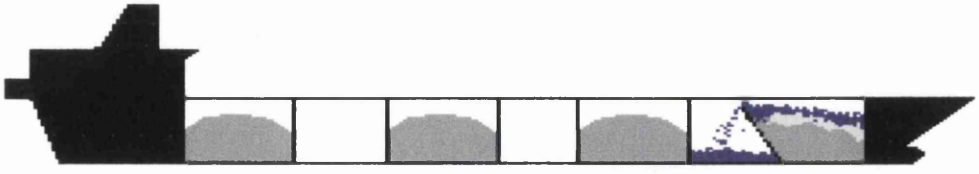

Figure 1.2.2 Damage scenario; after the flooding of hold # 1 the transverse bulkhead fails, leading to the flooding of hold # 2

A very similar scenario was revealed by an investigation into the loss of M/V *Derbyshire* [6]. She sank without a distress signal around September 10, 1980. The persistence and patience of the Derbyshire Families Association led to an investigation, which was initially speculative and later on-site, concluding in May 1998. It is the most important Bulk Carrier loss in the history of British shipping. An additional feature to the loss scenario is the flooding of the bow tank.

1.3 Reactions from IACS & IMO

The P&I clubs, insurance underwriters and the shipowners began demanding action from IACS in 1990. The reaction of IACS was to establish an Enhanced Survey Program (ESP) on the 1st July 1993. The program can be considered successful with the exception of the loss of the 22,021 tdw M/V *Leros Strength* and M/V *Albion II.* In 1997 IACS' goal was that by year 2003 75% of the Bulk Carrier fleet would comply with the new requirements for the ship structure. The new requirements involve higher reserves of strength in the transverse watertight bulkhead between holds number 1 and 2 and the double bottoms in way of number 1 hold [7].

The IMO requirements for the majority of Bulk Carriers up until 1991 can be seen in Appendix 1. In 1st of July 1991 an interim resolution was put in force to improve Bulk Carrier safety. The main aims were structural integrity of the vessel, seaworthiness and that loading procedures and transportation of cargo would not cause undue stresses. In 1995 draft amendments to SOLAS for new Bulk Carriers were introduced in an attempt to ensure a ship's ability to remain afloat following flooding, surveys of the structure and other requirements [3]. In 1996 the MSC adopted amendments to SOLAS Chapter VI which addressed the interaction between the ship and the bulk loading/discharging terminal. The latest action by the IMO is the adoption of the new SOLAS Chapter XII concerning the strength of Bulk Carriers, which will come into force on 1st July 1999, covering the following main topics [3]:

- New ships should have enhanced structures according to IACS Unified Requirements.
- Existing ships should also be assessed according to IACS Unified Requirements using the same timetable and in the form of an IMO standard.

- Loading instruments should be adopted again according to IACS.
- Finally, a definition of the Bulk Carrier was adopted which is acceptable to all the members.
- The EPS is officially recognised and accepted by the IMO.
- The suggestion that future work should be focused on ships with a length not exceeding 150 m (M/V *Leros Strength* length was 146 m).
- The call for fast implementation of the ISM code.

1.4 Evaluation of parameters and selection of those considered in the Study

Engineering ideology recommends that when confronted with a "situation/problem" that needs to be analysed, the subject should be broken down into various components. This leads to a number of simplified analyses, the results of which are appropriately combined to be applied to the initial stage and asses the "situation/problem".

The case we encounter can be subdivided into three major components: the input, the system and the output. The input is assumed to be the conditions that the vessel will encounter throughout its life. The system is the structural reaction to the specific environmental and other conditions. The output is the assessment of the reaction with respect to modes of failure that may lead to survival, partial or total damage.

Some consideration should be given to assessing the importance of each sub-component of the three major components. The aim of this study is not to perform a thorough structural analysis that is both costly and time consuming but to locate those sub-components of the system that are critical to the ability of the vessel to survive.

The input, defined as the conditions that the vessel will encounter throughout its life, can be subdivided into environmental and human applied input. The environmental input is subdivided into three categories: sea loads, corrosion and accidental loading. Furthermore, sea loads can be subdivided into global and local loads. As the characterism implies the first act overall on the ship's structure and the second in a specific area. Generally, global loads can be subdivided into the following:

- Still water loading although it does not appear to decrease the number of failures (pp 4), is a major structural load and was considered in the report.

- Low frequency, steady state, motion related wave excitation is the type of loading that dominates fatigue related failures and extreme vertical bending moment values; it will, therefore, be considered in the report.
- High frequency steady state wave excitation (springing), although infrequent, may cause severe structural damage. However, the crew of the vessel can control the phenomenon by altering the speed or the heading so it was not considered in this report.
- High frequency transient wave impact, resulting in slamming is frequent in bad weather but, again, the crew can control the loading by changing the speed and course so it was not considered.

Local loads:

- Still water external/internal static loads although not critical, was considered alongside the loading stated below.
- External hydrodynamic pressure as a result of waves is critical in bad weather and will, therefore, be considered.
- Slamming loads; the same applies as for global slamming.
- Cargo inertial loads were considered with respect to fatigue calculations.
- Liquid sloshing loads are not critical since Bulk Carriers have relatively few tanks, empty in most operating conditions, and if the tanks are loaded they rarely remain at between 20% to 70% capacity where sloshing is considered damaging to the structure, so they were not considered.
- Green water effects are associated with bad weather and can cause damage to the fore deck structure's fittings. They are not considered to be a major contributor to the losses, and will, therefore, not be considered.

Other Environmental input:

- Accidental Loading; human or mechanical related faults cause this type of loading and will, therefore, not be considered.
- Corrosion is probably the most important input since losses peak as age and increases. Corrosion margins were incorporated into the report.

Human related input:

- Loading / Unloading procedures were mentioned previously in this chapter but since they can be controlled they were not considered.

- Cleaning techniques are associated with corrosion and accidental localised loading, but since they can be controlled they were not considered.
- Inspection/Repairs are the only positive input and have been quite successful since the EPS began, with two exceptions.

The system is the structure of the vessel and can easily be subdivided into major structural components (e.g. double bottom, hopper tank etc). The areas that should concern us the most are those at which stress concentrations occur. Stress concentrations appear where a geometrical change occurs. The more abrupt the change, the higher the stress concentration will be. Since the structure has to serve a certain purpose its geometry is constrained by that purpose, as well as the initial cost and the operating cost. The single skin Bulk Carrier structure has been optimised throughout the years by experience and calculations in order to achieve the current configuration. This configuration, of course, has geometrical discontinuities, which give rise to stress concentrations. The major structural components define their locations by their borders. Naturally, other structural discontinuities can occur globally or locally as a result of sub-standard design or welding. This report focuses upon the inherent discontinuities of the Bulk Carrier structure rather than upon discontinuities that may exist as a special feature in a particular Bulk Carrier structure. Clearly, the general structural configuration is the cause of the Bulk Carrier losses, rather than the structural irregularities of specific Bulk Carriers.

The output is the result of the combination of the input and the system, the survival or failure, and how the failure of certain components may lead to the total failure or otherwise of the vessel.

Throughout this report the loading was calculated from first principals and using the rules of certain classification societies. The rules of the classification societies have been developed through years of research and experience. In the vast majority of the cases they have been reliable, fast and safe tools in the hands of designers. This analogy may prove helpful in understanding the problem and should provide confidence. The assessments with respect to failure were also evaluated using first principles. The reason behind the adoption of first principles is the clear overall understanding of the behaviour of the structure under loading. The results may be dubious regarding their accuracy since

assumptions need to be made with respect to boundary conditions. However the assumptions were assessed where possible so that a more clear opinion was formed with respect to their validity.

This Study commenced in the direction of investigating possible causes of Bulk Carriers structural failures despite compliance with the enforced Rules regarding the ship structure and the respective load-line regulations. However proceeding with this Study it was considered advisable to deal with certain aspects which either separately, as duly dealt with in each Chapter of the Study, or interrelated and combined can be the origin for the development of a structural failure. Each Chapter extended so far to establish its importance and eventually to give rise to a further investigation. In any case the present Study can provide valuable information for further considerations.

The four Chapters of the Study are covering to the extent possible the principal factors affecting the structure of the Bulk Carrier. However additional factors of equal importance are present and are indeed encountered in the actual service life of a Bulk Carrier, i.e. unusual loading and discharging conditions, unusual heavy weather conditions etc. It is therefore evident that the present Study is intended to cover part only of the actual problem however each Chapter and all combined address very important contributing factors to local and global structural failures.

For the last six years the Shipping Industry, IACS and IMO have concentrated their efforts to assess all main parameters that need to be addressed in design and operation of Bulk Carriers for existing vessels as well as for Newbuildings with a view that with proper utilisation, a ship will be safe for its trading purposes taking account of her operation, load-line procedures, stresses, fatigue and corrosion involved during her life service.

The main topics of the report are as follows:

- In Chapter 2 the vessel considered in the Study the single skin Bulk Carrier M/V *Victor* is presented with her particulars and midship section properties.
- In Chapter 3 the sea loads are discussed and evaluated. The extreme vertical bending moment acting on the midship section is calculated considering the hydrostatic and the hydrodynamic components. The fluctuating loading that causes fatigue damage is evaluated from the global loads: vertical bending moment, vertical shear force, horizontal

bending moment, horizontal shear force and torsional moment and the local loads: pressure fluctuation due to waves at the side shell and cargo inertial loading on the ship structure.

- In Chapter 4 the first principles methods are presented, which are based on beam theory, and are used to calculate the stresses incurred by the structure both globally and locally. A parametric study was included with respect to corrosion where considered significant.
- In Chapter 5 a finite element model is presented which was used to check the stresses calculated from the first principles analysis and additionally to evaluate the extreme vertical bending moment stresses that the vessel experiences. (A plated 3-D model was planned but was too large to run on the program as configured on the available workstation. Therefore a beam and bar 3-D model only was used with bars representing the in plane shear stiffness of panels.)
- In Chapter 6 the fatigue assessment is discussed that was carried out with respect to global and local loads for a section of the midship area.
- In Chapter 7 the current IACS regulations are reviewed.
- In Chapter 8 an overall discussion ends the report with main aim to draw together the conclusions of the previous chapters.

References

1. Isbester J.; "Bulk Carrier Practice", The Nautical Institute, London 1993, ISBN 1 870077 16 4.

2. Gratsos George A.: "Bulk carrier safety", Bimco Bulletin, Vol. 92, # 3, 1997, pp 20.

3. Williams, I., "New bulk carrier regulations", Bulk carrier safety, Bimco Special Bulletin, 1998

4. "Study Report on bulk carrier losses", N.K.K. , January 1992

5. "Bulk carrier safety – a position paper", IACS, Feb. 1997

6. M/V Derbyshire Surveys, UK/EC Assessors' Report

7. Middleton Ian, "The new bulk carrier rules", Seatrade Review, July 1997, pp26.

Bibliography

1. "Bulk Carriers – a great deal of work expected", International Shiprepair News, May/June 1997, pp 40.

2. Sommerville D. Robert, "Improving bulk carrier safety", Bimco Bulletin, Vol. 91, # 6, 1996, pp 40.

3. Middleton Ian, "Bulk carrier shock", Seatrade Review, January 1997, pp 18

4. "Bulk carrier safety", Bimco Bulletin, Vol. 92, # 4, 1997, pp 8.

5. "Bulk carrier safety", Bimco Bulletin, Vol. 92, # 1, 1997, pp 28.

6. "Questionnaire on bulk carriers", Bimco Bulletin, Vol. 91, # 5, 1996, pp 25.

7. "Draft bulk carrier safety regulations", Bimco Bulletin, Vol. 92, # 3, 1997, pp 6

8. "Bulk carriers – an update", Lloyd's Register. , March 1998

9. Petersen, S.S.," Safety the Bimco perspective", Bulk carrier safety, Bimco Special Bulletin, 1998

10. Montersen, B. N." Setting out Bimco's views and actions", Bulk carrier safety, Bimco Special Bulletin, 1998

11. Grey, M., "The history of bulk carrier safety and losses", Bulk carrier safety, Bimco Special Bulletin, 1998

12. Guest, A., "Questions still waiting for answers", Bulk carrier safety, Bimco Special Bulletin, 1998

13. "Steel re-inforcement of existing bulk carriers", Bimco Bulletin, Vol. 92, # 3, 1997, pp 12.

14. Bell, J., Smith, J.,"IACS meets its obligations", Bulk carrier safety, Bimco Special Bulletin, 1998

15. Mortensen N. B., "Bulk carrier safety – the view and role of an industry organisation", RINA Conference, Design and operation of bulk carriers, London, 1998

16. Plaza F., "IMO's work on safety of bulk carriers-an update", RINA Conference, Design and operation of bulk carriers, London, 1998

17. O'Neil William A., "Bulk carrier safety", Bimco, General Meeting, 2-4 June 1997, pp 53.

18. Lorentzen F., "Working together for safety", Bimco, General Meeting, 2-4 June 1997, pp 93

Appendix 1
Survivability requirements for bulk carriers assigned B - reduced freeboard
International Load Line Convention 1966

Regulation 27

7.d. The ship, when loaded to her summer load waterline, will remain afloat in a satisfactory condition of equilibrium after flooding of any single damaged compartment at an assumed permeability of 0.95 excluding the machinery space...

The relevant calculations may be based upon the following main assumptions:
- the vertical extent of damages equal to the depth of the ship;
- the penetration of damage is no more than B/5;
- no main transverse bulkhead is damaged; ...

Resolution A320(IX) (Adopted in Nov. 1975)
Regulation equivalent to regulation 27 of the International Convention on Load Lines 1966
Annex:

8.d. The ship when loaded to its summer load waterline, shall be able to withstand the flooding of any compartment or compartments, with an assumed permeability of 0.95 ... and shall remain in a satisfactory condition of equilibrium ...

Damage assumptions

12.d. Except where otherwise required by paragraph (10) (a) the flooding shall be confined to a single compartment between adjacent bulkheads...

Condition of equilibrium

13:The condition of equilibrium after flooding shall be regarded as satisfactory provided:
13.a: The final waterline after flooding, taking into account sinkage, heel and trim is below the lower edge of any opening through which progressive flooding may take place
...

Chapter 2

The vessel: M/V *Victor* Panamax Bulk Carrier, her Particulars and Midship Section Properties

2.1 General

The calculations for this report are based on the single skin Panamax Bulk Carrier M/V *Victor*. The vessel was built in Hitachi, Sakai shipyard in 1976. She was classed with ABS and has remained with the same classification society ever since. She has never suffered any kind of serious structural damage such as corrosion, cracking or buckling. She underwent a special survey in October 95 in which numerous gaugings were performed, finding all measured thicknesses to be within the margins set by the classification societies. She was/is operated in the tramp trade with usual cargo grain or bauxite.

2.2 Structural Arrangement

The main components of the Bulk Carrier structure, which is a single deck ship, are: double bottom, hopper tanks, single skin side shell, upper wing tanks, deck hatchways, cross deck and transverse bulkhead structure. They fulfil the basic requirements of every sea structure; firstly, to resist bending, shear and torsion and secondly, to provide a watertight envelope.

The double bottom consists of the bottom plating, the inner bottom plating, the bottom girders and floors, and the inner bottom and bottom longitudinal stiffeners. The first two contribute to the lower flange of the hull girder as principal longitudinal members. Also, they resist local loading; in the first case hydrostatic and in the second, cargo induced. The remaining sub-components fulfil the two main requirements of distribution of loading and stiffening of the plating. The girders and floors may also provide the subdivision of the double bottom for ballast or fuel tanks.

Hopper tanks consist of the bottom plating, the bilge plating, the side shell plating, the hopper tank sloping plating, the longitudinal stiffeners on the two previous platings and the hopper transverse ring web. They serve the same purposes as the equivalent sub-components of the double bottom and also act as torsion resistant boxes.

The side shell is the simplest of all the components. The main sub-component is the side shell plating, which is stiffened by the transverse side shell stiffeners. It forms a connection between the upper and lower part of the structure. It also acts as a web for the hull girder and is a principal part of the watertight envelope. Throughout the vessel's life

it will be subject to hydrodynamic, hydrostatic and cargo inertial loads. Accidental loading involving piers or other vessels during port operations is not infrequent and internal during loading/discharge or cleaning operations. Some vessels have, on the external face of their side shell, "bumpers" to ease this type of loading.

The upper wing tanks can be subdivided into deck plating and longitudinal stiffeners, side shell plating and longitudinal stiffeners, topside sloping tank plating and longitudinals, vertical strake and transverse ring frames. They serve equivalent purposes to the hopper tanks' components, but in the upper part of the vessel.

The hatchways essentially have two components. The hatch coaming, which contributes to the hull girder, provides the base for the hatch and with its height alters the flow of water on board. The hatch provides a watertight cover for the hold ensuring the good condition of cargo and the water-tightness of the hold.

The transverse bulkhead structure includes the following sub components. The upper stool resists transverse torsion loads and provides a structural connection between the deck structure and the transverse bulkhead. The lower stool has an equivalent purpose to the upper stool, but in the lower part of the vessel. The combination of the transverse bulkhead with the stools, the cross deck and the double bottom provides transverse strength. The transverse structure also provides a watertight subdivision of the holds.

The cross deck can be subdivided into the deck plating, the deck longitudinals and the transverse stiffeners as secondary stiffeners. It enhances the transverse strength of the vessel and reduces torsion loads.

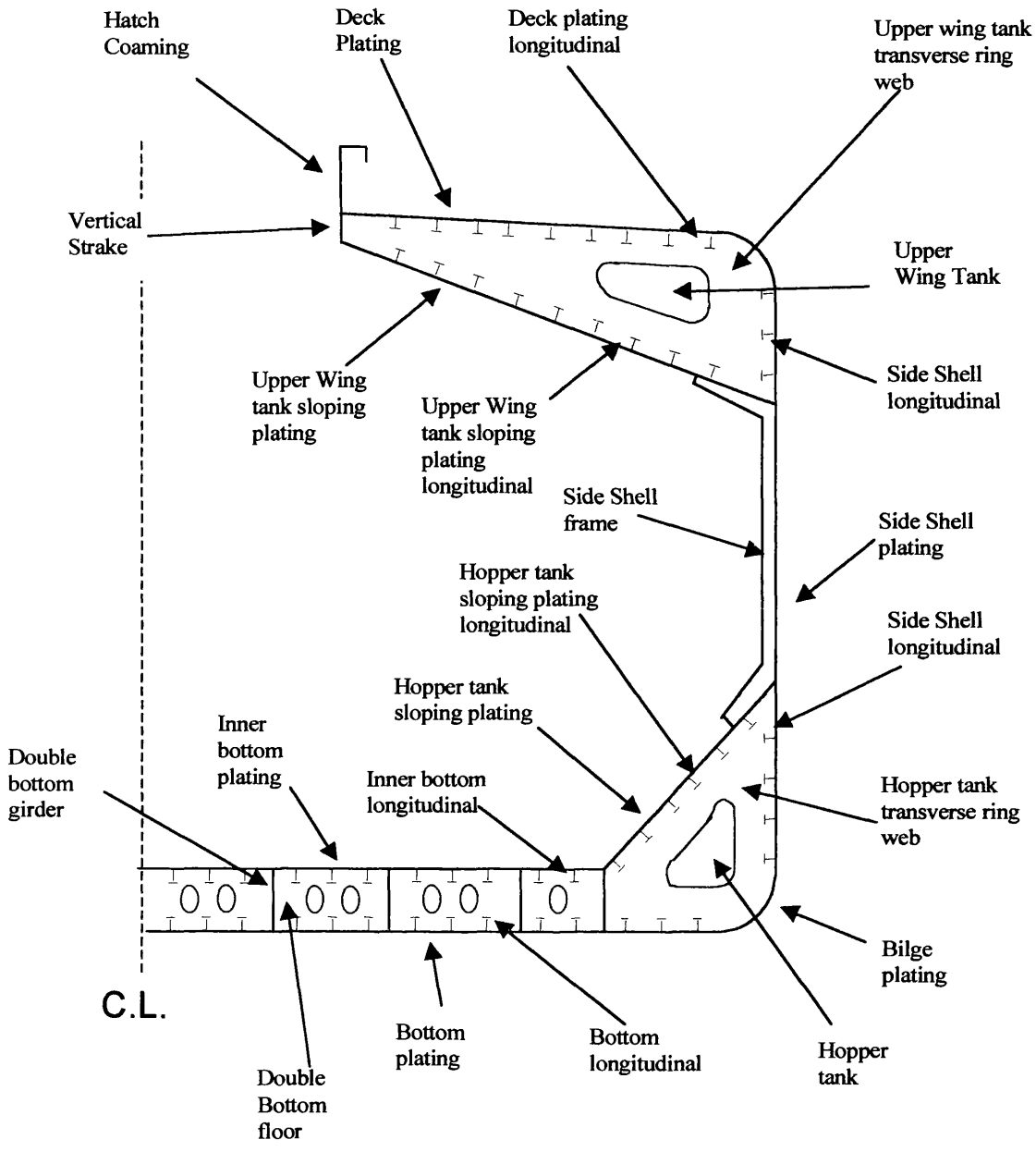

Figure 2.2.1 Midship section

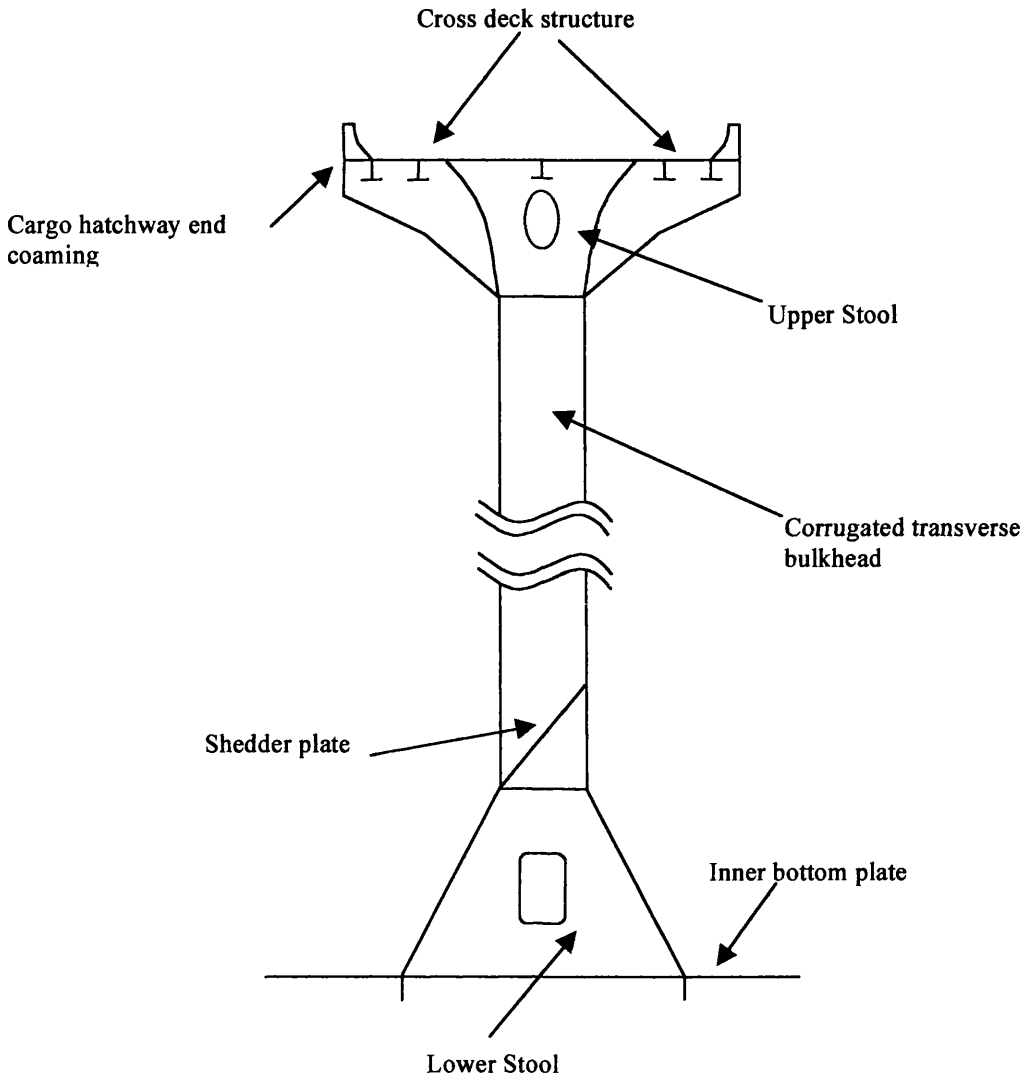

Figure 2.2.2 Corrugated transverse watertight bulkhead

2.3 Principal characteristics of the vessel

2.3.1 Principal Particulars of M/V *Victor*.

The Principal Particulars of M/V *Victor* are [1].

1.General

Operator:	Endeavour Shipping CO. S.A.
Port of registry:	MONROVIA, LIBERIA
Kind of ship:	Bulk carrier
Keel laid:	25th JAN. 1976
Launched:	23rd JULY 1976

Delivered:	15th NOV. 1976
Shipyard:	HITACHI, SAKAI SHIPYARD
Yard number:	4461

2.3.2 Principal dimensions

Length, over all:	225.000 m
Length, registered:	216.761 m
Length, between perpendiculars:	215.000 m
Breadth, moulded:	32.200 m
Depth, moulded:	17.800 m
Designed load draft, moulded:	12.400 m
Scantling draft, moulded:	12.400 m
Summer freeboard (from deck mark:	4.487 m
Summer load draft, extreme:	12.450 m
Corresponding full load displacement:	72,981 kt (71,828 L.T.)
Block coefficient at full load draft:	0.8249
Prismatic coefficient at full load draft:	0.8304
Water plane coefficient at full load draft:	0.8875
Midship section coefficient at full load draft:	0.9934

2.3.3 Classification and Regulations

Classification:	American Bureau of Shipping + A1 E, "Bulk Carrier", "Strengthened for the Carriage of Ore Cargoes-Holds No.2, 4 &6 may be empty", + AMS and + ACCU
Regulations:	International Convention for the Safety of Life at Sea, 1960. International Load Line Convention, 1960. Liberian Maritime Laws and Regulations. Tonnage Regulations. International Tele-communication Convention, 1967. Suez and Panama Canal Rules Including Tonnage Measurements.

2.3.4 Speed

Maximum. trial speed at ballast condition of displacement (45% full) and at maximum continuous output of the main engine. 17.639 knots
Sea speed at full-loaded condition and at continuous service output of the main engine with 15% of sea margin. 15.300 knots

2.3.5 Type of ship

Type of ship:	Single deck type bulk carrier with F'cle deck.
Stem:	Bulbous type.
Stern:	Transom type.

2.3.6 Tonnage

Gross tonnage:	30592.2 t (Liberia)
Net tonnage:	23585 t (Liberia)

2.3.7 Dead-weight

Light weight:	11,607 kt (11,424 L.T.)
Dead-weight:	61,374 kt (60,404 L.T.)

2.3.8 Complement

Officer:	12 persons
Crew:	27 persons
Other:	2 persons
Total:	41 persons

2.3.9 Propelling machinery

Main engine:	Hitachi Sulzer 8rind Vertical, 2-stroke, single acting, direct reversible, crosshead type, turbo- charged, welded design.
Propeller:	Aerofoil solid type 1set Material: Manganese bronze Diameter: 6,000 mm Pitch: 4,125 mm Pitch ratio: 0.6875 Exp. area ratio: 0.6417

2.4 Midship section properties

The calculations of the midship section properties were performed using the computer program C.S.S.P. [2]. The midship section was defined using "nodes" and "plates", the former being points on the midship section where a geometrical change occurred, the latter being dependent upon the former. All the dimensions used in the C.S.S.P. program are moulded. Millimetres are the input unit for length and kilograms per cubic meter for density. The output of the program consists of:

1. The input file containing the definition of "nodes" and "plates" and other input data such as density of the material, etc.
2. Mass parameters including section mass and moments of inertia at the centre of gravity in x, y and z directions.
3. Strength data including structural area centre of gravity and the second moment of inertia about the y axis.
4. Torsion constant
5. Co-ordinates of the shear centre and the shear area in y, yz and z directions and shear flows in the plates as a result of a unit shear.

The sectional properties of the vessel were calculated with regard to four conditions. The "as built" condition and three other conditions taking corrosion margins of 10%, 20% and 30%. These corrosion margins were selected because the first is considered acceptable by classification societies [3,4] but anything greater than twenty percent is not. The moment of inertia of the hull girder in the different conditions is shown in table 2.4.1. Part of the output can be found in Appendix 2.

Condition/Corrosion margin	Second moment of area about the neutral axis mm^4
Midship Section as built (0%)	1.8857E+14
Midship Section (10%)	1.6971E+14
Midship Section (20%)	1.5086E+14
Midship Section (30%)	1.3200E+14

Table 2.4-1 Corrosion margins and second moments of area about the neutral axis of the midship section

References

1. Principal particulars ,M/V *Victor*

2. Das, P. K., "Background formulation in CSSP program and shear flow calculations of typical example problems", BMT ltd, 1986

3. "Guide for Dynamic Based Design and Evaluation of Bulk Carrier Structures", ABS, March 1995

4. Valsgard, S., Andreassen E., Kim S.K., (1998), Development of ultimate Hull girder Capacity, Proceedings of the Conference Design and Operation of Bulk Carriers, London

Appendix 2

Output of computer program that calculates midship section properties.

Output of CSSP (units in mm and kg)

Case 1 0% corrosion margin

```
0  PROGRAM CSSP (VAS ISSUE 2) P.K.DAS
 NA/W506 MARK IBM1      COMPILED ON 05/07/83
 COMPUTED ON         AT TIME 10:45:19
 CALCULATION OF SHIP SECTIONAL PROPERTIES


0M/V VICTOR

NO. GRID POINTS= 99  NO. PLATES =103NO. WEIGHTS =  0

 LENGTH OF SEGMENT=  1.00    SCALE=    1.00
0KEY=  212  REFERENCE DENSITY OF STRUCTURE= 0.78000000E+04
SECTIONAL PROPERTY RESULTS


 SECTION MASS     =  2.7153E+10
0CO-ORDINATES OF C.G.          Z =  7.5062E+03   Y =  0.0000E+00
0MOMENT OF INERTIA AT C.G. ABOUT  Z    =  3.5756E+18
 MOMENT OF INERTIA AT C.G. ABOUT YZ    =  0.0000E+00
 MOMENT OF INERTIA AT C.G. ABOUT  Y    =  1.4709E+18
 MOMENT OF INERTIA AT C.G. ABOUT  X    =  5.0464E+18




              STRENGTH DATA
0STRUCTURAL AREA    =  3.4812E+06
0CO-ORDINATES OF ELASTIC CENTRE  Z =  7.5062E+03   Y =  0.0000E+00
02ND. MOMENT OF AREA AT CENTRE ABOUT  Z =  4.5840E+14
 2ND. MOMENT OF AREA AT CENTRE ABOUT YZ =  0.0000E+00
 2ND. MOMENT OF AREA AT CENTRE ABOUT  Y =  1.8857E+14
0NUMBER OF LOOPS USED FOR Z SHEAR =            5
0NUMBER OF LOOPS USED FOR Y SHEAR AND TORSION =  6 PLUS ONE CHECK LOOP IF
SYMMETRIC SECTION SPECIFIED

0TORSIONAL CONSTANT =  1.0190E+13
```

Case 2 10% corrosion margin

0 PROGRAM CSSP (VAS ISSUE 2) P.K.DAS
NA/W506 MARK IBM1 COMPILED ON 05/07/83
COMPUTED ON AT TIME 14:41:48
CALCULATION OF SHIP SECTIONAL PROPERTIES

0M/V VICTOR
NO. GRID POINTS= 99 NO. PLATES =103NO. WEIGHTS = 0
LENGTH OF SEGMENT= 1.00 SCALE= 1.00
0KEY= 212 REFERENCE DENSITY OF STRUCTURE= 0.78000000E+04

SECTIONAL PROPERTY RESULTS

SECTION MASS = 2.4438E+10
0CO-ORDINATES OF C.G. Z = 7.5062E+03 Y = 0.0000E+00
0MOMENT OF INERTIA AT C.G. ABOUT Z = 3.2180E+18
MOMENT OF INERTIA AT C.G. ABOUT YZ = 0.0000E+00
MOMENT OF INERTIA AT C.G. ABOUT Y = 1.3238E+18
MOMENT OF INERTIA AT C.G. ABOUT X = 4.5418E+18

STRENGTH DATA
0STRUCTURAL AREA = 3.1331E+06
0CO-ORDINATES OF ELASTIC CENTRE Z = 7.5062E+03 Y = 0.0000E+00
02ND. MOMENT OF AREA AT CENTRE ABOUT Z = 4.1256E+14
2ND. MOMENT OF AREA AT CENTRE ABOUT YZ = 0.0000E+00
2ND. MOMENT OF AREA AT CENTRE ABOUT Y = 1.6971E+14
0NUMBER OF LOOPS USED FOR Z SHEAR = 5
0NUMBER OF LOOPS USED FOR Y SHEAR AND TORSION = 6 PLUS ONE CHECK LOOP IF SYMMETRIC SECTION SPECIFIED
0SHEAR LOOPS DEFINED BY PLATE NUMBERS ARE

0TORSIONAL CONSTANT = 9.1714E+12

Case 3 20% corrosion margin

0 PROGRAM CSSP (VAS ISSUE 2) P.K.DAS
NA/W506 MARK IBM1 COMPILED ON 05/07/83
COMPUTED ON AT TIME 14:45:50
CALCULATION OF SHIP SECTIONAL PROPERTIES

0M/V VICTOR
NO. GRID POINTS= 99 NO. PLATES =103NO. WEIGHTS = 0

LENGTH OF SEGMENT= 1.00 SCALE= 1.00
0KEY= 212 REFERENCE DENSITY OF STRUCTURE= 0.78000000E+04

SECTIONAL PROPERTY RESULTS

SECTION MASS = 2.1723E+10
0CO-ORDINATES OF C.G. Z = 7.5062E+03 Y = 0.0000E+00
0MOMENT OF INERTIA AT C.G. ABOUT Z = 2.8604E+18
MOMENT OF INERTIA AT C.G. ABOUT YZ = 0.0000E+00
MOMENT OF INERTIA AT C.G. ABOUT Y = 1.1767E+18
MOMENT OF INERTIA AT C.G. ABOUT X = 4.0371E+18

STRENGTH DATA
0STRUCTURAL AREA = 2.7850E+06
0CO-ORDINATES OF ELASTIC CENTRE Z = 7.5062E+03 Y = 0.0000E+00
02ND. MOMENT OF AREA AT CENTRE ABOUT Z = 3.6672E+14
2ND. MOMENT OF AREA AT CENTRE ABOUT YZ = 0.0000E+00
2ND. MOMENT OF AREA AT CENTRE ABOUT Y = 1.5086E+14
0NUMBER OF LOOPS USED FOR Z SHEAR = 5
0NUMBER OF LOOPS USED FOR Y SHEAR AND TORSION = 6 PLUS ONE CHECK LOOP IF SYMMETRIC SECTION SPECIFIED
0SHEAR LOOPS DEFINED BY PLATE NUMBERS ARE

0TORSIONAL CONSTANT = 8.1524E+12

Case 4 30% corrosion margin

0 PROGRAM CSSP (VAS ISSUE 2) P.K.DAS
NA/W506 MARK IBM1 COMPILED ON 05/07/83
COMPUTED ON AT TIME 14:46:07
CALCULATION OF SHIP SECTIONAL PROPERTIES

0M/V VICTOR
NO. GRID POINTS= 99 NO. PLATES =103NO. WEIGHTS = 0

LENGTH OF SEGMENT= 1.00 SCALE= 1.00
0KEY= 212 REFERENCE DENSITY OF STRUCTURE= 0.78000000E+04

SECTIONAL PROPERTY RESULTS

SECTION MASS = 1.9007E+10
0CO-ORDINATES OF C.G. Z = 7.5062E+03 Y = 0.0000E+00
0MOMENT OF INERTIA AT C.G. ABOUT Z = 2.5029E+18
MOMENT OF INERTIA AT C.G. ABOUT YZ = 0.0000E+00
MOMENT OF INERTIA AT C.G. ABOUT Y = 1.0296E+18
MOMENT OF INERTIA AT C.G. ABOUT X = 3.5325E+18

STRENGTH DATA
0STRUCTURAL AREA = 2.4369E+06
0CO-ORDINATES OF ELASTIC CENTRE Z = 7.5062E+03 Y = 0.0000E+00
02ND. MOMENT OF AREA AT CENTRE ABOUT Z = 3.2088E+14
2ND. MOMENT OF AREA AT CENTRE ABOUT YZ = 0.0000E+00
2ND. MOMENT OF AREA AT CENTRE ABOUT Y = 1.3200E+14
0NUMBER OF LOOPS USED FOR Z SHEAR = 5
0NUMBER OF LOOPS USED FOR Y SHEAR AND TORSION = 6 PLUS ONE CHECK LOOP IF SYMMETRIC SECTION SPECIFIED
0SHEAR LOOPS DEFINED BY PLATE NUMBERS ARE

0TORSIONAL CONSTANT = 7.1333E+12

Chapter 3

Extreme and Fluctuating Sea Loads

3.1 Introduction to extreme and fluctuating loading

The structure of a vessel suffers as a result of its sea loads throughout its life. The engineer responsible for assessing the strength of the structure needs to subdivide the loading into extreme and fluctuating loading in order to asses the corresponding modes of failure. Extreme loading is defined as the most severe loading that the structure will undergo within a specified period of time (usually 20 or 100 years). Fluctuating loading is defined as loading constituted by stress cycles suffered by the vessel throughout its life, causing crack initiation and propagation.

3.2 Extreme Loading

The hull girder extreme load depends on the distribution of both gravitational and buoyancy forces along the ship's length. Buoyancy distribution is composed of two different effects: the static and the dynamic. The static depends upon the underwater shape of the vessel, and the dynamic upon the interaction between the underwater shape and waves. In order to simplify the analysis, calculations will be carried out for each individual effect and the results will be collated.

3.2.1 Introduction to Still Water Loading

Uneven distribution of weight and buoyancy along a ship's length causes bending, the reason being that larger buoyancy forces than gravitational or the opposite will be applied to sections of the ship's length. If the buoyancy forces have a bigger magnitude than the gravity forces at a group of sections in the middle of the vessel then the bending is termed "hogging", the opposite being termed "sagging". Figure 3.2.1 illustrates sagging. Longitudinal shear forces are forces that tend to break or shear the ship across, as illustrated in figure 3.2.2.

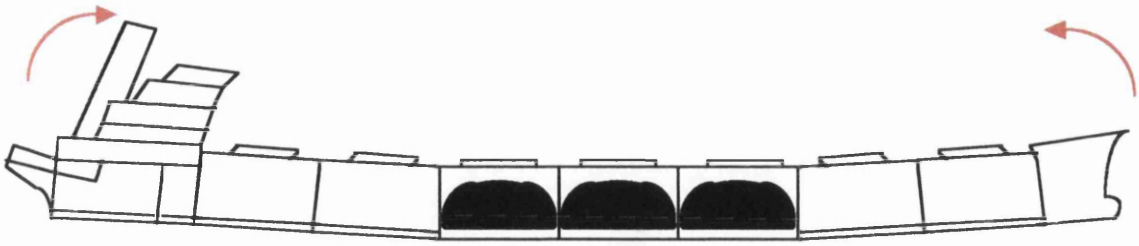

Figure 3.2.1 The sagging moment illustrated above will result in compression at the deck and tension at the bottom.

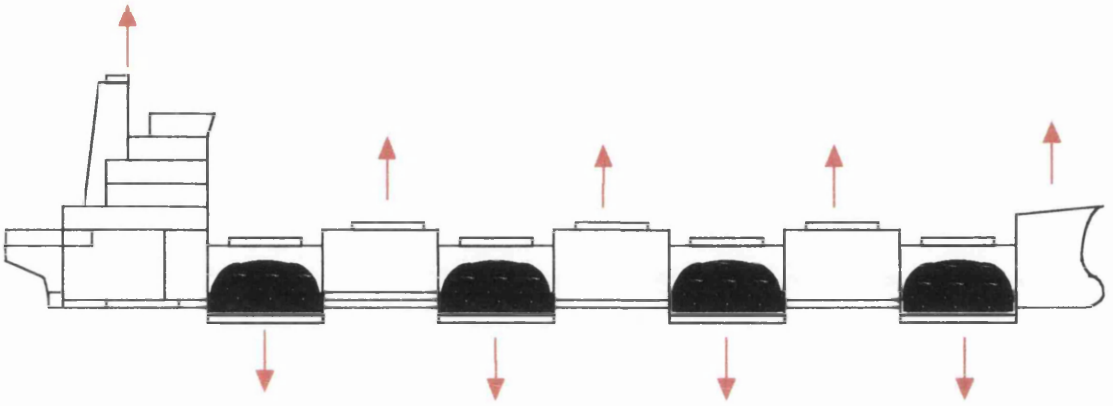

Figure 3.2.2 The shear effects will tend to break the ship with maximum value where the difference between the weight and the buoyancy.

3.2.2 Weight distribution

Buoyancy distribution effects, as mentioned above, depend upon the underwater shape of the vessel. The underwater shape is calculated based on the lines plan and the corresponding draft of the vessel for its corresponding loading condition. Therefore, to calculate these drafts we need the weight distributions for the conditions that we intend to study. The weight distribution is composed of the sum of the conditional weight curve and the basic weight curve. The former includes the weights of a particular condition, listed in the vessel's 'Trim and Stability book'. The latter includes only the weights that are present in the lightship condition and is constant for all conditions. Each weight is distributed over a length determined by the frame spacing. Unfortunately, the weight distribution of the vessel was not available so an approximate weight distribution was calculated based on the Bilge-Coffin diagram, which is essentially a trapezoid with the centre corrected with respect to the longitudinal centre of gravity of the vessel. The

approximation does not incorporate the weight of the machinery, which was added at the end of the calculations.

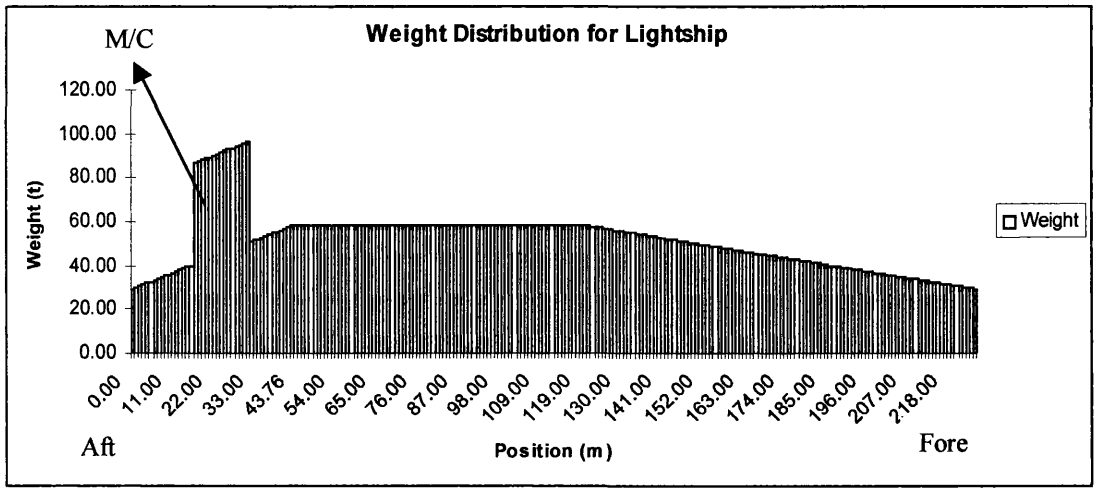

Figure 3.2.3 The Lightship weight distribution

3.2.3 Still Water Loading

The load distribution is the algebraic sum of the weight distribution and the buoyancy distribution. According to simple beam theory, if we integrate once the load distribution along the ship's length, we will calculate the distribution of the vertical shear force and twice the distribution of the still-water bending moment. These calculations can be carried out using a calculator as in the 'Trim and Stability book', based on a method developed by ABS. The most difficult part of the calculations is in determining the draft and trim of the vessel. The calculations are tedious and repetitive so a computer package was used.

The still-water vertical bending moments and vertical shear forces were calculated for ten conditions using the computer package Autohydro. The first five conditions are described in the 'Trim and Stability book' [1]. Five more conditions were considered; one variant for the described conditions, with each variant having hold #1 flooded. The variant conditions were studied because according to statistical data the majority of the Bulk Carriers that suffered structural damage had the #1 hold flooded. The results can be seen in table 3.2-1.

Conditions	Max. B.M. (kN-m)	Max. Shear (kN)
Heavy Ballast at Departure	1078943 (Sagging) at 11.15f	-46460 at 1.650a
Heavy Ballast at Departure with #1 hold damaged	632637 (Hogging) at 44.850a	42559 at 22.350f
Grain Load at Departure	461374 (Sagging at 32.05a	-20414 at 73.650a
Grain Load at Departure with #1 hold damaged	613252 (Hogging) at 29.550f	-27536 at 70.350f
Grain Load at Arrival	385052 (Sagging) at 18.45a	-18246 at 73.650a
Grain Load at Arrival with #1 hold damaged	619815 (Hogging) at 27.950f	-27546 at 70.350f
Ore Load at Departure	1226976 (Hogging) at 11.950f	-58199 at 70.350f
Ore Load at Departure with #1 hold damaged	1689929 (Hogging) at 11.950f	-71760 at 70.350f
Ore Load at Arrival	1277065 (Hogging) at 11.15f	-58075 at 70.350f
Ore Load at Arrival with #1 hold damaged	1711207 (Hogging) at 11.950f	-71554 at 70.350f

Table 3.2-1 Loading conditions with the corresponding vertical bending moments and shear forces.

The 'Trim and Stability book' [1] includes the maximum bending moments for intact conditions. Comparing the results, we can conclude that the real weight distribution of the lightship should be lighter in the middle area since sagging moments have greater values and hogging moments smaller values with respect to the 'Trim and Stability book'. The position of the maximum bending moments is reasonably close, with the exception of the Grain Load at Arrival Condition. The difference between the Grain Load Arrival Condition and the Grain Load Departure Condition is that three fuel tanks positioned between the midship and the fore end of the superstructure and one ballast tank underneath the aft end of the superstructure are empty. The comparison can be seen in Table 3.2-2.

Conditions	Maximum Bending Moments (kN-m)	
	Trim & Stability Booklet	Autohydro
Heavy Ballast at Departure	907268 (Sagging) at 9.981f	1078943 (Sagging) at 11.15f
Grain Load at Departure	359212 (Sagging) at 23.512a	461374 (Sagging at 32.05a
Grain Load at Arrival	225159 (Sagging) at 3.121f	385052 (Sagging) at 18.45a
Ore Load at Departure	1353024 (Hogging) at 10.48f	1226976 (Hogging) at 11.950f
Ore Load at Arrival	1421881 (Hogging) at 9.71f	1277065 (Hogging) at 11.15f

Table 3.2-2 Comparison of results produced by computer program Autohydro and those listed in the trim and stability booklet.

The maximum bending moment occurs for the Ore Load in the Arrival condition. It is interesting to note that for in each damage case the maximum bending moments are larger than the values produced for the equivalent intact conditions except for the heavy ballast condition.

3.2.4 Rule based still water bending moment

The maximum allowable still water bending moment as calculated from the rules (ABS rules) [2] is:

$$M_{ss} = -k_S C_1 L^2 B(C_b+0.7)10^{-3} \text{ sagging moment} \qquad 3.2.4.1$$

$$M_{sh} = +k_H C_1 L^2 B(8.167-C_b)10^{-3} \text{ hogging moment} \qquad 3.2.4.2$$

Where:

k_S = 65
k_H = 15
C_1 = $10.75-[(300-L)/100]^{1.5} = 9.966$ for 150<L<300m
L = 215 m (Lpp)
B = 32.2 m (max. breadth)
C_b = 0.829 (summer loadline)

Therefore:

M_{ss} = -1474261 kN-m maximum allowable sagging moment

M_{sh} = 1632761 kN-m maximum allowable hogging moment

3.2.5 Discussion

The still-water longitudinal strength calculations were carried out for five intact and five damaged conditions. The differences between the values for maximum bending moments listed in the 'Trim and stability booklet' and the values calculated occur as a result of the assumed weight distribution and the methods of calculation. None of the maximum vertical bending moments exceeds the values stated by the rules for intact conditions. The maximum still-water vertical bending moment for the cases in which the vessel is intact is for the Ore Load Arrival condition (1226976 kN-m (hogging)) (figure 3.2.4.) and for the damaged cases the same condition (1711207 kN-m (hogging) (figure 3.2.5), which exceeds the value calculated by the rules). The conditions are graphically represented in Appendix 3 along with their strength curves. High shear force values have been calculated for the alternate conditions in the fore end of the structure however the correction for the effect of local forces at transverse bulkheads was not incorporated in the calculations.

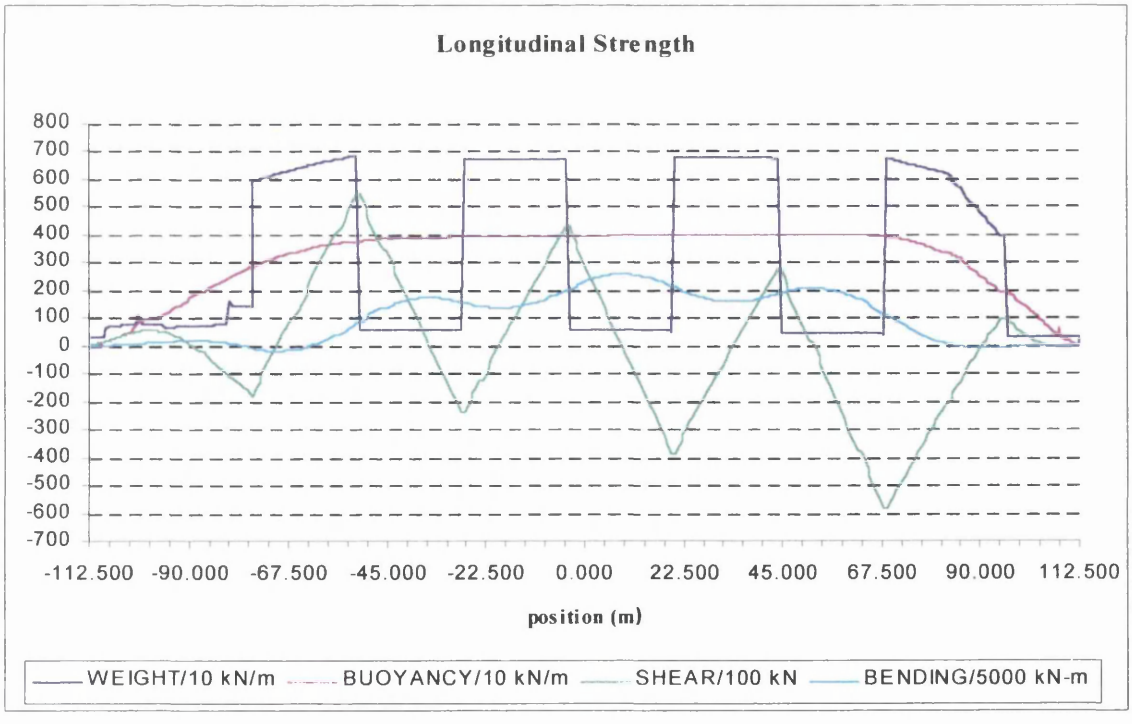

Figure 3.2.4 Ore load arrival condition longitudinal strength curves.

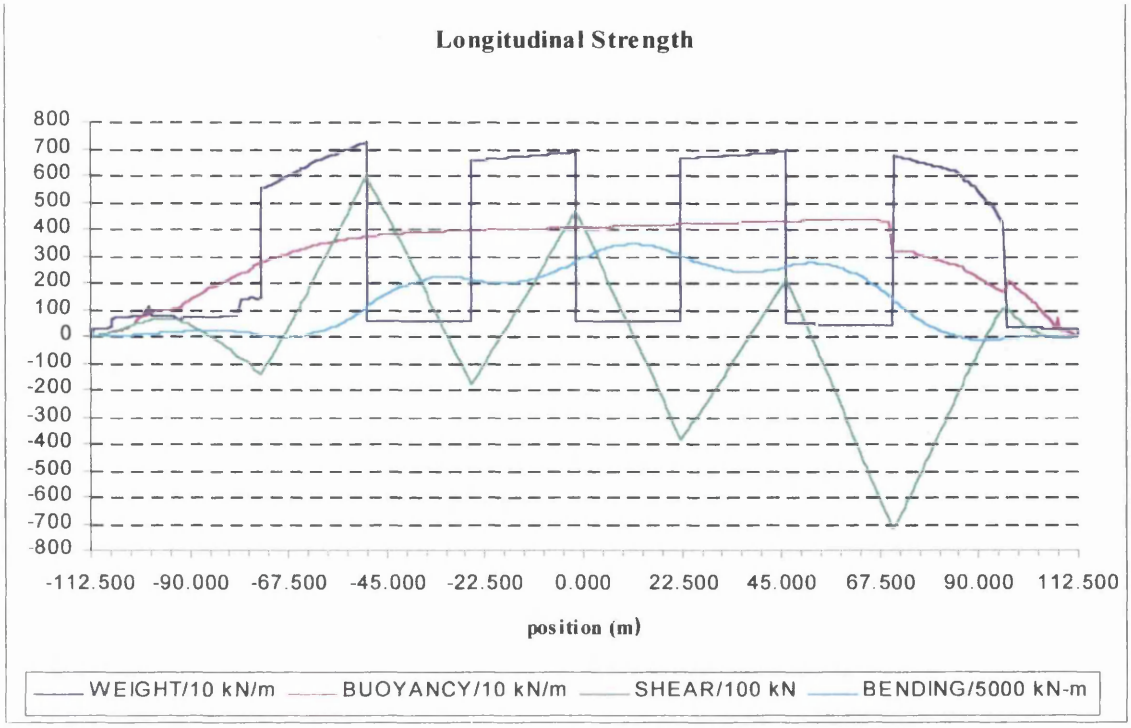

Figure 3.2.5 Ore load arrival with hold 1 damaged condition longitudinal strength curves.

3.2.6 Introduction to Global Extreme Wave Loading

Loading of the structure due to waves can be subdivided into global and local loads or internal and external loads. The most important global load by far is the vertical bending moment. For the sake of these calculations the hull girder is considered to be stiff so that the wave excitation does not cause vibrations (springing) within the vessel. Hughes [3] describes the methodology of including the impact effects by considering the wave impact response separately and assuming that the hull girder is modeled as a flexible beam, and then combining the results. Wave impact effects such as bottom slamming or bow flare impact and springing effects are not considered for the reasons described in the introduction. Predicting the extreme vertical bending moment is not simple although the methodology has existed since the late 60's. The method is sensitive to the following input:

- Scatter diagram
- Wave and Directional spectrum
- Transfer functions
- The approach used to extrapolate/interpolate the extreme value

3.2.7 Literature Survey

The development of the strip theory approach to the calculation of ship motions by Korvin and Kroukorsky led to the methodology for the calculation of shear, torsion and bending moment in regular waves, initially developed by Jacobs and enhanced by Salvensen, Tuck and Faltinsen [4].

St. Denis and Pierson [5], working on the assumption that both waves and the ship's short-term responses are stationary stochastic processes, accomplished the extension of regular wave results by predicting various ship responses to those of short-crested irregular seas. Subsequently, the long-term prediction method was first developed by Bennet [6] for the analysis of full-scale stress data. Variations and enhancements to the initial long-term prediction procedure have been made, including those of Guedes Soares [7], Ochi [8], Lewis and Zubaly [6] and Mansour [9]. Every method predicts the short-term probabilities in the same way and then calculates the long-term probabilities; the differences lie in the area of initial input, the succession of combining the input and also in the mathematical methods used to perform the interpolation/extrapolation. This project adopts the methodology presented at the Extreme Loads Response symposium of 1981 by Lewis and Zubaly [6].

3.2.8 Scatter diagram

The sea-state scatter diagram is a collection of probabilities of occurrences of combinations of significant wave heights and mean zero-crossing periods measured every one or three hours over a period of several years. The Global Wave Statistics data [10] contains a collection of scatter diagrams available for each of the four seasons and their combination. The data is also subdivided into certain areas of ocean called Marsden zones (see Appendix 4). This report has combined zones 8,9,11,15,16 and 17. The initial range of significant wave heights is 0.5 meters to 14 meters, with respect to mean zero-crossing periods from 3.5 seconds to 14.5 seconds. Projects regarding weather conditions in the North Atlantic area have reported an increase in significant wave height values compared to those of the past [11], which is probably a result of global warming. In order to incorporate this effect, the wave scatter diagram was expanded into wave heights up to

19.5 meters because the aim of the calculations is to estimate/extrapolate the most probable extreme value over periods of twenty and one hundred years. The method of Fang and Hogben [12] estimates the probability distributions of wave periods given the probability distribution of the wave heights. The input to the procedure is the probability distribution of the wave's significant heights, the significant wave heights and the mean zero-crossing periods. The method distributes the probabilities of occurrence of the significant wave heights to the combined probabilities of occurrence of significant wave heights and mean zero-crossing periods.

The probability distribution of the wave heights up to 19.5 was calculated by applying the method [13] outlined below:

- Obtain the probability of occurrence for each wave height. Plot the occurrence probability with respect to wave height using Fisher –Tippet II distribution (–ln(-ln(1-Q)) against ln(Hs) where Q is probability of occurrence and Hs is significant wave height).
- A best-fit line should be drawn, thereby extrapolating the probabilities of occurrence of significant wave heights up to 19.5 with 1-meter steps. Figure 3.2.6 illustrates the distribution.

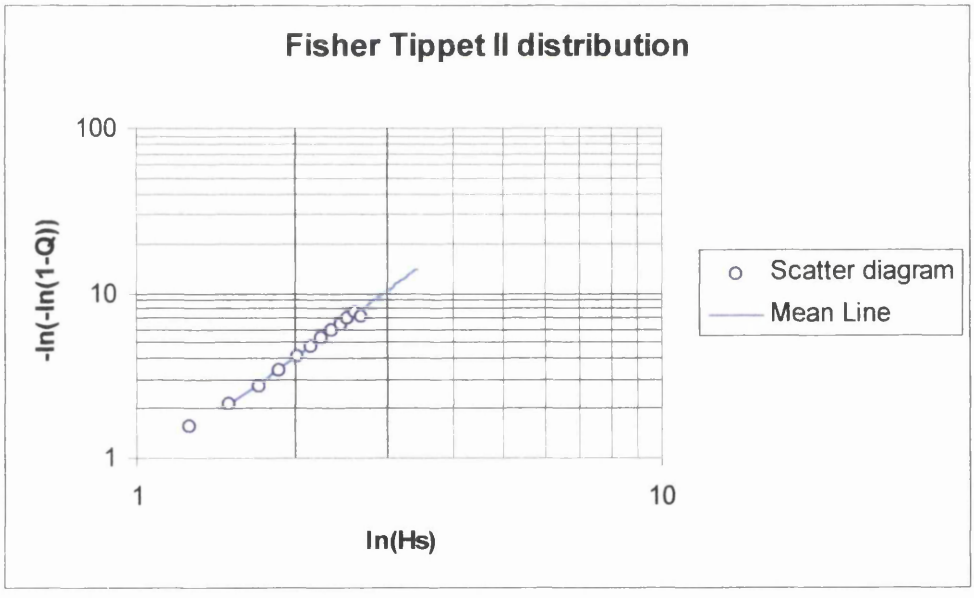

Figure 3.2.6 The Fisher-Tippet II distribution used to predict the probabilities of occurrence of the significant wave heights

Once obtained, the probability of occurrences for the wave heights were introduced to the equation of the long-term joint probability density of wave heights and periods (3.2.8.1)

$$f(h,t) := \frac{1}{2\cdot\pi\cdot\sqrt{1-\rho ht^2}\cdot\sigma h\cdot\sigma t}\cdot e^{\left[-\frac{1}{2\cdot\left(1-\rho ht^2\right)}\cdot\left[\left(\frac{h-\mu h}{\sigma h}\right)^2+\left(\frac{t-\mu t}{\sigma t}\right)^2-2\cdot\rho ht\cdot\left(\frac{h-\mu h}{\sigma h}\right)\cdot\left(\frac{t-\mu t}{\sigma t}\right)\right]\right]\cdot\left[1-\frac{Cs}{6}\cdot\left[3\cdot\left(\frac{h-\mu h}{\sigma h}\right)-\left(\frac{h-\mu h}{\sigma h}\right)^3\right]\right]}$$

3.2.8.1

Where:

$\sigma t := 0.244 - 0.0225\mu H$

$\mu T := 3.925 + 1.439\mu H$

$\mu t := \ln(\mu T) - \frac{\sigma t^2}{2}$

$\rho ht := 0.415 + 0.049\mu H$

The formulas listed above are regression formulas except the third one.

And

h = lnHs: Hs denotes significant wave height

t = lnT : T denotes mean zero crossing period

μt and μh are mean values of t and h in one data set

σt and σh are standard deviations of h and t in one data set

ρht is correlation coefficients of h and t

Cs is skewness parameter

$$Cs := \frac{\sum_{i=1}^{n}\left(h_{i,j}-\mu h\right)^3\cdot V_{i,j}}{\sigma h^3}$$

3.2.8.2

f(h,t) denotes the probability of occurrence of the specific combination of h and t

The expanded sea-state scatter diagram was subsequently used to calculate the most probable extreme vertical bending moment in twenty years and in one hundred years. The

contours of the initial scatter diagram and the numerical representations of the two scatter diagrams can be found in Appendix 5.

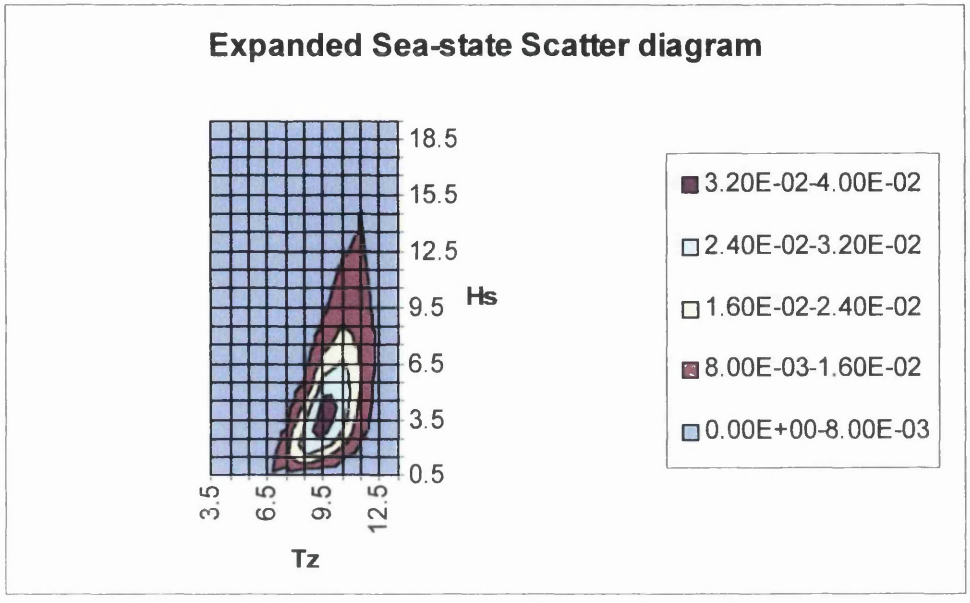

Figure 3.2.7 Expanded Scatter Diagram

3.2.9 Wave and Directional Spectrum

The wave spectrum defines the distribution of energy among the different hypothetical regular wave components having various frequencies. The wave spectrum chosen for this study is the I.S.S.C. (Special case to Pierson-Moskowitz) wave spectrum, which permits wave period and significant wave height to be assigned separately. It has the form:

$$S(\omega) = \frac{0.11 \cdot Hs^2}{\omega_1} \cdot \left(\frac{\omega}{\omega_1}\right)^{-5} \cdot e^{\left\{-0.44\left(\frac{\omega}{\omega_1}\right)^{-4}\right\}} \qquad 3.2.9.1$$

Where:

$$\omega_1 = \frac{2 \cdot \pi}{Ta} \qquad 3.2.9.2$$

ω: Wave frequency

H_s: Significant wave height

T_a: Average wave period

The sea surface is composed of waves travelling in different directions with different wave heights and periods, so a directional spreading function should be introduced to include the wave energy with respect to direction. Some directional spectrums have been formulated with the main difference being their mathematical complexity (e.g. Mitsuyasu/Goda [13]). Pierson and St. Dennis [7] introduced the directional spreading function adopted.

The formulae is:

$$G(\theta) = \frac{2}{\pi} \cdot \cos^2 \theta \qquad \text{when } |\theta| \leq \frac{\pi}{2}$$

$$G(\theta) = 0 \qquad \text{when } |\theta| \geq \frac{\pi}{2} \qquad 3.2.9.3$$

So the wave and directional spectrum is:

$$S(\omega,\theta)=G(\theta)*S(\omega) \qquad 3.2.9.4$$

3.2.10 Transfer function and Response spectrum

The transfer functions are the responses of the structure to a unit wave height for every frequency. They were calculated using the computer package Hydro of Kokcums, which is based on the strip theory developed by Vugts [14]. The main simplification of the strip theory is that the vessel is divided into 'strips' and, subsequently, the various forces are calculated in two dimensions. The shear forces, bending moments and torsion are calculated by integration of the relevant forces acting on the various 'strips' [15]. In many cases strip theory has been strongly supported by experiments. However it is essential to note the limitations [16]:

- Strip theory is a high-frequency theory (it is more applicable to head and bow sea waves than to quartering and following seas for a ship with forward speed.)
- The theory does not properly account for the interaction between the steady wave system and the oscillatory effects of ship motions. This particularly applies when the froude number exceeds or is equal to 0.4. The froude number of the vessel studied is 0.17.
- The effects of slamming and green water are not taken into consideration.

- Strip theory has shown questionable results when the length to beam ratio is low. However, the vessel considered is a Panamax bulk-carrier with a relatively high length to beam ratio.

The calculation of the response spectrum simply involves the multiplication of the squared transfer function by the wave and directional spectrum.

$$\text{Response Spectrum} = \text{Wave} + \text{Directional Spectrum} \cdot \text{Transfer Function}^2$$

This equation is valid only if we assume that the response of the structure is linear with respect to wave height at a specific frequency and that the response at a specific frequency is independent of the response at other frequencies. Conventional linear theory is computationally efficient and produces reasonably good and widely accepted results regarding ship motions and wave frequency loads. However when non-linear effects appear, the linear frequency domain analysis is no longer as accurate as the 3D-time domain analysis. Shin, Chung, Lin, Zhang and Engle [17] discuss the linear and the non-linear methods of analysis for a fine form container ship. They mention that the non-linear effects except of bow flare and bottom slamming include the vertical bending moment, roll motion, the associated loads to the roll motion and wave pressure near the waterline. However they state that the non-linear method should not replace the linear method due to its complexity and time required but should rather complement when more accuracy is required. Stiansen, Jan and Liu [18] performing a structural analysis on a container ship show that the relation of wave induced moments with the wave height is almost linear near the midship section but at stations remote from the midship section non linear effects are more dominant. The project considers the wave bending moments only at the midship section, which as stated above their relationship with the wave height should be almost linear. However if non-linear effects have to be considered and a 3D non-linear approach is unavailable, Mansour and Wasson [19] present charts that can be used in conjunction with linear strip theory so that non-linear sagging and hogging moments can be estimated.

3.2.11 Statistics and extreme vertical bending moment prediction

Assuming that the frequencies are independent of each other and the response is narrow banded, the short-term probability distribution will be Rayleigh. Dalzell, Maniar and Hsu [20] found that for an ocean-going dry Bulk Carrier: 'The assumption that the short-term wave-induced moment fits the Rayleigh distribution would be reasonable if not always true'. The short-term narrow-banded cumulative Rayleigh distribution associates the probability of exceeding a certain amplitude x with the variance in the following way:

$$P(x_1 > x) = e^{-\frac{x^2}{2 \cdot m_o}} \qquad 3.2.11.1$$

Where:

$P(x_1>x)$ is the probability of exceedance of the value x by the value x_1

m_o is the variance (volume under the response spectrum)

x_1 is any amplitude chosen randomly

The long-term formulation is based on combining the short-term formulation with a number of parameters, which describe the various situations that the vessel may encounter. These are:

- Significant wave height of the sea
- Mean zero-crossing period of the sea
- Spreading of the waves
- Heading of the ship
- Loading condition
- Speed

The loading condition and the speed are defined as input to the strip theory calculations, so the transfer functions are based upon them, assuming an equal probability for each heading incorporates the ship's heading. This assumption is conservative since the crew of the vessel will try to avoid headings known to induce severe loads upon the ship's structure (e.g. following seas). Assuming the spreading function mentioned previously incorporates the spreading of the seas. Weighting by the probability of

occurrence of each combination includes the significant wave height and mean zero crossing period.

The long-term cumulative distribution is, therefore in mathematical terms:

$$Q(x_1 > x) = \sum_{H_s}\sum_{T_z} e^{-\frac{x^2}{2 \cdot m_o}} \cdot p(H_s, T_z, h) \qquad 3.2.11.2$$

Where:

$Q(x_1>x)$ is the probability of exceeding the value x by the value x_1.

m_o is the variance (volume under the response spectrum).

x_1 is any amplitude chosen randomly.

H_s is significant wave height.

T_z is mean zero crossing period.

h denotes heading.

$P(H_s, T_z, h)$ is the probability of occurrence of the combined H_s, T_z and heading.

The formulation of the long term distribution assumes that the same number of cycles of load are induced by each situation. Ochi [21] has shown that for each situation a different number of cycles of load will occur. In order to incorporate this effect we need to calculate the total number of cycles and then include a factor that is the number of cycles of the situation divided by the total number of cycles. This will, in effect, produce a weighted sum with respect to the number of cycles. Zumbaly and Lewis [6] carried out calculations for a SL-7 container ship both with and without taking into consideration the effect, and found 0.4% of a difference. Therefore, the effect was not considered in the calculations.

A weighted sum of probabilities of exceeding a range of values was calculated, and the same procedure that was used to extrapolate the significant wave heights was used to estimate the vertical bending moment with a probability of occurrence of 10^{-8} (approximately 20 years) and 10^{-9} (approximately 100 years). Fortran was used to perform the calculations and in appendix 7 the flow chart of the program is shown.

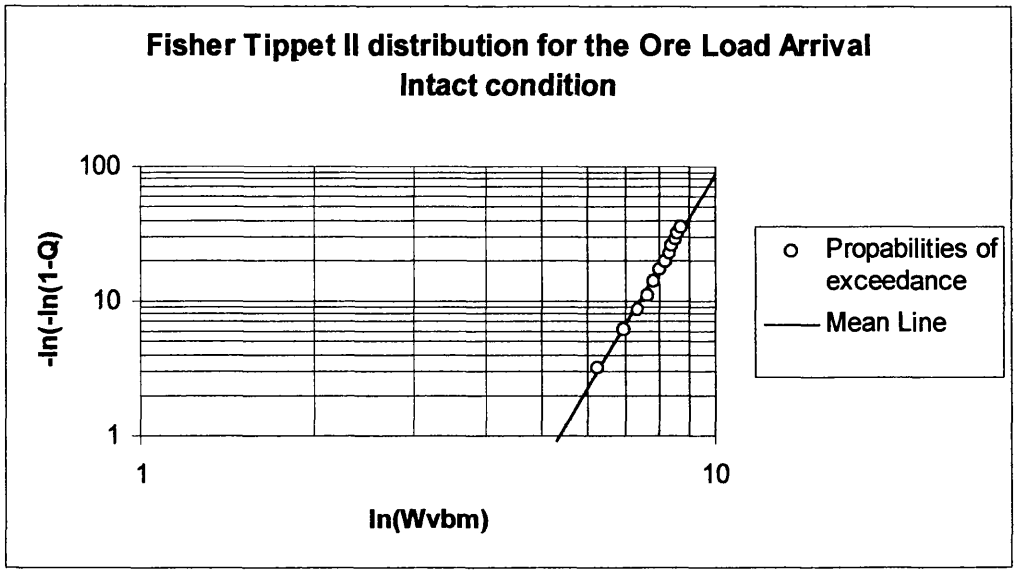

Figure 3.2.8 The Fisher-Tippet distribution for the midship section at the Ore Load Arrival Condition (intact)

The results are:

Condition	Wave Scatter	V.B.M.	Q_e
Intact	Initial	3346210 (kN-m)	10^{-8}
Intact	Initial	3808940 (kN-m)	10^{-9}
Intact	Expanded	6139050 (kN-m)	10^{-8}
Intact	Expanded	6820320 (kN-m)	10^{-9}
Damaged	Initial	2865870 (kN-m)	10^{-8}
Damaged	Initial	3264350 (kN-m)	10^{-9}
Damaged	Expanded	4920040 (kN-m)	10^{-8}
Damaged	Expanded	5443620 (kN-m)	10^{-9}

Table 3.2-3 Predicted wave vertical bending moments with their probability of occurrence, damaged or intact load-case and scatter diagram used.

3.2.12 Rule based wave induced bending moments

The rule wave induced vertical bending moment amidships expressed in kN-m, are given from the following expressions:

$M_{ws} = -k_1 C_1 L^2 B(C_b+0.7)10^{-3}$ maximum allowable sagging moment 3.2.12.1

$M_{wh} = -k_2 C_1 L^2 B C_b 10^{-3}$ maximum allowable hogging moment 3.2.12.2

Where:

k_1 = 110
k_2 = 190
C_1 = $10.75-[(300-L)/100]^{1.5}$ for 150<L<300m
L = 215 m (Lpp)
B = 32.2 m (max. breadth)
C_b = 0.829 (summer loadline)

Therefore: M_{ws} = -2490008 kN-m maximum allowable sagging moment

M_{wh} = 2328023 kN-m maximum allowable hogging moment

3.2.13 Discussion

The wave induced bending vertical bending moments with probabilities exceeding 10^{-8} and 10^{-9}, which are equivalent to twenty and hundred years respectively, have been calculated. Two conditions were studied. The first one was ore load arrival condition and the second was the equivalent when hold #1 is damaged. The results show that the intact condition values are larger, so they will be used for our comparison with the ultimate bending moment capacity of the midship section. The expansion of the scatter diagram although mathematically successful, provided results that could be considered very conservative, even unrealistic, for a Bulk Carrier. The results of the calculation where the expanded scatter was used will be discarded for the rest of the project. They show us a tendency that should be studied very seriously since the climate changes are an unavoidable reality in today's world.

The superimposition of the wave induced vertical bending moment and still-water loading is shown on the table below.

Probability of occurrence	Still water vertical bending moment	Wave induced vertical bending moment	Total vertical bending moment
10^{-8}	1277065 (kN-m)	3346210 (kN-m)	4623275 (kN-m)
10^{-9}	1277065 (kN-m)	3808940 (kN-m)	5086005 (kN-m)

Table 3.2-4 Combination of wave and still water vertical bending moments.

3.3 Fluctuating Wave Loading

All loads that vary with respect to magnitude and/or direction cause stress variations in the structure, which leads to fatigue damage. The most important varying loads in a ship's structure are those induced by waves. Globally, the ship, acting like a beam, suffers from horizontal and vertical bending, horizontal and vertical shear forces and torsion. Locally, the pressure fluctuations cause some damage mainly to the side shell and bottom structure.

There are three main ways of considering these loads and, subsequently, the fatigue damage they cause [22]:

- The deterministic method where selected load cases are studied. The stress range is determined by the load cases assuming that they will cause the maximum and minimum stresses.
- The spectral method where the sea is regarded as superimposition of waves and the response is considered linearly dependent to the wave height. The stress occurring during the entire operational lifetime can be obtained from an assessment of all sea-states in the principal regions, where their frequency of occurrence is described by long-term statistics, and from the assumed ship course, speeds and loading conditions.
- The time domain method is particularly realistic. The random loads are calculated using wave spectra and the resulting stresses are analysed over a representative period of time. The draw back is the computational effort needed.

3.3.1 Hull structure global loading

The spectral method was selected for the calculations of fatigue loading. The theory used to predict the heave, pitch, sway, roll and yaw motions as well as the wave induced vertical and horizontal forces, bending moments, and torsional moments is strip theory and the computer package used is Hydro by Kokcums. The output of the program includes the motions and the loads for a section but not the pressure loading which is dealt in the next section. The results for loads and motions were produced with respect to non-dimensionalised amplitude and phase and with respect to loads can be seen in

appendix 6.

3.3.2 Hull structure local loading

Global loads mainly influence the structure of small vessels. The structures of larger vessels need to be strengthened with respect both to local and global loads. The side shell structure, by way of the neutral axis, is greatly affected by local loads. A transverse structural component is designed to sustain local transverse loads. The double bottom, especially in the fore of any large ship, is affected by inertial cargo loading, particularly if the cargo transported is of a high-density ($\cong 3$ t/m^3). In the following two sections the procedure used for the calculation of the local loads will be discussed.

3.3.3 External shell structure hydrodynamic pressure due to waves

Low-frequency dynamic wave induced pressures on the ship hull are usually calculated using strip theory or diffraction theory with some corrections made at the waterline level to account for the non-linearities [13]. Unfortunately, the Hydro computer package does not include water-pressure calculations and no other programs were available to perform these type of calculations, so a methodology was adopted [13] to calculate the water-pressure stresses' transfer function.

In still water the pressure increases hydro-statically following the formula $p = -\rho g z$ were z is zero at the waterline and positive above the waterline. The introduction of waves alters the pressure distribution, since at the wave crest we have an increase of pressure but at the wave trough either a decrease or better suction will occur.

Linear wave theory was selected to model the pressure distribution, mainly because of its simplicity and applicability. Linear wave theory is a regular wave theory simulating waves of the same form without changing the shape. The main disadvantage of the linear wave theory is that the procedure used to establish a mathematical relation between the potential function and the wave period, height and length assumes that the wave heights are small. This assumption restricts the theory to only those waves, which have small wave height. This restriction can be avoided by assuming that the highest region in the pressure distribution is simulated by hydrostatic pressure.

The effect of the pressure fluctuations are of interest, so the procedure used to calculate them was that of superimposing the pressure distribution when the wave reached the maximum and minimum height. The subtraction of the two pressure distribution profiles gave us the pressure fluctuation. The pressure profiles and their equations are outlined in the figures below.

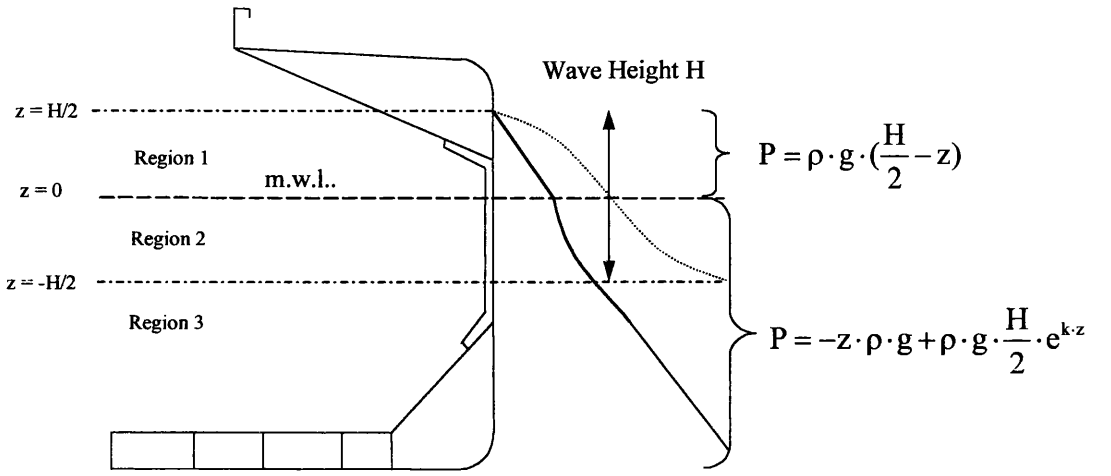

Figure 3.3.1 Pressure distribution when the wave reaches the maximum height

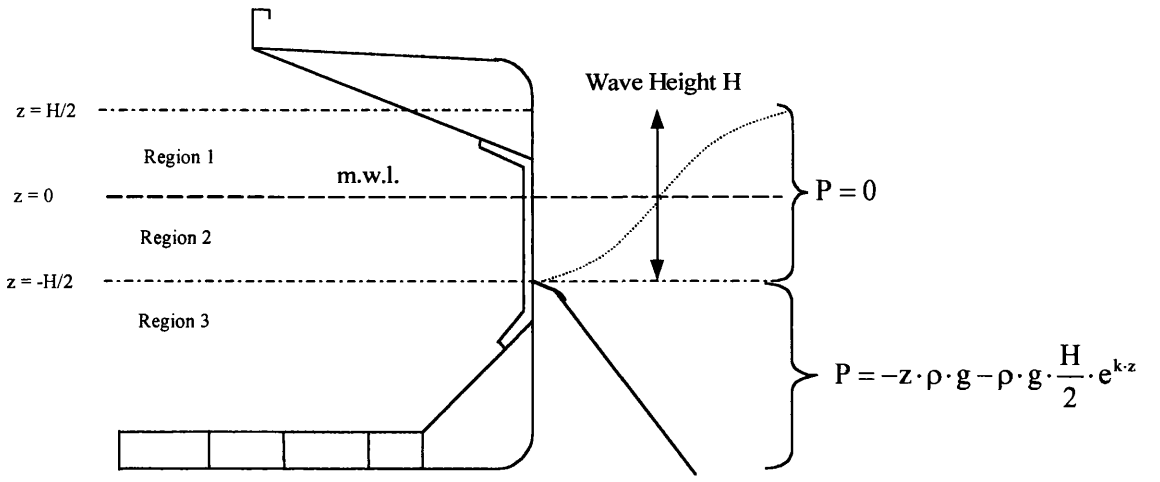

Figure 3.3.2- The pressure distribution when the wave trough occurs.

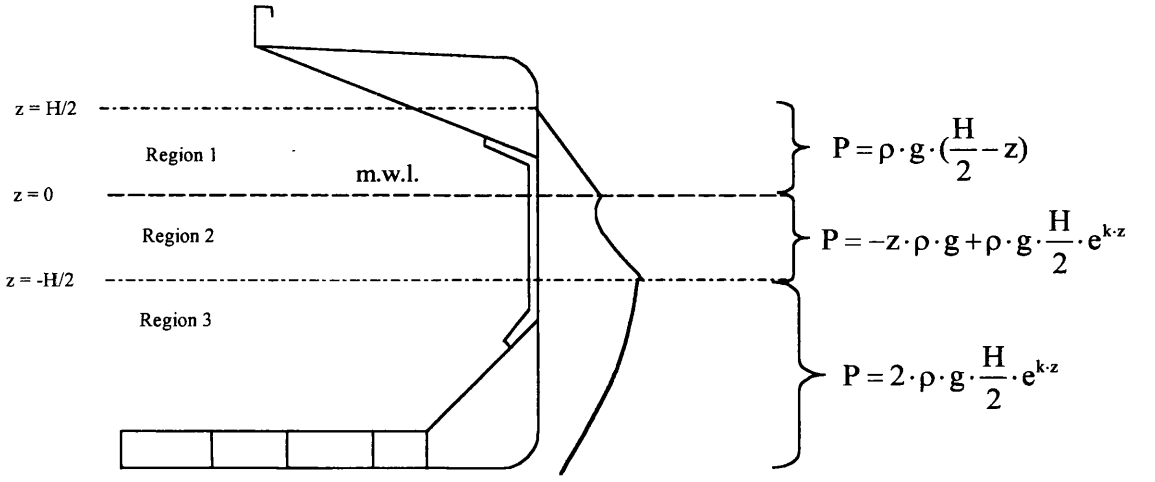

Figure 3.3.3- Pressure fluctuation in a wave.

The model of pressure fluctuations does not include the alterations in the pressure profile caused by the existence of the hull. The hull will diffract small waves changing their wave height (essentially making it double). Medium-height waves will diffract but some portion of the energy will pass under the hull. Large waves will not be affected by the presence of the hull. This effect, although complex, could be modelled by multiplying the pressure-fluctuation model by function depending on wave length and the breadth of the vessel (equation 3.3.3.3). The phenomenon should be also a function of ship's draught, ship's speed and water depth. The equation modelling the phenomenon is purely speculative and the intention of its existence is to provide a physical insight into the problem. Liapis and Faltinsen [23] studied the diffraction problem of a fixed slender ship in incident regular deep-sea waves coming from two directions. They used a 3D theory, which involved the solution of the Helmoholtz equation problem for cross sections along the ship. The results were compared with experiments and were found satisfactory. The same results were studied in order not to prove the accuracy of equation 3.3.3.3 but its physical insight. The comparison can be found in the first section of Appendix 8 where the graphical representation exhibits the physical insight of the equation. The waves come not only from zero or ninety degrees but also from all possible angles. The effect could be simulated by introducing a function with respect to the relative angle between the direction of the wave and the ship (equation 3.3.3.4). Again as for the equation 3.3.3.3 the aim of presenting the equation is to provide a physical insight into the phenomenon described. In the second section of Appendix 8 a comparison is made using

the results presented in a paper by Liapis and Faltinsen [23]. As for equation 3.3.3.3 its physical insight is clearly shown. Last but not least, the motions of the hull are incorporated into the model so that the position at which the pressure fluctuation is calculated is 'monitored'. The motion is included in the model by the assumption of a pseudo wave height and a pseudo distance from the mean waterline using the equations listed below.

$$H_p = 2 \cdot \left[\left(\frac{H}{2} - heave_{amplitude} \cdot \cos(heave_{phase}) \right)^2 + (heave_{amplitude} \cdot \sin(heave_{phase}))^2 \right]^{0.5} \quad 3.3.3.1$$

The equations listed below form the pressure fluctuation model.

$$P_i = f_d \cdot f_h \cdot P_{(R+M)i} \quad 3.3.3.2$$

$$f_d = 1 + e^{-\frac{L}{B}} \quad 3.3.3.3$$

$$f_h = \frac{1 + \sin\theta}{2} \quad 3.3.3.4$$

$$P_{(R+M)i} = \begin{cases} \rho \cdot g \cdot \left(\frac{H_p}{2} - z_p \right) .....if...z > 0 \\ -z_p \cdot \rho \cdot g + \rho \cdot g \cdot \frac{H_p}{2} \cdot e^{k \cdot z} ...if...0 \geq z \geq -\frac{H_p}{2} \\ 2 \cdot \rho \cdot g \cdot \frac{H_p}{2} \cdot e^{k \cdot z} .....if...z < -\frac{H_p}{2} \end{cases} \quad 3.3.3.5$$

Where:

P_i: The pressure fluctuation at point I

f_d: A function of ship breadth and wave characteristics to include the diffraction of waves

H: Wave height

L: Wave length

B: Breadth of the ship taken into consideration

f_h : A function of ship heading

θ : Heading of the vessel with respect to the waves

$P_{(R+M)i}$ Pressure fluctuation at point i including the effect that point I will move according the vessel's motion

This project considers a model simulated by equation (3.3.3.5).

The wave pressure fluctuation near the waterline presented above is considered to be a simple but realistic approach and its accuracy is subject to the assumptions and simplifications discussed. Experiments or a 3D non-linear method are required in order to numerically prove or disprove the accuracy of the assumed water pressure fluctuation. Unfortunately time and materialistic constraints did not allow the research in such a direction

3.3.4 Cargo inertial loads on ship's structure

Due to the motion vessels suffer from accelerations which not only influence the crew/passengers and the performance of the ship's systems but also the structure may suffer from high internal and external, fluctuating and extreme loading especially at the bow area were the most severe accelerations occur.

The accelerations were computed using the results of the motion amplitudes and phases leading to the distributed loading on the structure.

$$\gamma_v = -\omega_e^2 \cdot (\text{heave}_{\text{amplitude}} \cdot e^{i \cdot \text{heave}_{\text{phase}}} - 1 \cdot \text{pitch}_{\text{amplitude}} \cdot e^{i \cdot \text{pitch}_{\text{phase}}}) \qquad 3.3.4.1$$

$$\gamma_h = -\omega_e^2 \cdot (\text{sway}_{\text{amplitude}} \cdot e^{i \cdot \text{sway}_{\text{phase}}} - 1 \cdot \text{roll}_{\text{amplitude}} \cdot e^{i \cdot \text{roll}_{\text{phase}}}) \qquad 3.3.4.2$$

Where:

ω_e : Frequency of encounter

l : Distance from centre of motion which for simplicity was assumed to be the midship section. In reality it depends on the fore and aft underwater shape and lies near the midship section.

γ_v : Vertical acceleration

γ_h : Horizontal acceleration

3.3.5 Discussion

In the previous sections a methodology was described for the calculation of both local and global fluctuating loading. The methodology adopted for the pressure fluctuations can be enhanced in three areas. The first is the adoption of higher order wave theory, which will result in a more realistic pressure profile. The second is the incorporation of the difference that occurs between the situation where the vessel heaves with respect to waves and the situation which; the waves rise with respect to the vessel. The third is the incorporation of the two effects discussed in section 3.3.3 (equations 3.3.3.3 and 3.3.3.4). The two effects should be studied more thoroughly so that their mathematical formulation is more accurate.

The next chapter discusses the response of the structural components using first principals so that we can asses the extreme and fluctuating loading discussed in this chapter.

References

1. Trim and Stability booklet of M/V *Victor*

2. "Guide for Dynamic Based Design and Evaluation of Bulk Carrier Structures", ABS, March 1995

3. Hughes, O., "Ship structural design: a rationally based, computer-aided, optimization approach.", John Willey & Sons, New York, 1983

4. Salvensen, N., Tuck, E.O., Faltinsen, O, "Ship Motions and Sea Loads", SNAME, Annual Meeting, Nov. 12-13, 1970

5. St. Denis M., Pierson W.J., "On the motion of Ships in Confused Seas", Trans. SNAME, vol. 61, 1953

6. Lewis, E.V., Zubaly, R. B., "Predicting Hull Bending Moments for Design", SNAME, Extreme Loads Response Symposium, 1981, paper D

7. Guedes Soares C, "Probabilistic Methods for Structural Design", Comett, 1993, Lisbon, Instituto Superior Tecnico.

8. Ochi, M.K., "Wave Statistics for the Design of Ships and Ocean structures", Trans. SNAME, 1978

9. Mansour, A., Faulkner, "On Applying the Statistical Approach to Extreme Sea Loads and Ship Hull Strength", Trans. RINA, 1972

10. Hobgen, H. and Lumb, "Ocean Wave Statistics", National Physics Laboratory, H.M. Stationery Office, London, 1967

11. "Storm warning: shipping slow to react", Fairplay, 4th June 1998.

12. Fang, Z. S., Hogben, N., "Long term Statistics of wave heights and periods", The Naval Architect, 1980

13. Barltrop N.D.P., Adams A.J.,(1991), "Dynamics of Fixed Marine Structures", London, Butterworth-Heinemann, 3rd Edition

14. Vugts, J. H., "The hydrodynamic forces and ship motions in oblique waves", Nederlands Ship Research Center, Report 150 S, December 1971

15. Salvensen, N., Tuck, E.O., Faltinsen, O., "Ship Motions and Sea Loads" , SNAME Trans. Vol. 78, 1970

16. Faltinsen O.M., "Sea Loads on Ships and Offshore Structures", Cambridge,

Cambridge University Press, 1990.

17. Yung-Sup Shin, J. S. Chung, W. M. Lin, S. Zhang and A. Engle, "Dynamic loadings for structural analysis of fine form container ship based on a non-linear large amplitude motions and loads method", SNAME, Transactions, Vol. 105, 1997, pp 127-154

18. S. G. Stiansen, H. Y. Jan and D. Liu, "Dynamic Stress Correlation for the SL-7 Containership", SNAME, Transactions, Vol. 87, 1979, pp 64-98

19. A. E. Mansour and J. P. Wasson, Charts for Estimating Non-linear Hogging and Sagging Bending Moments", Journal of Ship Research, SNAME, Vol. 39, 1995, pp 240-249

20. Dalzell, J. F., Maniar N. M., Hsu, M. W.,: "Examination of Service and Stress data of three Ships for Development of Hull Girder Load Criteria", SSC – 287,1979

21. Ochi, M. K., "Wave statistics for the design of ships and ocean structures", Trans. SNAME,1978

22. Fricke W., Petershagen H., Paetzold H., "Fatigue strength of ship structures" , GL- Technology, Hamburg, August, 1997

23. N. Liapis and O. M. Faltinsen, "Diffraction of Waves around a Ship", Journal of Ship Research, SNAME, Vol. 24, No. 3, Sept. 1980, pp 147-155

ppendix 3
ongitudinal strength for ten loading conditions
Heavy Ballast Condition Departure

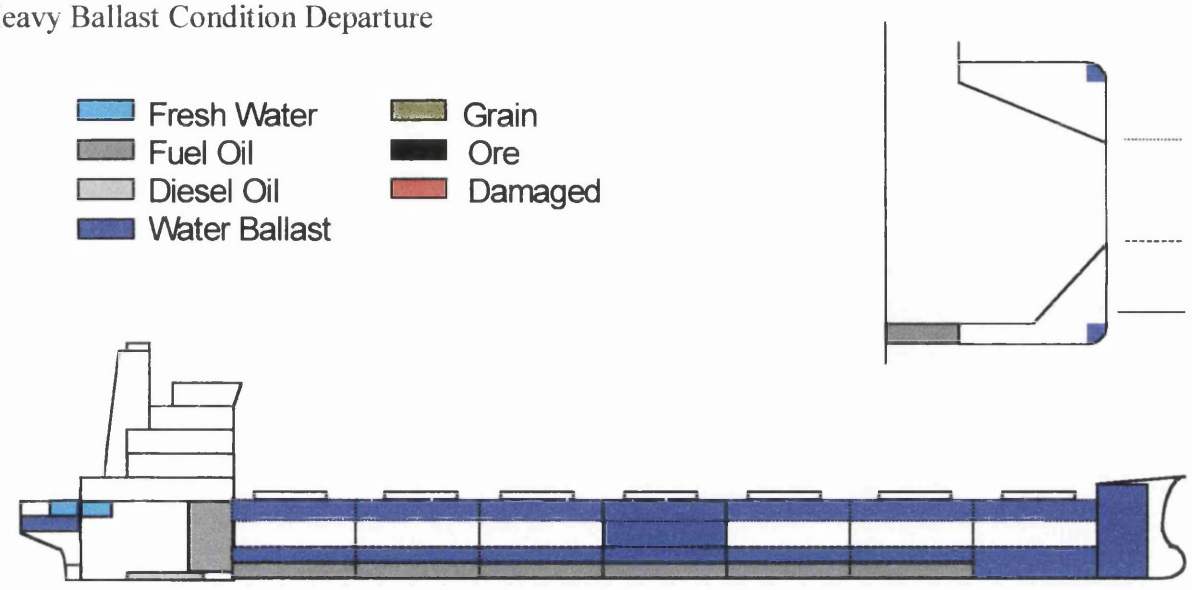

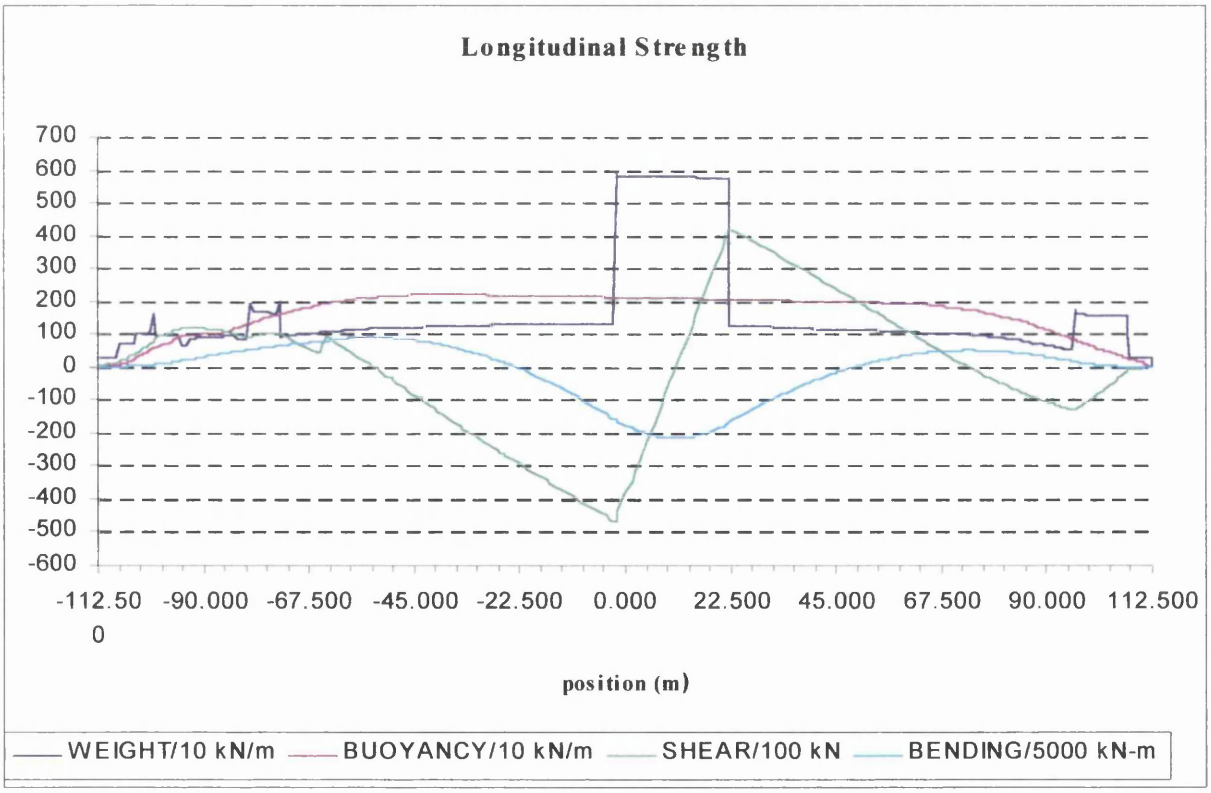

Heavy Ballast Condition Departure Hold 1 damaged

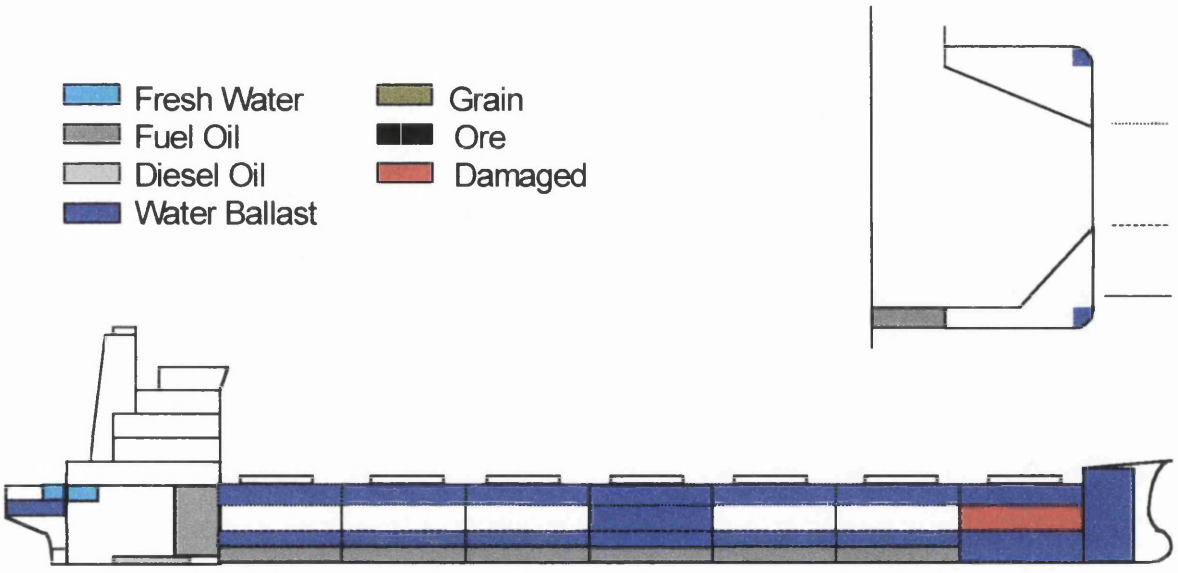

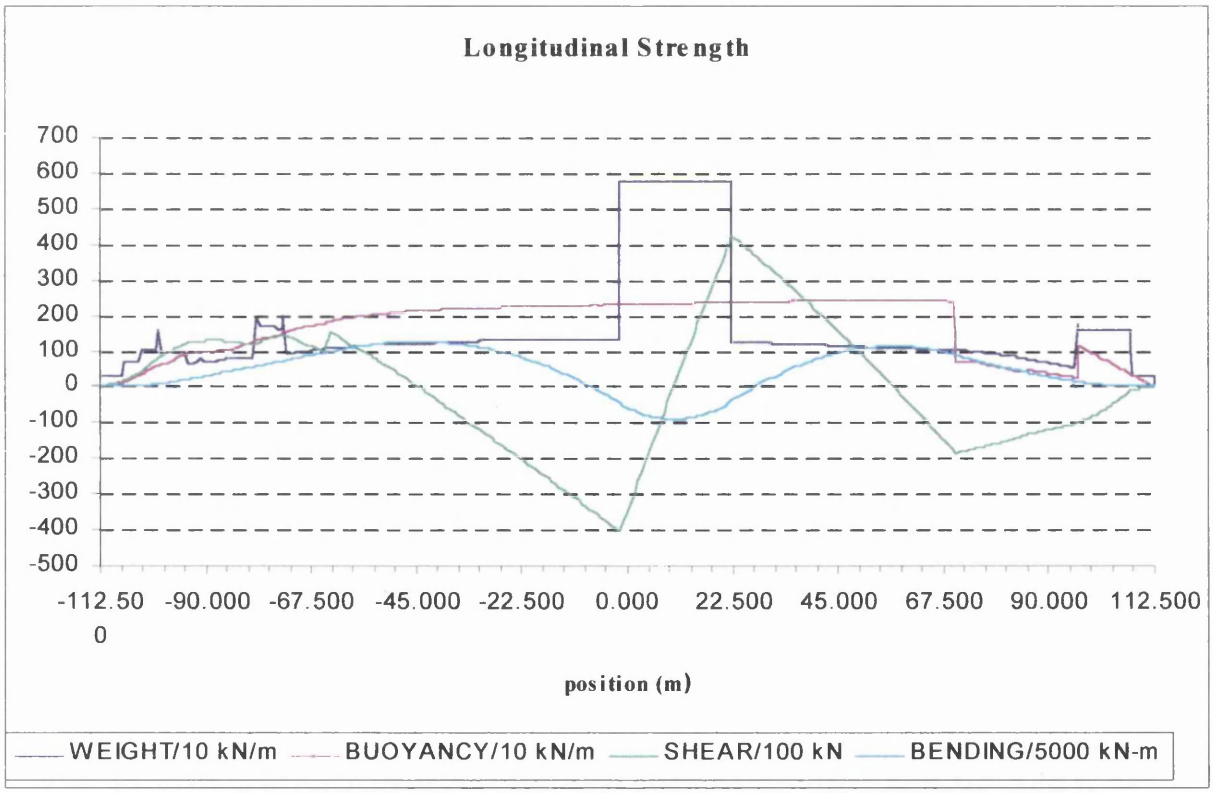

Grain Load Condition Departure

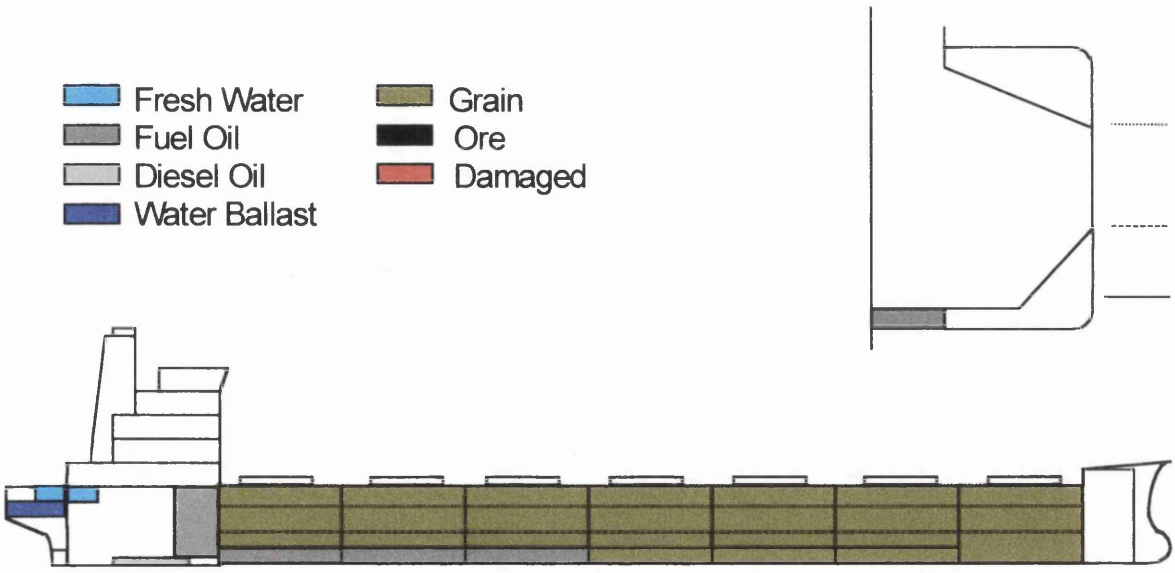

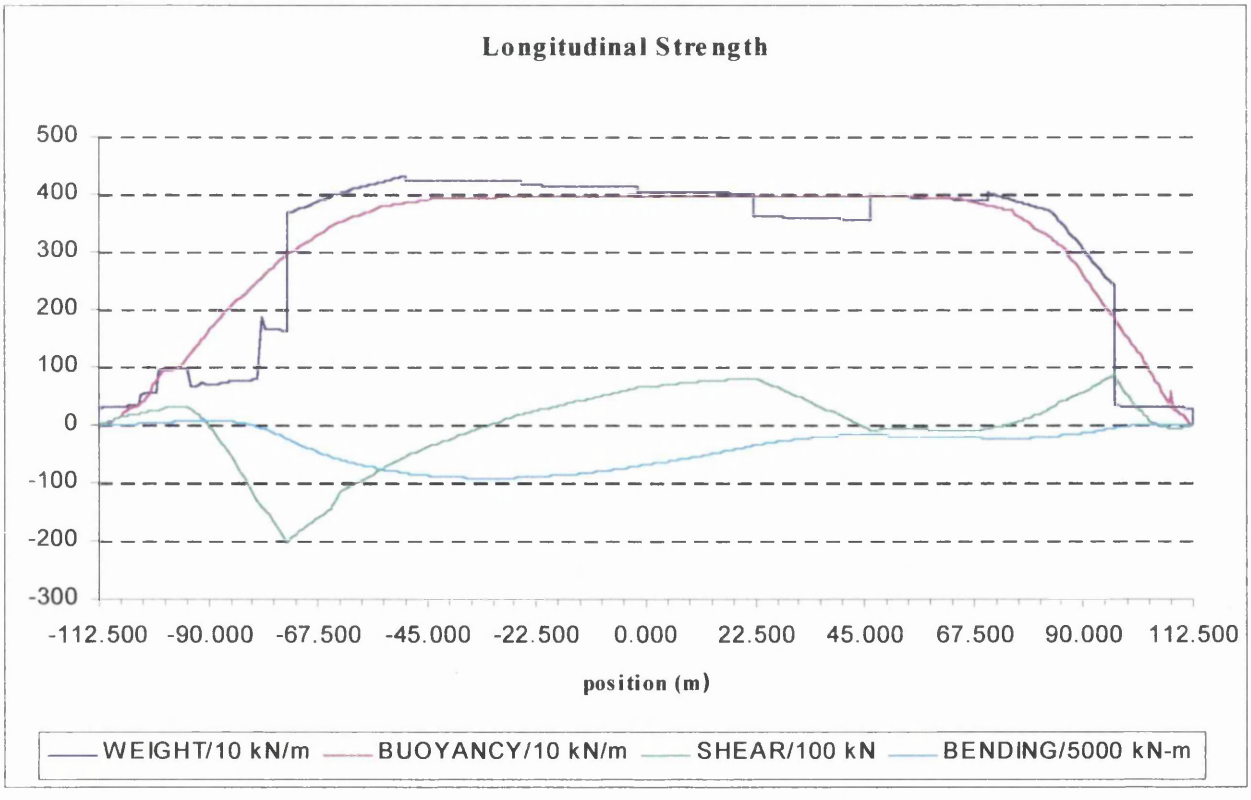

Grain Load Condition Departure Hold 1 damaged

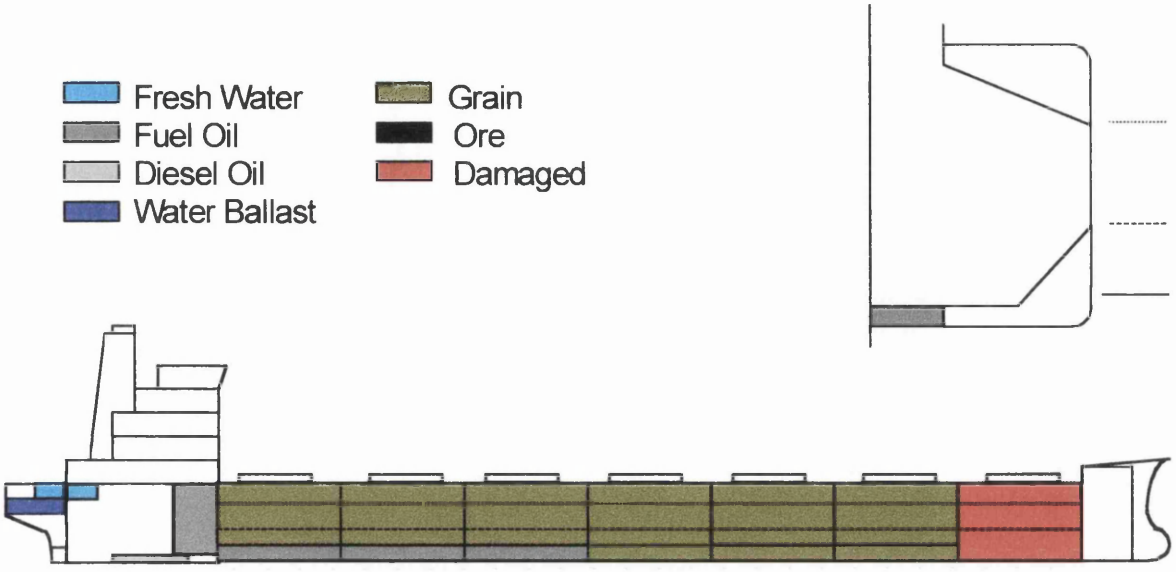

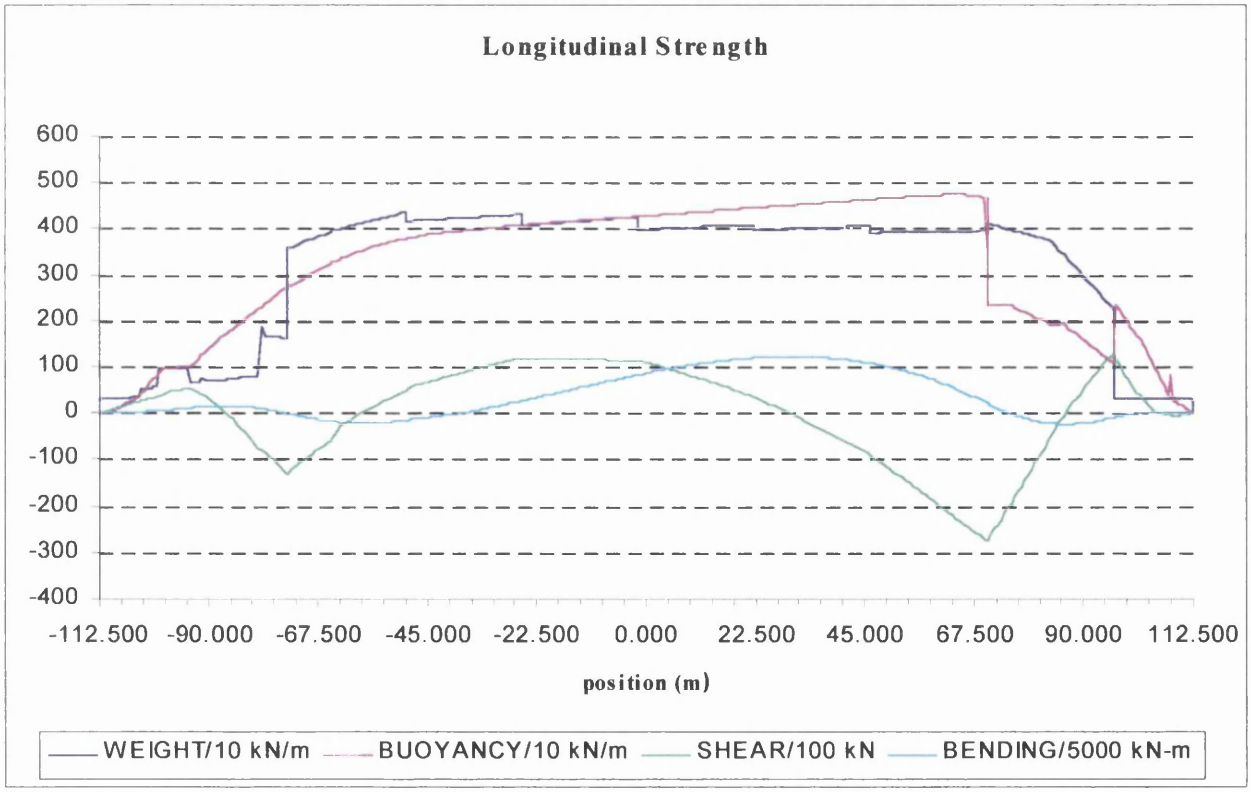

Grain Load Condition Arrival

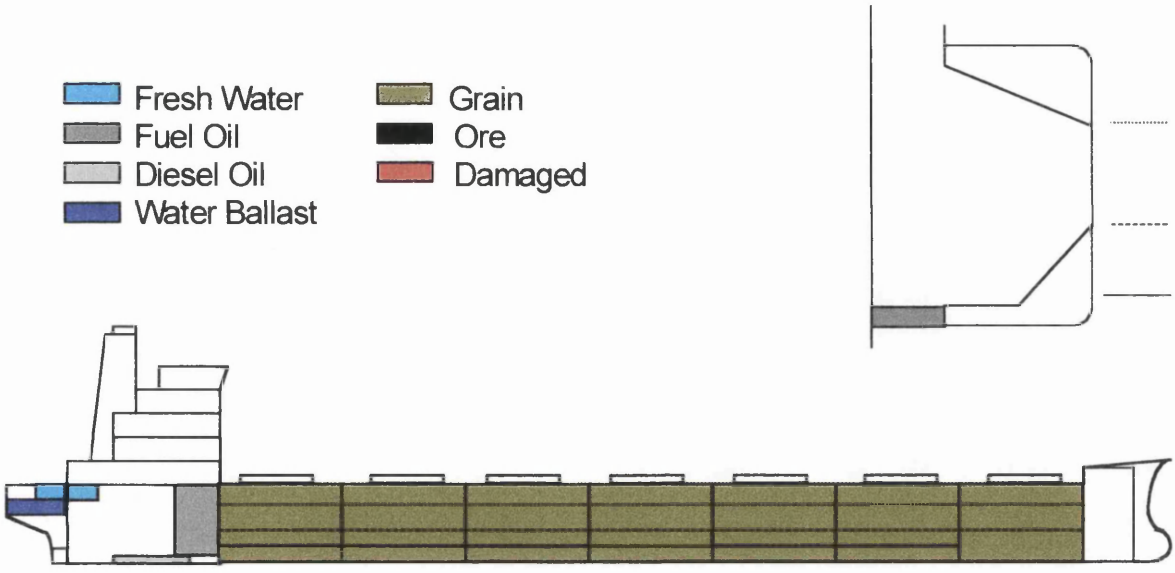

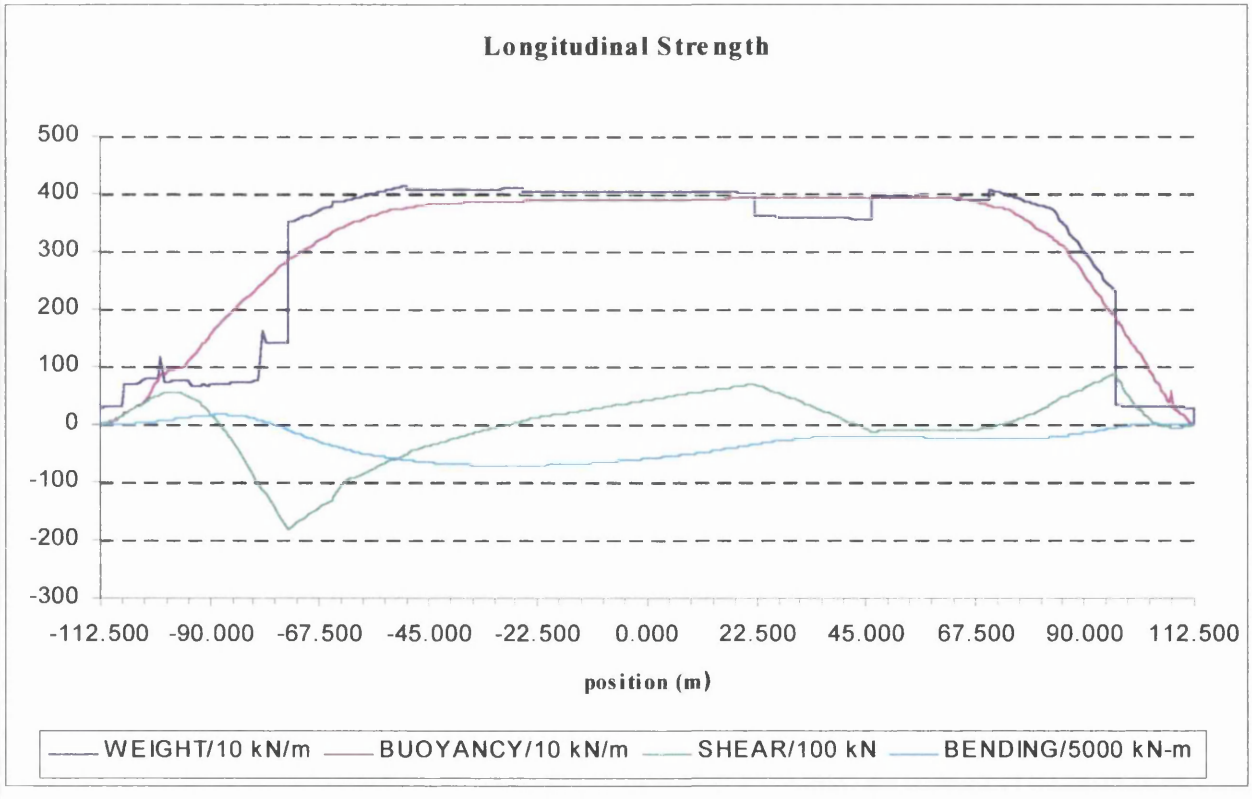

Grain Load Condition Arrival Hold 1 damaged

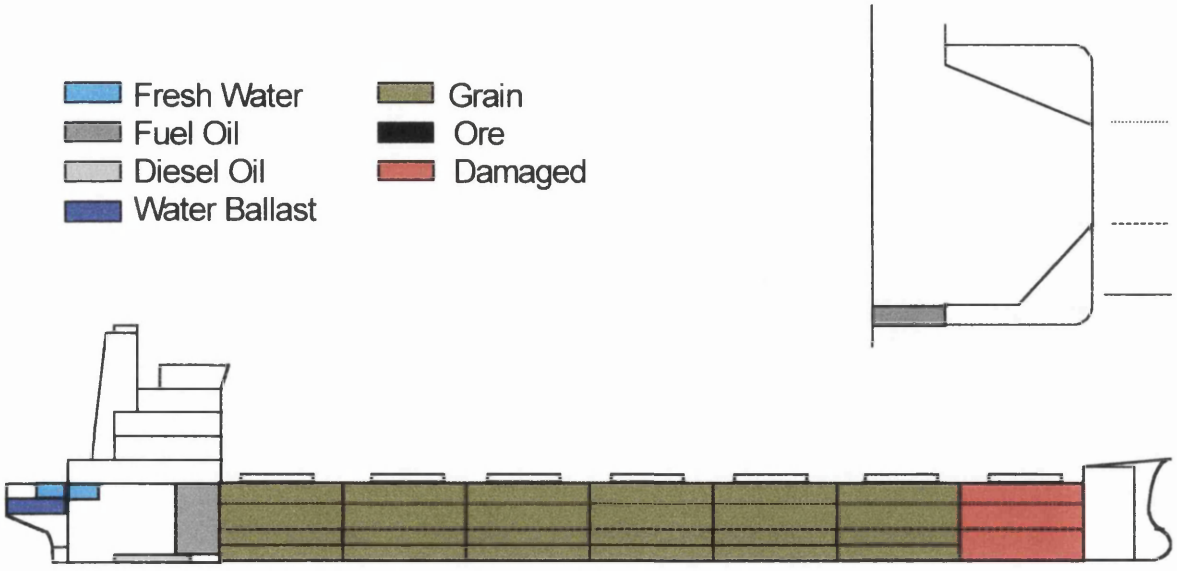

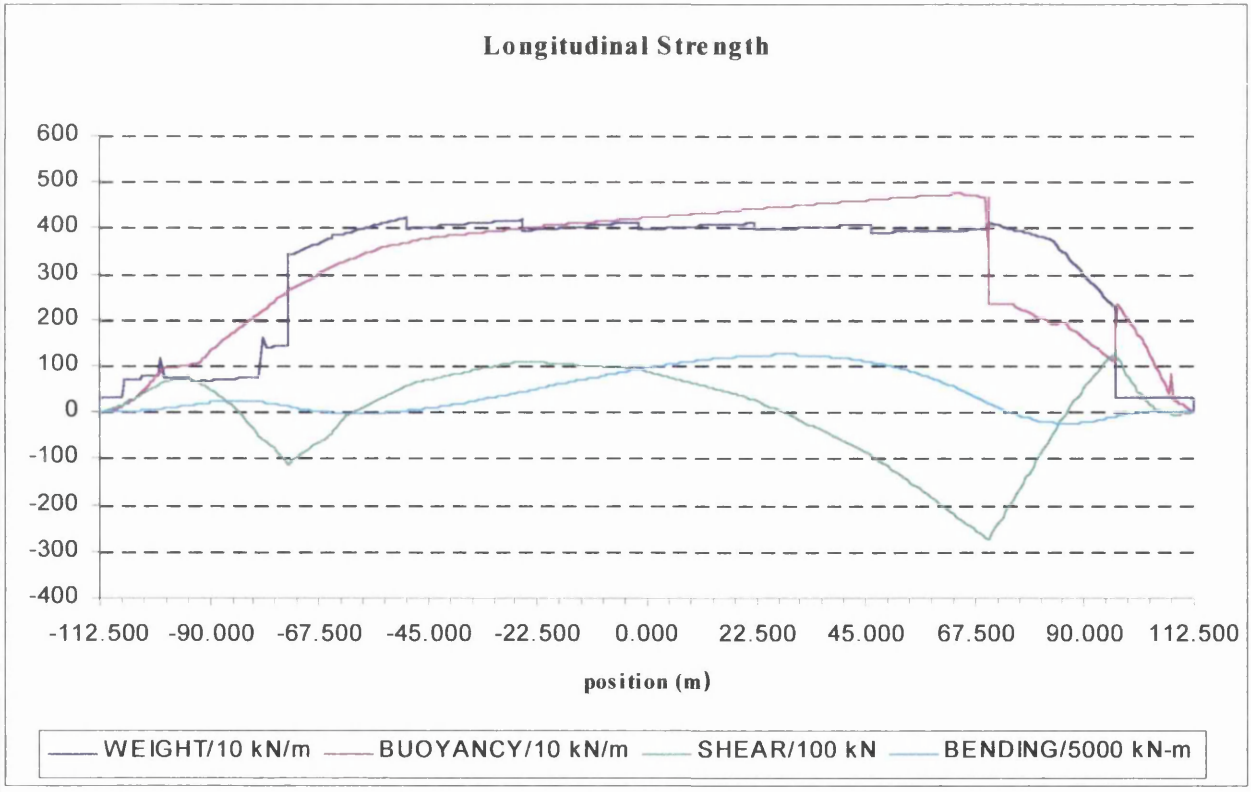

. Ore Load Condition Departure

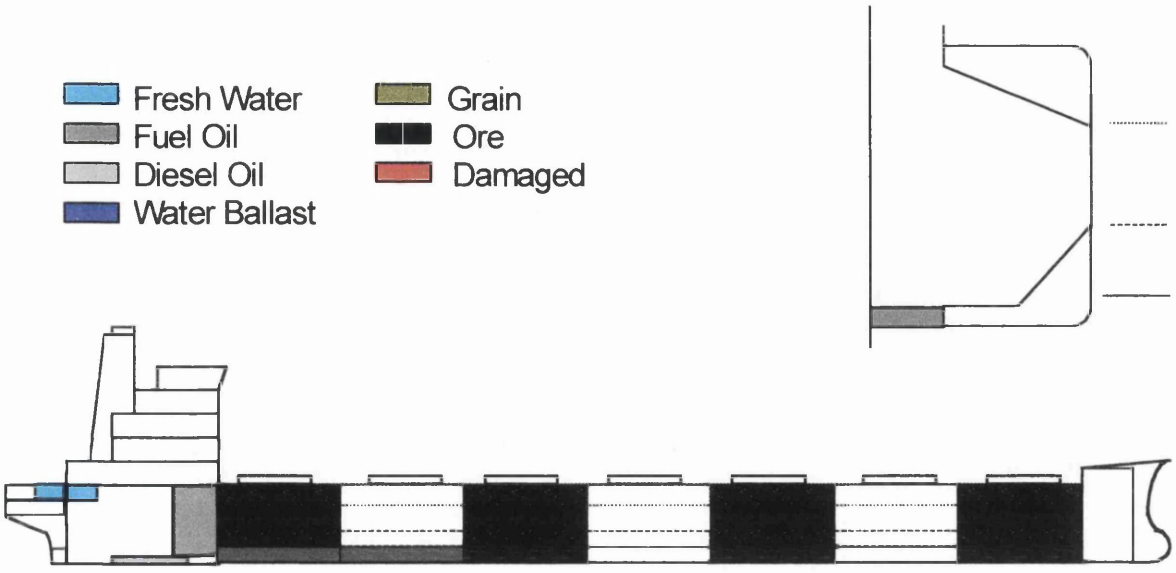

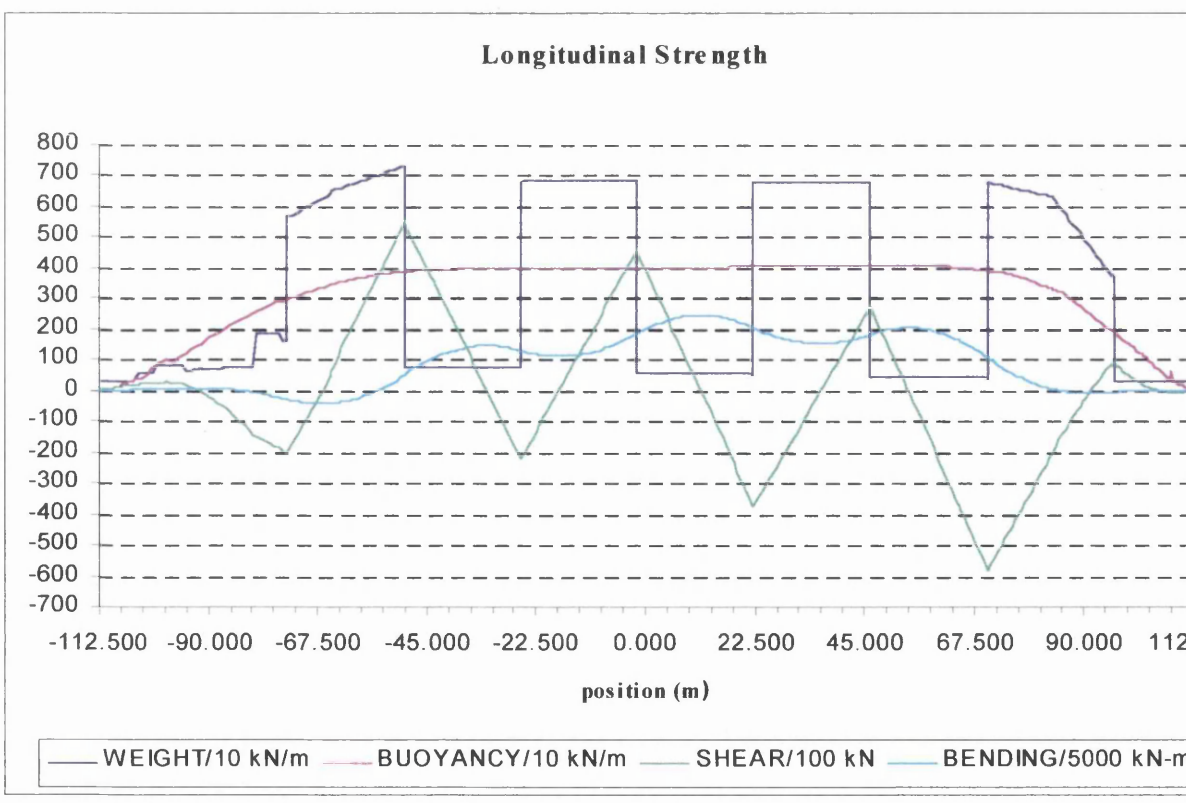

. Ore Load Condition Departure Hold 1 damaged

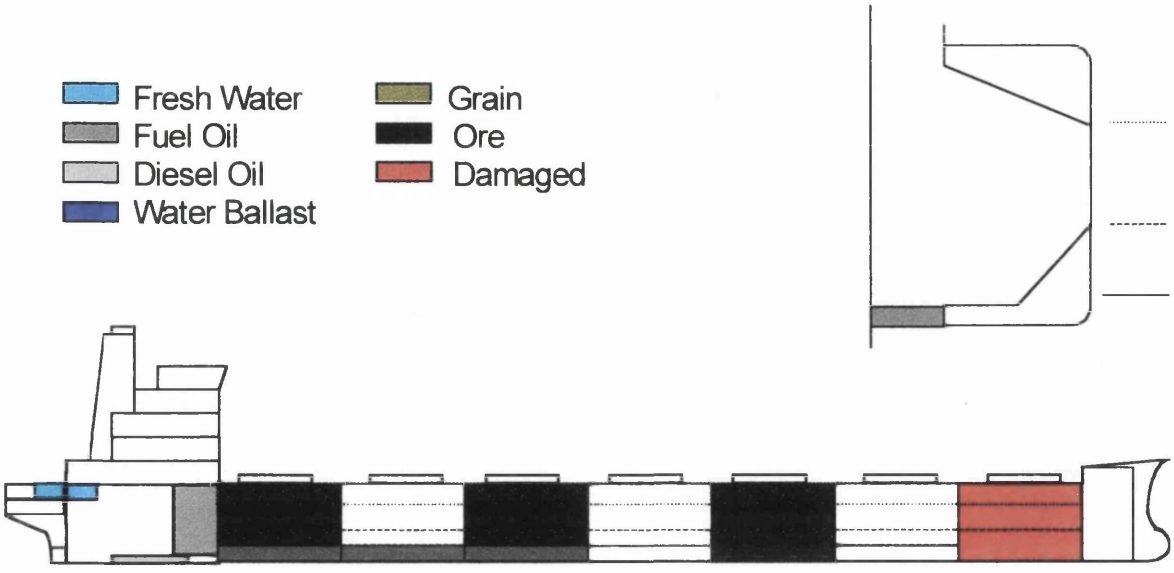

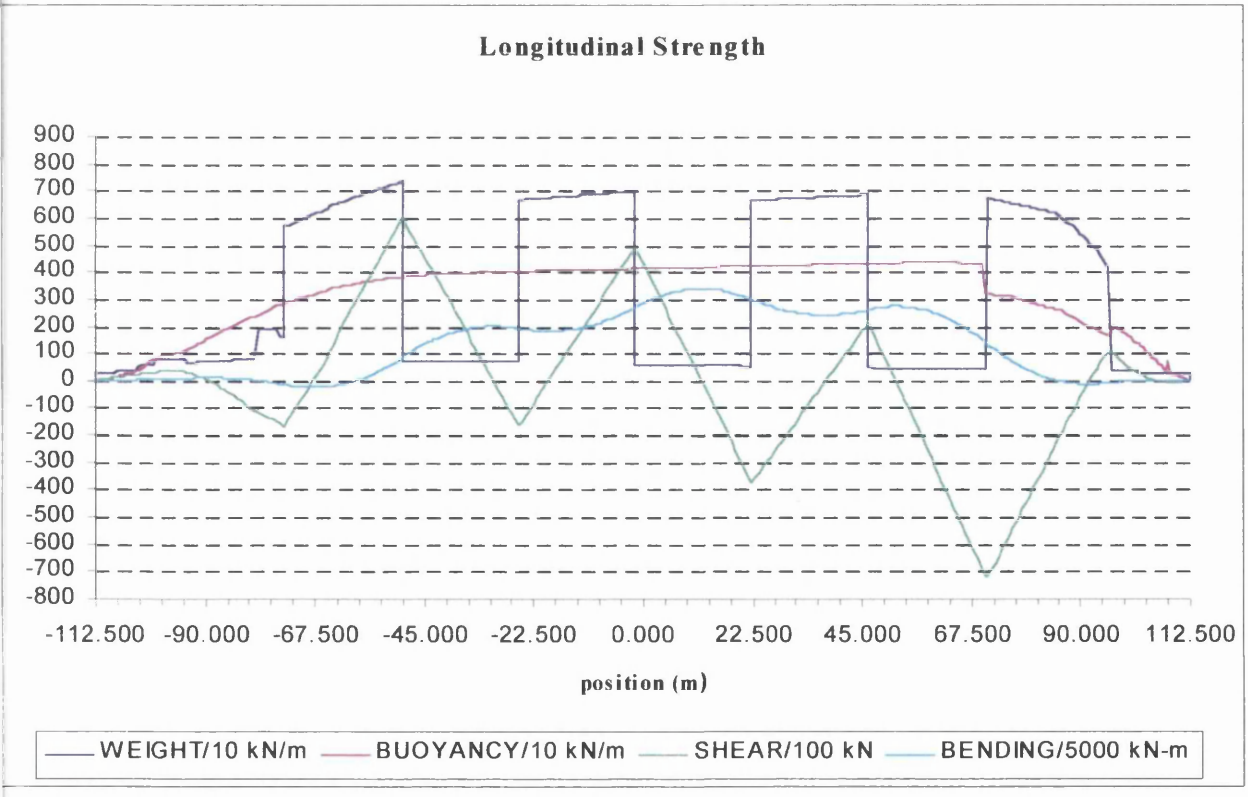

. Ore Load Condition Arrival

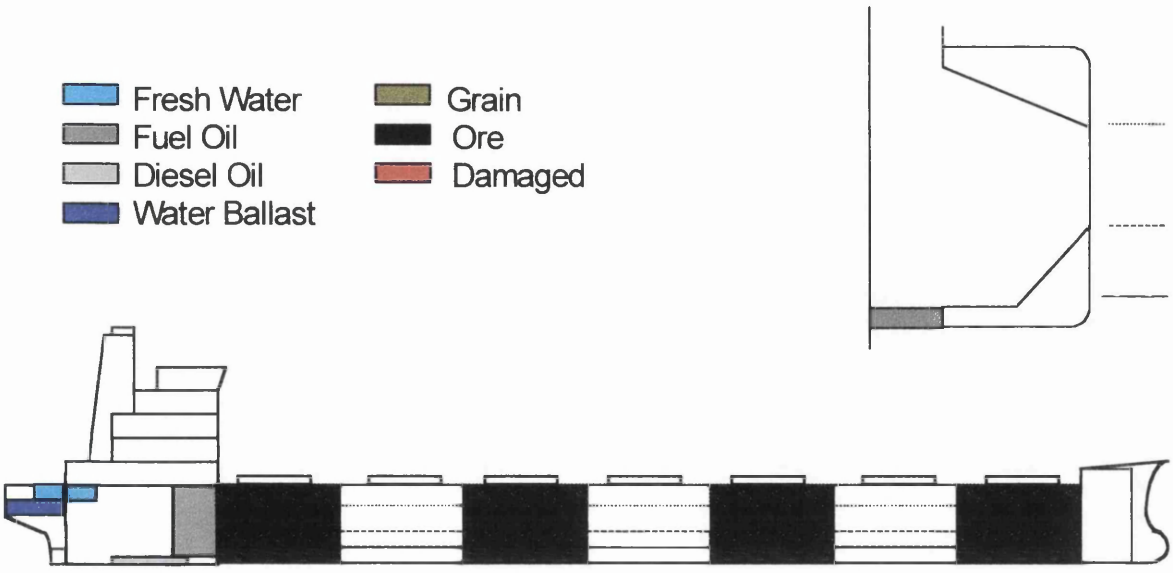

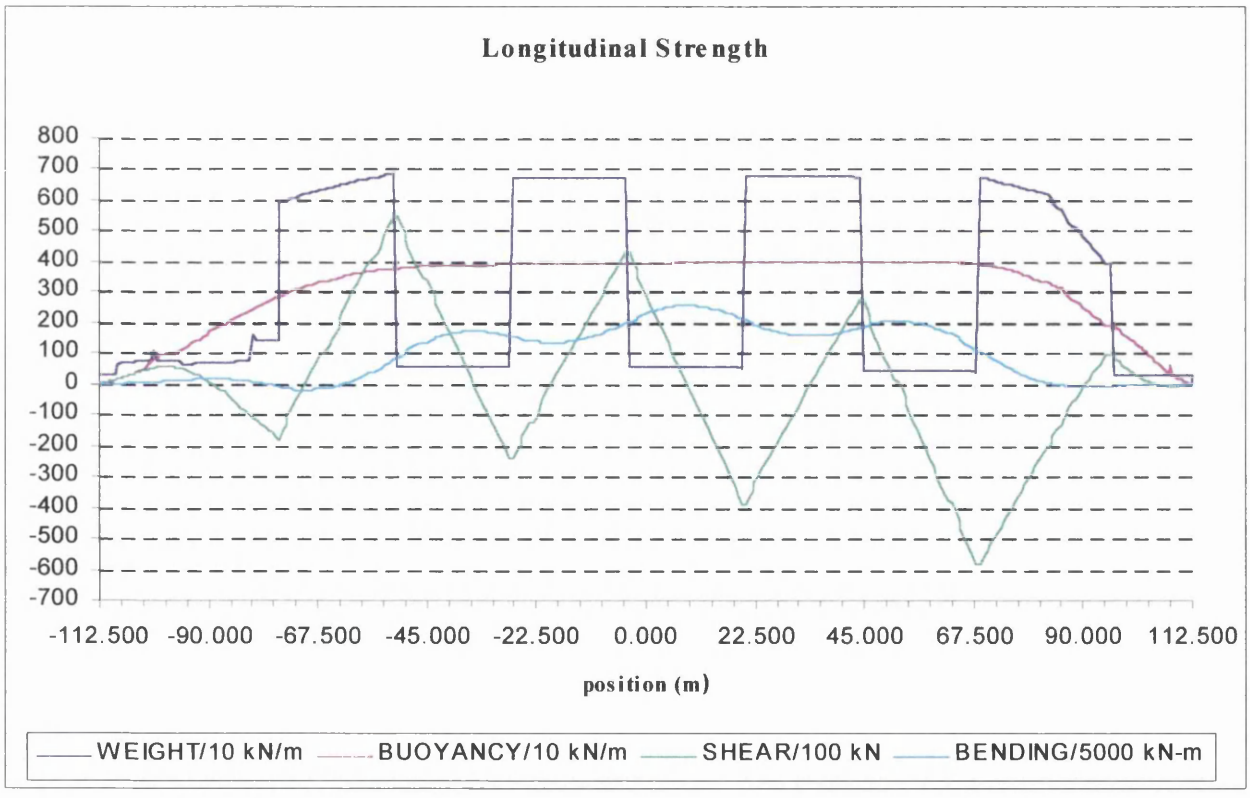

0. Ore Load Condition Arrival Hold 1 damaged

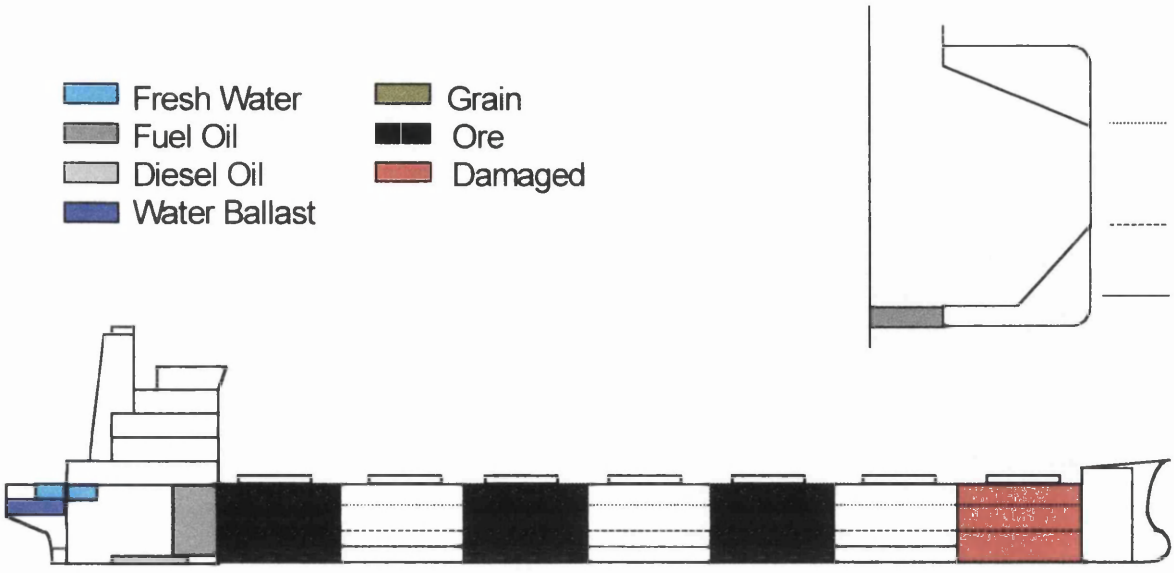

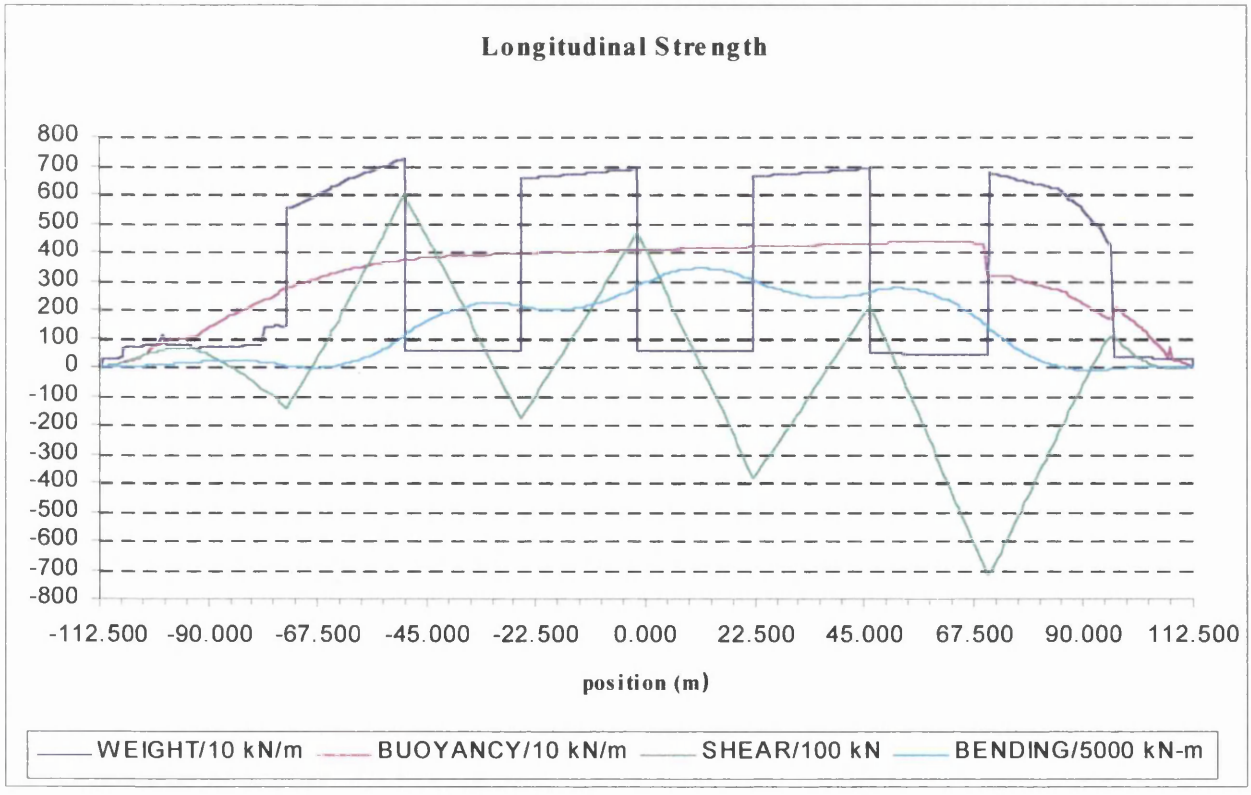

Appendix 4 Marsden squares on the World map

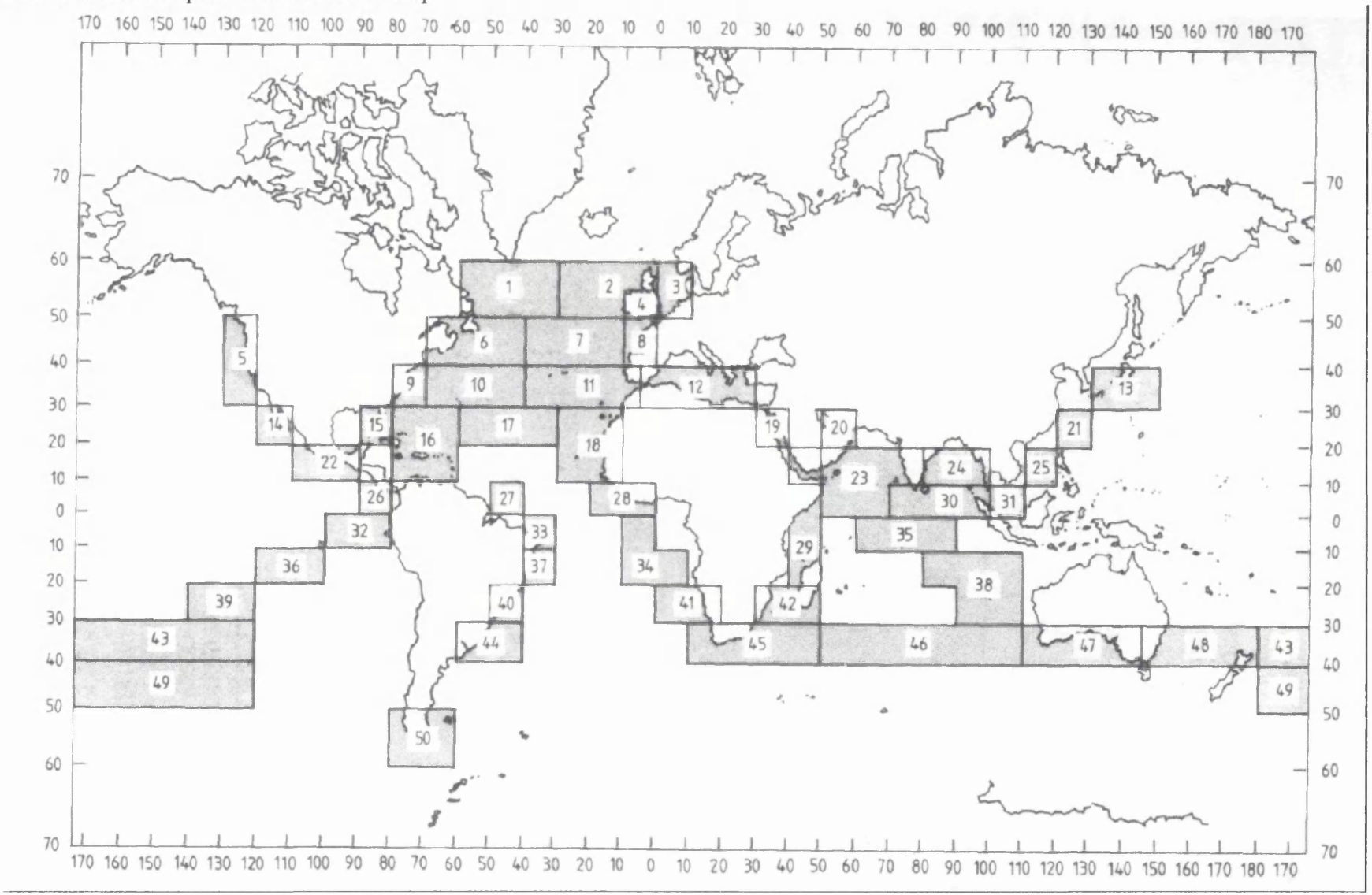

Appendix 5 Initial and Expanded scatter diagrams

Initial Scatter diagram												
Hs/Tz	3.5	4.5	5.5	6.5	7.5	8.5	9.5	10.5	11.5	12.5	13.5	Totals
0.5	2.74E-03	1.52E-02	2.72E-02	2.64E-02	1.39E-02	4.07E-03	7.57E-04	1.02E-04	1.10E-05	1.14E-06	0.00E+00	9.04E-02
1.5	4.66E-04	7.50E-03	2.94E-02	6.28E-02	7.16E-02	4.24E-02	1.47E-02	3.44E-03	6.02E-04	8.63E-05	1.07E-05	2.33E-01
2.5	1.00E-04	2.52E-03	1.32E-02	3.99E-02	7.32E-02	6.90E-02	3.63E-02	1.22E-02	2.94E-03	5.53E-04	8.71E-05	2.50E-01
3.5	2.40E-05	8.13E-04	5.04E-03	1.77E-02	4.30E-02	5.56E-02	3.94E-02	1.73E-02	5.31E-03	1.24E-03	2.36E-04	1.86E-01
4.5	6.29E-06	2.68E-04	1.89E-03	6.99E-03	1.99E-02	3.21E-02	2.85E-02	1.54E-02	5.71E-03	1.58E-03	3.53E-04	1.13E-01
5.5	1.86E-06	9.31E-05	7.28E-04	2.71E-03	8.37E-03	1.59E-02	1.67E-02	1.07E-02	4.61E-03	1.47E-03	3.73E-04	6.17E-02
6.5	5.71E-07	3.44E-05	2.94E-04	1.09E-03	3.44E-03	7.31E-03	8.82E-03	6.45E-03	3.17E-03	1.14E-03	3.22E-04	3.21E-02
7.5	1.43E-07	1.33E-05	1.25E-04	4.61E-04	1.44E-03	3.31E-03	4.46E-03	3.66E-03	2.00E-03	7.97E-04	2.48E-04	1.65E-02
8.5	1.43E-07	5.43E-06	5.56E-05	2.06E-04	6.26E-04	1.52E-03	2.24E-03	2.02E-03	1.21E-03	5.29E-04	1.79E-04	8.59E-03
9.5	0.00E+00	2.43E-06	2.60E-05	9.74E-05	2.85E-04	7.13E-04	1.13E-03	1.11E-03	7.26E-04	3.41E-04	1.24E-04	4.55E-03
10.5	0.00E+00	1.14E-06	1.26E-05	4.81E-05	1.36E-04	3.46E-04	5.86E-04	6.17E-04	4.33E-04	2.18E-04	8.47E-05	2.48E-03
11.5	0.00E+00	5.71E-07	6.29E-06	2.47E-05	6.83E-05	1.74E-04	3.09E-04	3.48E-04	2.60E-04	1.40E-04	5.76E-05	1.39E-03
12.5	0.00E+00	2.86E-07	3.29E-06	1.33E-05	3.53E-05	9.03E-05	1.67E-04	1.99E-04	1.58E-04	8.99E-05	3.90E-05	7.95E-04
13.5	0.00E+00	1.43E-07	1.71E-06	7.29E-06	1.90E-05	4.81E-05	9.23E-05	1.15E-04	9.66E-05	5.80E-05	2.64E-05	4.65E-04
14.5	0.00E+00	1.43E-07	2.29E-06	1.00E-05	2.56E-05	6.19E-05	1.24E-04	1.71E-04	1.61E-04	1.10E-04	5.67E-05	7.23E-04
Totals	3.34E-03	2.65E-02	7.80E-02	1.58E-01	2.36E-01	2.33E-01	1.54E-01	7.38E-02	2.74E-02	8.35E-03	2.20E-03	1.00E+00

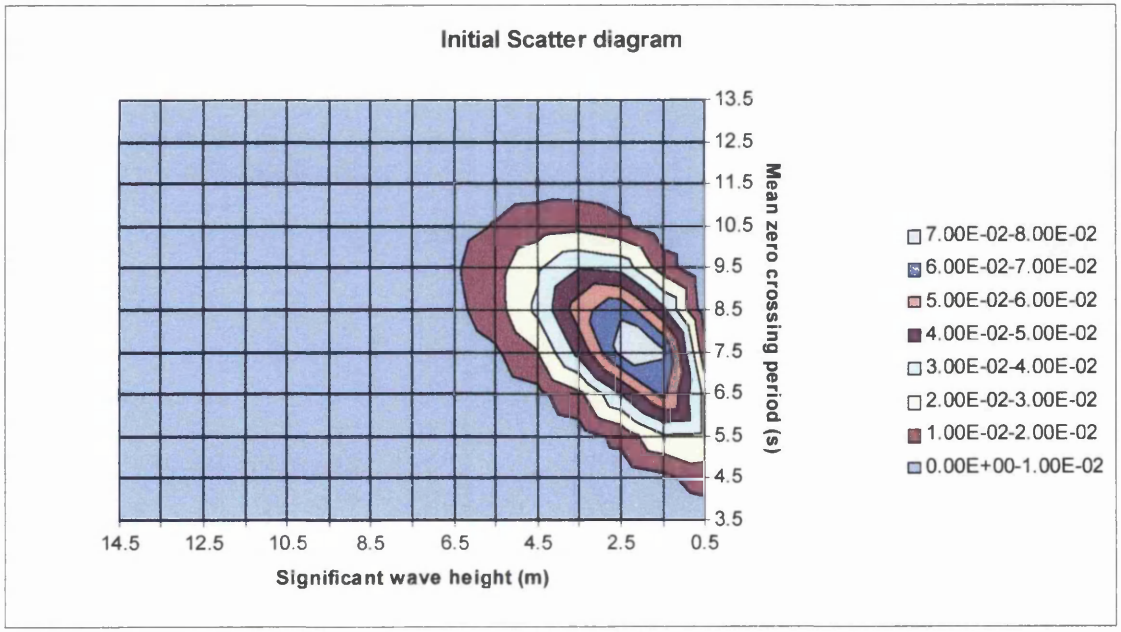

Expanded Scatter diagram												
Hs/Tz	3.5	4.5	5.5	6.5	7.5	8.5	9.5	10.5	11.5	12.5	13.5	Totals
0.5	5.99E-04	3.32E-03	5.95E-03	5.77E-03	3.04E-03	8.90E-04	1.66E-04	2.23E-05	2.41E-06	2.49E-07	0.00E+00	1.98E-02
1.5	6.42E-11	8.05E-07	1.67E-04	3.21E-03	1.38E-02	2.18E-02	1.74E-02	8.49E-03	2.90E-03	7.63E-04	1.65E-04	6.87E-02
2.5	4.09E-13	3.59E-08	2.74E-05	1.31E-03	1.08E-02	2.76E-02	3.12E-02	1.97E-02	8.12E-03	2.43E-03	5.71E-04	1.02E-01
3.5	9.77E-17	2.30E-10	1.39E-06	2.53E-04	5.02E-03	2.24E-02	3.55E-02	2.66E-02	1.15E-02	3.28E-03	6.85E-04	1.05E-01
4.5	5.56E-20	2.13E-12	7.60E-08	4.49E-05	1.95E-03	1.47E-02	3.24E-02	2.94E-02	1.39E-02	4.00E-03	7.93E-04	9.72E-02
5.5	1.53E-22	4.58E-14	6.21E-09	9.07E-06	7.37E-04	8.57E-03	2.54E-02	2.81E-02	1.50E-02	4.59E-03	9.24E-04	8.33E-02
6.5	2.09E-24	2.44E-15	8.25E-10	2.29E-06	2.95E-04	4.81E-03	1.83E-02	2.44E-02	1.48E-02	4.99E-03	1.07E-04	6.87E-02
7.5	1.22E-25	3.10E-16	1.80E-10	7.47E-07	1.32E-04	2.75E-03	1.28E-02	1.99E-02	1.38E-02	5.21E-03	1.22E-03	5.58E-02
8.5	2.60E-26	8.63E-17	6.32E-11	3.20E-07	6.75E-05	1.65E-03	8.88E-03	1.59E-02	1.25E-02	5.28E-03	1.38E-03	4.57E-02
9.5	1.71E-26	4.90E-17	3.46E-11	1.80E-07	4.03E-05	1.07E-03	6.35E-03	1.26E-02	1.11E-02	5.28E-03	1.56E-03	3.80E-02
10.5	3.03E-26	5.27E-17	2.86E-11	1.31E-07	2.81E-05	7.59E-04	4.74E-03	1.02E-02	9.91E-03	5.26E-03	1.75E-03	3.26E-02
11.5	1.29E-25	1.00E-16	3.45E-11	1.22E-07	2.30E-05	5.93E-04	3.75E-03	8.49E-03	8.96E-03	5.28E-03	1.99E-03	2.91E-02
12.5	1.17E-24	3.20E-16	5.90E-11	1.45E-07	2.21E-05	5.14E-04	3.16E-03	7.35E-03	8.29E-03	5.38E-03	2.28E-03	2.70E-02
13.5	2.12E-23	1.62E-15	1.39E-10	2.13E-07	2.47E-05	4.94E-04	2.85E-03	6.66E-03	7.90E-03	5.60E-03	2.66E-03	2.62E-02
14.5	7.04E-22	1.25E-14	4.40E-10	3.88E-07	3.20E-05	5.26E-04	2.77E-03	6.35E-03	7.81E-03	5.97E-03	3.16E-03	2.66E-02
15.5	4.01E-20	1.40E-13	1.83E-09	8.58E-07	4.77E-05	6.22E-04	2.90E-03	6.39E-03	8.01E-03	6.55E-03	3.83E-03	2.84E-02
16.5	3.72E-18	2.23E-12	9.74E-09	2.28E-06	8.17E-05	8.13E-04	3.27E-03	6.79E-03	8.57E-03	7.41E-03	4.78E-03	3.17E-02
17.5	5.36E-16	4.87E-11	6.55E-08	7.22E-06	1.59E-04	1.17E-03	3.97E-03	7.63E-03	9.58E-03	8.68E-03	6.11E-03	3.73E-02
18.5	1.15E-13	1.42E-09	5.46E-07	2.69E-05	3.51E-04	1.86E-03	5.20E-03	9.09E-03	5.59E-03	5.26E-03	8.03E-03	3.54E-02
19.5	3.51E-11	5.36E-08	5.56E-06	1.16E-04	8.72E-04	3.23E-03	7.30E-03	5.72E-03	6.83E-03	6.60E-03	1.09E-03	4.16E-02
Totals	5.99E-04	3.32E-03	6.15E-03	1.08E-02	3.75E-02	1.17E-01	2.28E-01	2.60E-01	1.85E-01	9.78E-02	5.39E-02	1.00E+00

Appendix 6

Transfer functions at the midship section for vertical bending moment, vertical shear force, horizontal bending moment, horizontal shear force and torsional moment for three intact conditions and one damaged (only vertical bending moment)

Ore Load Condition T.F for midship

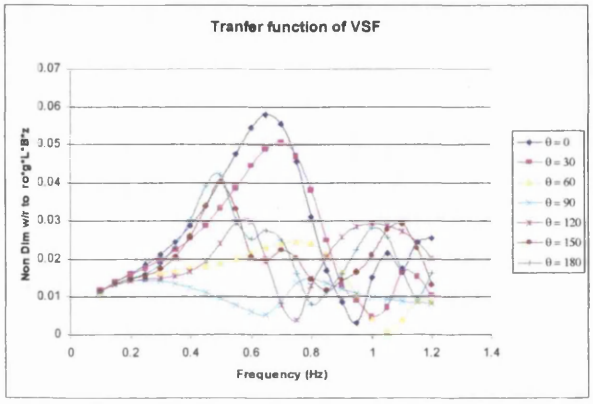

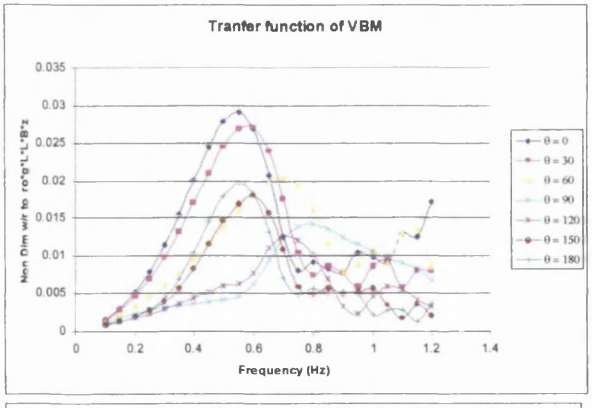

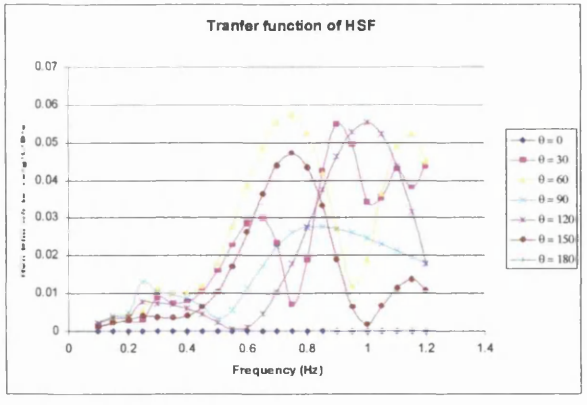

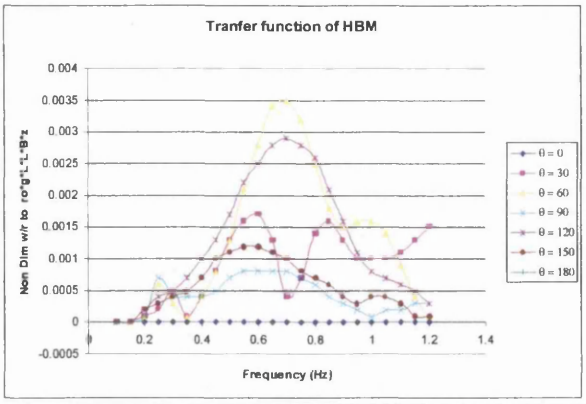

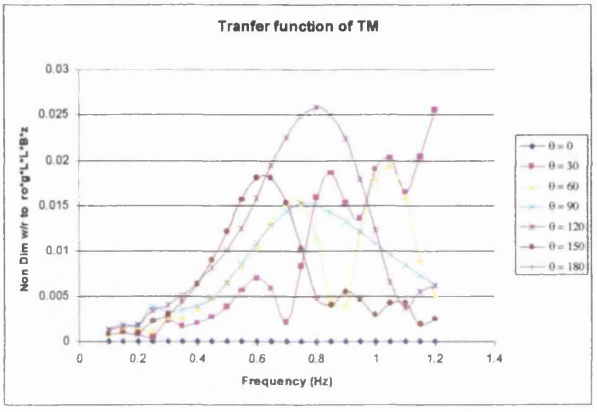

Damaged Condition Transfer Function

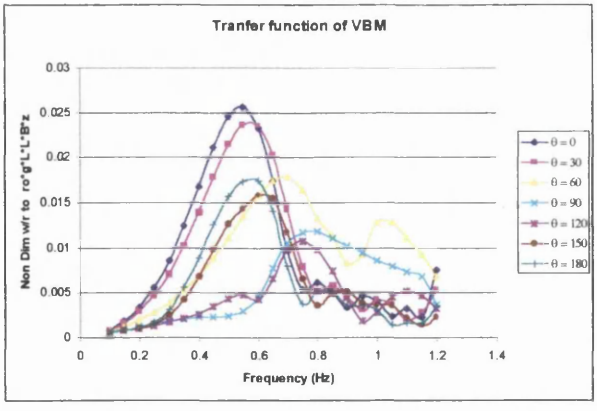

Grain Load Condition T.F. for midship

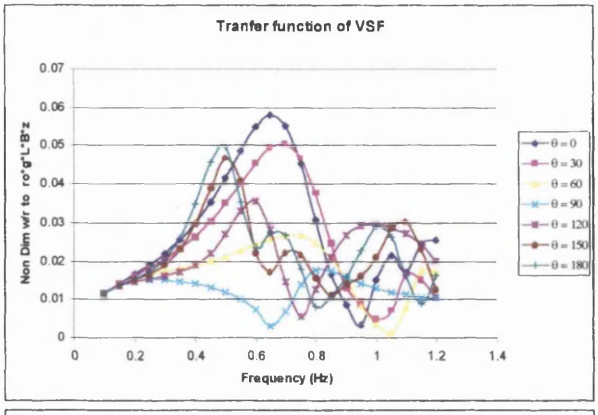

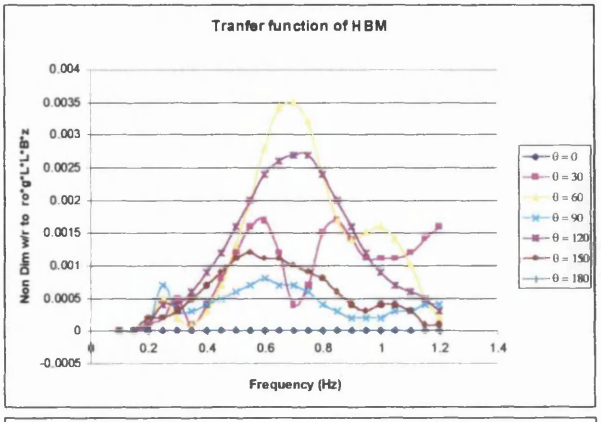

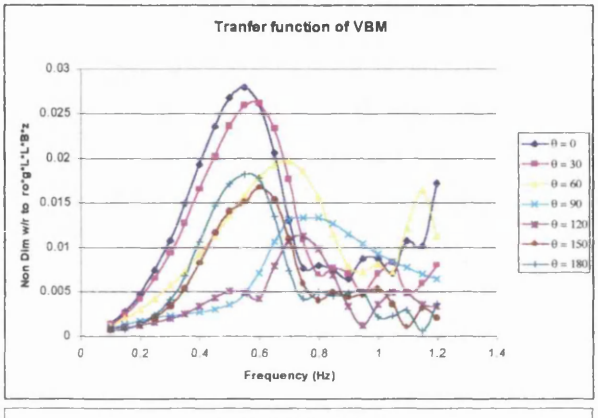

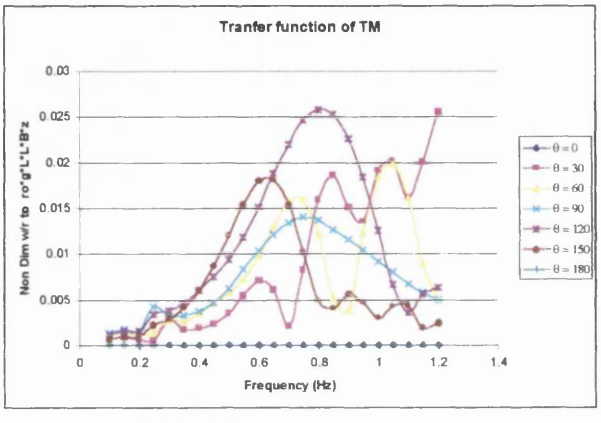

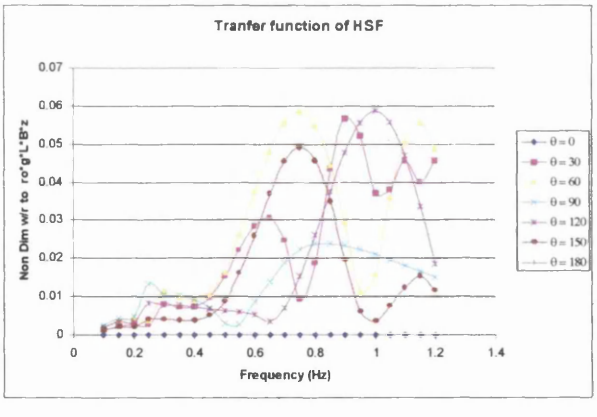

Heavy Ballast Condition T. F. for midship

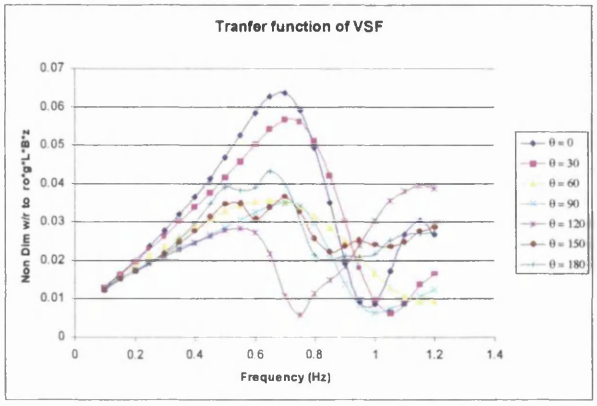

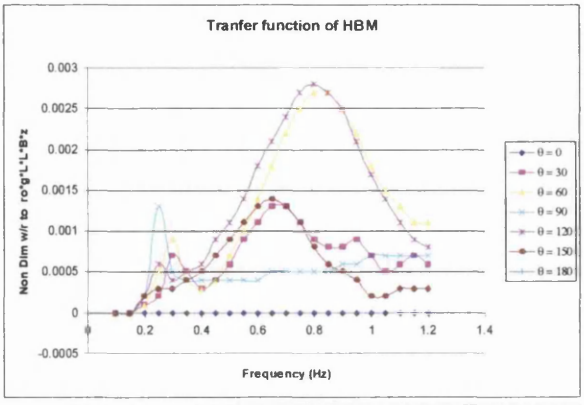

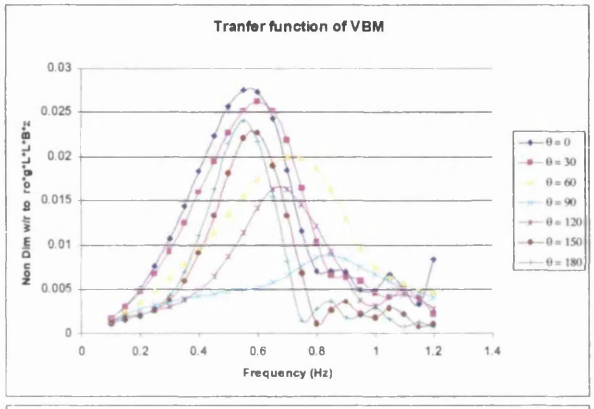

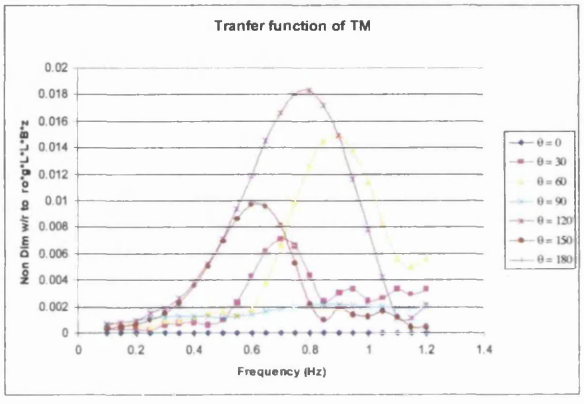

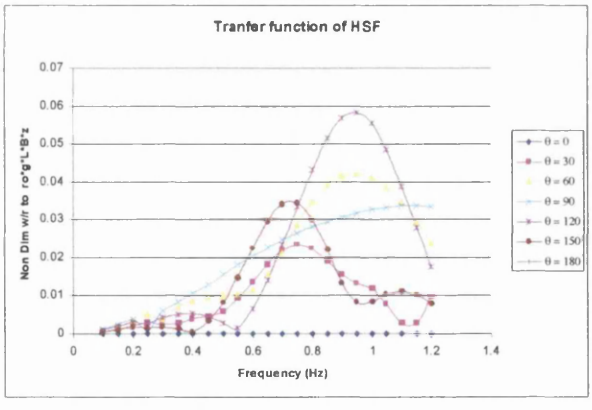

Appendix 7 Flowchart for Fortran program calculating the probability of exceedance for vertical bending moment at the midship section.

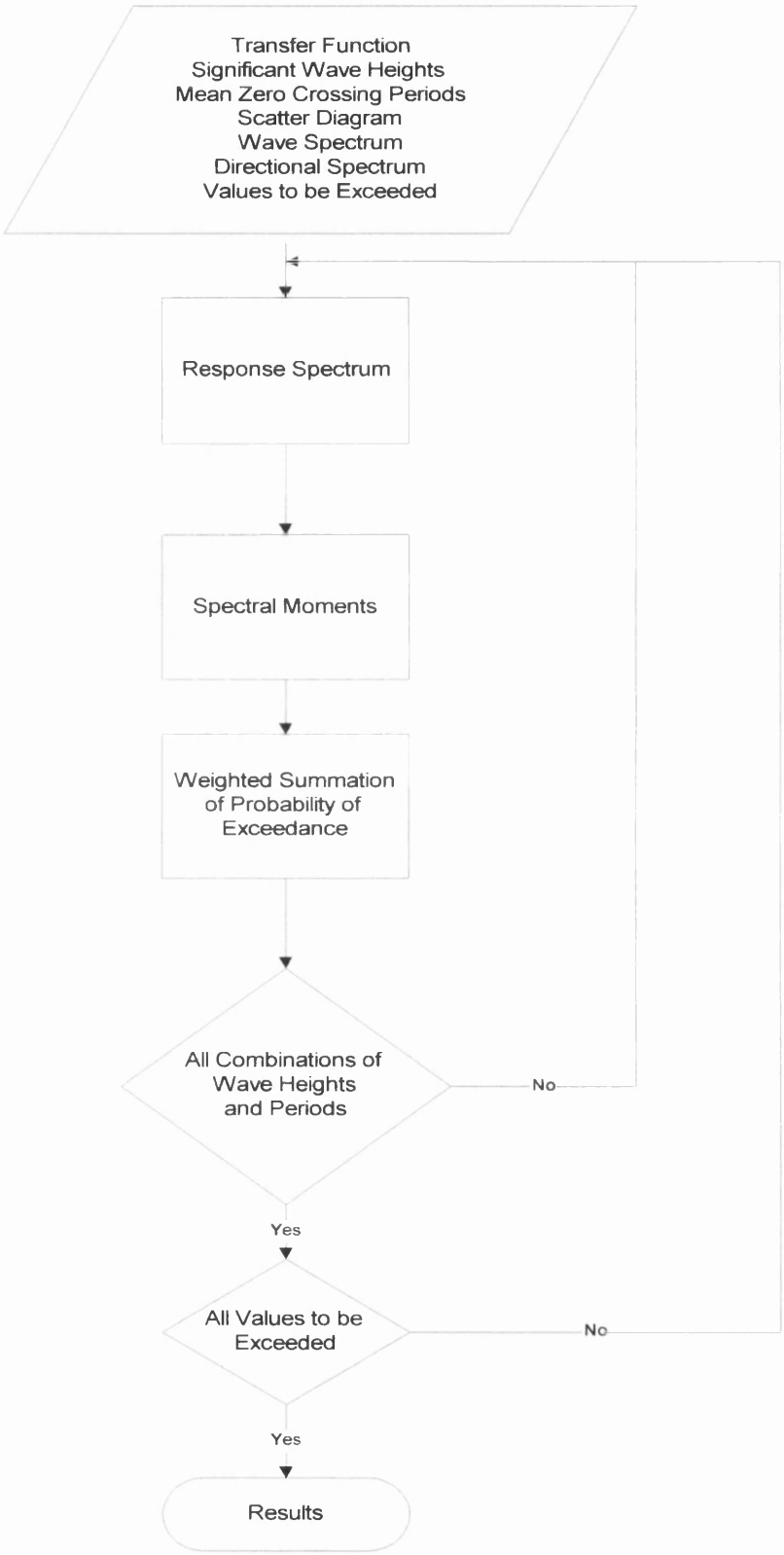

Appendix 8 Assesment of assumed functions regarding wave diffraction and wave heading influence on wave induced pressure on the ship's side.

Wave Diffraction Influence

X = 45 degrees **Midships**	Column 1 Fig. 13 from Paper* λ/L = 1,235 (λ=305 m)	Column 2 Fig. 10 from Paper* λ/L = 1(λ=247 m)	Column 3 Ratio of columns	Column 4 Fig. 4 from Paper* λ/L = 0,5(λ=123,5 m)	Column 5 Ratio of columns
Point (θ degrees)	$p/\rho g\zeta_\alpha$	$p/\rho g\zeta_\alpha$	1 and 2	$p/\rho g\zeta_\alpha$	1 and 4
67,5	1,174	1,304	1,111	1,217	1,037
90	1,511	1,641	1,086	1,946	1,288
Table A8.1		Mean Ratio =	1,099	Mean Ratio =	1,162

X = 45 degrees **St. 2,5**	Column 1 Fig. 14 from Paper* λ/L = 1,235 (λ=305 m)	Column 2 Fig. 11 from Paper* λ/L = 1(λ=247 m)	Column 3 Ratio of columns	Column 4 Fig. 5 from Paper* λ/L = 0,5(λ=123,5 m)	Column 5 Ratio of columns
Point (θ degrees)	$p/\rho g\zeta_\alpha$	$p/\rho g\zeta_\alpha$	1 and 2	$p/\rho g\zeta_\alpha$	1 and 4
67,5	1,098	1,228	1,119	1,217	1,109
90	1,391	1,554	1,117	2,043	1,469
Table A8.2		Mean Ratio =	1,118	Mean Ratio =	1,289

X = 45 degrees **St. 8,5**	Column 1 Fig. 12 from Paper* λ/L = 1,235 (λ=305 m)	Column 2 Fig. 9 from Paper* λ/L = 1(λ=247 m)	Column 3 Ratio of columns	Column 4 Fig. 3 from Paper* λ/L = 0,5(λ=123,5 m)	Column 5 Ratio of columns
Point (θ degrees)	$p/\rho g\zeta_\alpha$	$p/\rho g\zeta_\alpha$	1 and 2	$p/\rho g\zeta_\alpha$	1 and 4
67,5	1,141	1,152	1,010	1,152	1,010
90	1,815	1,652	0,910	1,891	1,042
Table A8.3		Mean Ratio =	0,960	Mean Ratio =	1,026

Length of ship = 247m
Breadth of ship = 40,6m

$$f_d = 1 + e^{-\frac{\lambda}{B}}$$

Wave length λ	**f_d (Equation 3.3.3.3)**	**Ratios** Midships	St. 2,5	St. 8,5
100	1,085	–	–	–
123,5	1,048	1,162	1,2888	1,0257
150	1,025	–	–	–
200	1,007	–	–	–
247	1,002	1,099	1,118	0,9599
250	1,002	–	–	–
300	1,001	–	–	–
305,045	1,001	1,000**	1,000**	1,000**
350	1,000	–	–	–

Table A8.4

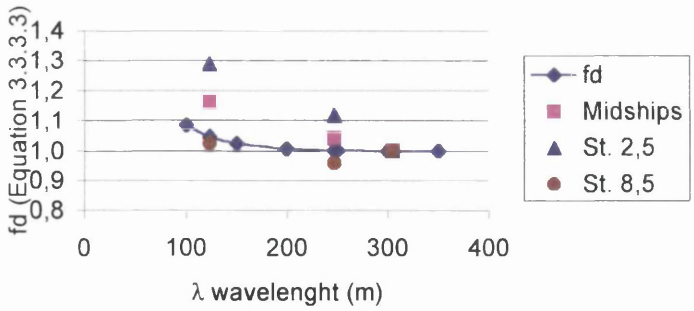

Figure A8.1 Graphical comparison of the wave diffraction function and the 3D theory resulys

* N. Liapis, O. M. Faltinsen, "Diffraction of Waves Around a Ship", Journal of Ship Research, Vol 24, No.3, Sept. 1980, pp. 147-155
** Assumed values so that comparison is possible

Wave heading Influence

λ/L = 0,5	Fig. 4 from Paper*	Fig. 7 from Paper*	
Midships	X = 45 degrees	X = 85 degrees	
Point (θ degrees)	$p/\rho g\zeta_\alpha$	$p/\rho g\zeta_\alpha$	Ratio
45	0,435	0,652	0,667
67,5	1,239	1,391	0,891
90	1,946	2,109	0,923
Table A8.5		**Mean Ratio =**	**0,827**

λ/L = 0,5	Fig. 5 from Paper*	Fig. 8 from Paper*	
St. 2,5	X = 45 degrees	X = 85 degrees	
Point (θ degrees)	$p/\rho g\zeta_\alpha$	$p/\rho g\zeta_\alpha$	Ratio
45	0,478	0,674	0,710
67,5	1,217	1,348	0,903
90	2,043	2,000	1,022
Table A8.5		**Mean Ratio =**	**0,878**

λ/L = 0,5	Fig. 3 from Paper*	Fig. 6 from Paper*	
St. 8,5	X = 45 degrees	X = 85 degrees	
Point (θ degrees)	$p/\rho g\zeta_\alpha$	$p/\rho g\zeta_\alpha$	Ratio
45	0,500	0,609	0,821
67,5	1,152	1,283	0,898
90	1,891	2,000	0,946
Table A8.5		**Mean Ratio =**	**0,888**

$f_h = (1+ \sin(X))/2$

Wave Heading	**fh**	**Mean Ratios (3D theory values)**		
degrees (X)	**(Equation 3.3.3.4)**	Midships	St. 2,5	St. 8,5
45	0,854	0,827	0,878	0,888
50	0,883	---	---	---
60	0,933	---	---	---
70	0,970	---	---	---
80	0,992	---	---	---
90	1,000	1,000**	1,000**	1,000**

Table A8.5

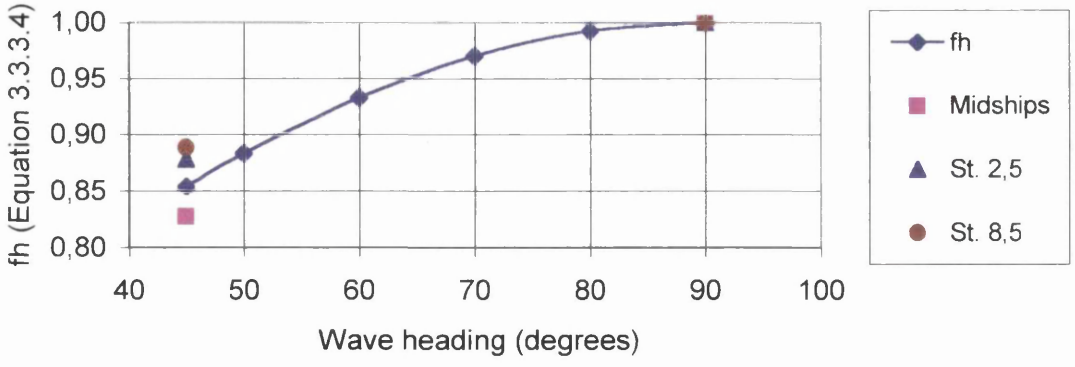

Figure A8.2 Graphical comparison of the wave heading function and the 3D theory results

* N. Liapis, O. M. Faltinsen, "Diffraction of Waves Around a Ship", Journal of Ship Research, Vol 24, No.3, Sept. 1980, pp. 147-155

** Assumed values so that comparison is possible

Chapter 4

Study of Stresses developing in the Structure using Principal Models corresponding to the dominant Ship Structure Characteristics

4.1 Introduction to the structural behaviour of the models applied

The behaviour of the structure studied is analysed in this chapter. The first part describes a simplified procedure for calculating the ultimate hull girder bending moment, and the results are compared with the extreme vertical bending moments calculated in the previous chapter. The second part discusses local structural behaviour, the various associated assumptions and the stress transformations. Of particular interest is the accuracy of simple models applied to the complex structure of a bulk carrier.

4.2 Literature Survey

The earliest writings dealing with structures are those of Archimedes (287-212 B.C). Around seventeen hundred years later, the basics of the theories regarding structures, general physics and mathematical tools for their manipulation were developed by a group of mathematicians/physicians, including Galileo and Newton. A great number of modern books have been written on the subject of structures, and the majority of them include the basic principles of stress, strain, force etc. Coates, Coutie and Kong [1] include the basic principles and their application to finite element analysis. Meriam and Kraige [2], Benham and Crawford [3], Cook and Young [4] and Rees [5] have described the basic principles and their application to engineering problems in an academically oriented way. Young [6], on the other hand, enhanced a book written by Roark, which presents a large collection of formulas, facts and principles suitable for fast first principle analysis. Hughes [7] describes the methodology of ship structural optimisation and presents a respectable amount of information regarding ship structural behaviour and response.

Most of the books mentioned above contain at least one chapter regarding torsion. The chapter included in the book by Cook and Young [4] is the most informative, containing the theory for solid or hollow, open or closed and multicellular sections. It also discusses warping in a simplified manner. Kollbrunner and Basler [8] discuss the subject of torsion very thoroughly, in fact their book could be considered to encapsulate this century's knowledge regarding torsion, even though it was written around thirty years ago. A one-dimensional finite element procedure for analysis of the coupled torsional-bending response of thin-walled beam structures such as ship hulls is presented

by Pedersen [9]. His aim is to provide a simplified method of analysing the effects of torsion on container ship structures, which, due to their very large hatch openings, suffer significant torsional loads. A similar methodology regarding the same problem is presented by Senjanovic and Fan [10], who consider a pontoon that consists of a channel middle part and rectangular tub peaks.

With respect to ultimate bending moment capacity calculations, Rutherford and Caldwell [11] discuss the buckling and post-buckling behaviour of compressed stiffeners and plates. They also describe an incident where a VLCC broke its back, and compare this situation with theoretical results provided by their approach. Paik [12] provides a description of his approach towards ultimate hull girder capacity, this being the idealised structural unit method for ultimate strength analysis of large-size plated structures such as ships. In the same paper, other aspects of ship design and evaluation are discussed. Damonte, Figari and Porcari [15] describe a methodology for calculating the ultimate longitudinal bending moment of the hull girder. They also discuss the uncertainties that originate from the loads and strength assessment. Hughes [7] discusses in depth the major factors of the ultimate longitudinal hull girder capacity and presents two methods for the calculation. The first is detailed, but the second is much faster due to the assumptions that are made. The results for a box girder structure are compared with experiments and good agreement is shown overall. Dow [14] also discusses the problem of evaluating the hull girder ultimate bending moment capacity and behaviour under quasi-static loads and whipping response. Gordo and Guedes Soares [15] present a method by which to estimate the ultimate moment based on a simplified approach for representing the collapse strength of beam columns. The results are compared with experiments, other approaches and finite elements.

4.3 Hull structure global behaviour

The stresses and shear stresses induced by global loading on the hull girder were and are considered to be very important to the structural integrity of the vessel. The classification societies started their rule-based design by considering only global loads and hence the structural properties of the midship section. The shipyard and the ship-

owner determined the rest of the structure's scantlings. However, it should be noted that the length of the ships then was shorter than that of today.

The calculations regarding stresses and shear stresses affecting the hull girder are based on the following assumptions:

- The hull girder is idealised as a hollow thin-wall box beam.
- The hull girder is elastic, and strain in the longitudinal direction varies linearly with respect to the neutral axis.
- Shear lag effects are not included in the analysis (plane sections of the hull girder remain plane).
- Warping effects due to torsion are excluded from the analysis (plane sections of the hull girder remain plane).
- Dynamic effects are included by superimposition of the still water bending moment and the extreme wave induced bending moment.

The above assumptions allow us to use the following equations for the calculations regarding stresses and shear stresses. They are written in a format whereby the stresses and shear stresses are calculated based on their equivalent loading.

$$\sigma_{VBM} = \frac{VBM \cdot y}{I_{yy}} \qquad 4.3.1$$

$$\sigma_{HBM} = \frac{HBM \cdot x}{I_{xx}} \qquad 4.3.2$$

$$\tau_{VSF} = \frac{VSF \cdot q_v}{t} \qquad 4.3.3$$

$$\tau_{HSF} = \frac{HSF \cdot q_h}{t} \qquad 4.3.4$$

$$\tau_{TM} = \frac{TM \cdot q_t}{t} \qquad 4.3.5$$

Where:

VBM : Vertical Bending moment

y : Distance from neutral axis of the point at which the stress is calculated.

I_{yy} : Inertia of section from the neutral axis

σ_{VBM} : Resultant stress due to VBM

HBM : Horizontal Bending moment

x : Distance from centre-line of the point at which the stress is calculated

I_{xx} : Inertia of section from the centre-line

σ_{HBM} : Resultant stress due to HBM

VSF : Vertical Shear force

q_v : Vertical shear flow per unit of vertical shear force at the point of interest

t : Thickness at point of interest

τ_{VSF} : Resultant vertical shear stress

HSF ; Horizontal Shear stress

q_h : Horizontal shear flow per unit horizontal shear force at the point of interest

τ_{HSF} : Resultant horizontal shear stress

TM : Torsion moment

q_t : Shear flow per unit torque

The structural properties (inertia etc.) were calculated using a computer program, and the results can be found in chapter 2.

4.3.1 Ultimate hull girder capacity

4.3.1.1 Introduction

The hull is a three-dimensional structure containing many components, and its collapse involves combinations of plastic collapse and buckling. Two overall modes of collapse - longitudinal and transverse - exist, since the transverse frames are orthogonal to the longitudinal frames. The transverse frames are sized to support transverse loads and therefore the longitudinal collapse will occur between adjacent frames. A section

between frames is then critical for longitudinal ultimate strength. This section should be in the middle of the hold amidships because of the large hatch opening.

A panel collapse involves the loss of total load carrying capacity, so when it happens, the load previously carried by the panel is distributed to the remaining panels. As a result, the ultimate hull girder capacity can be determined only by an incremental analysis whereby, when a panel fails, it can be considered non-existent for the rest of the calculations. Various computer programs have been developed to perform the calculation of the hull girder ultimate strength (e.g. Lloyd's Register hull girder ultimate strength program no. 20203).

4.3.1.2 Approximate calculations of Ultimate strength

A simplified method, presented by Hughes [7], is adopted here. It possesses sufficient accuracy for most design applications. In the majority of ship structures the stiffeners are identical or differ only moderately in size and spacing. The collapse of one stiffener as a result of an imposed strain coincides with the collapse of the adjacent panels. There is, therefore, no need to perform the calculations for each stiffener-plate.

The first step is calculating the ultimate strength of the panels induced to in-plane compression and bending using the formulas for the collapse of the panel in two major modes, these being plate collapse and stiffener collapse (Appendix 9). It is worth mentioning that a third mode occurs when bending induces large tensile forces in the stiffener and compressive forces at the plate. However, for this mode to occur the bending must be large, which is not the case in our example. The panel with the lowest value is used for the calculation of the ultimate strain. The value is then compared with the average hull girder bending strain. The calculations take into account that the extreme vertical bending moment is hogging, so the bottom panels are checked for buckling and the deck panels for tensile yield. Then the curvature of the hull girder ϕ_o at which the first panel will collapse is:

$$\phi_o = \underset{i=1}{\overset{Np}{MIN}}\left\{\left|\frac{(\varepsilon_{a,u})_i}{y_i}\right|, \left|\frac{(\varepsilon_y)_i}{y_i}\right|\right\} \qquad 4.3.1.2.1$$

Where:

ϕ_o: The curvature of the hull girder at which the first panel collapses

Np: Number of panels

i: Panel considered

$\varepsilon_{\alpha,\upsilon}$: Ultimate strain

ε_y Average elastic hull girder bending strain

y_I: The distance from the elastic neutral axis of the panel's cross section

And the corresponding value of ultimate strength is

$$M = E \cdot I \cdot \phi_o \qquad 4.3.1.2.2$$

The procedure continues the iterations in the same way but distinguishes between tensile yield failure and compressive collapse. When a panel fails during tensile yield there is no immediate shedding of its load; it continues to carry the load it had when the tensile yield failure occurred, and is therefore ignored for the rest of the calculations. However, when a panel fails under compression it is assumed that the load it carried is distributed to the rest of the panels. This is incorporated into the calculations by recalculating the inertia and the remaining structural properties excluding the panel in which failure occurred. We performed only the first step in the iteration and the result is shown in the table below, with the extreme vertical bending moment and the bending moment capacity with respect to tensile yield.

Applied vertical bending moment	4623275 kN m
Simplified method for capacity (0% corrosion)	5451000 kN-m
Simplified method for capacity (10% corrosion)	4737000 kN-m
Simplified method for capacity (20% corrosion)	3863000 kN-m
Tensile yield capacity(0% corrosion)	6246000 kN-m
Tensile yield capacity(10% corrosion)	5621000 kN-m
Tensile yield capacity(20% corrosion)	4997000 kN-m

Table 4.3-1 Ultimate and tensile hull girder capacity with corrosion margins.

The safety factor is 1.179 for the hull girder capacity and 1.35 for yield capacity, which are low values relative to the usual 1.6-1.7 values. The reason is probably the scatter diagram used for the calculation of the wave loading.

4.4 Hull structure local behaviour

As mentioned previously, classification societies initially regulated only the scantlings of the mid-ship section. The length of the ships built gradually increased and local failures began to occur as a result of both extreme loading and fatigue. Of course, the classification societies reacted to the situation and provided regulations for the rest of the structure.

4.4.1 Local structural components considered

The structural behaviour of the components that comprise the vessel's watertight envelope is not straightforward. It is determined by the boundary conditions of each component, which interact by deforming and restraining the other components so that the structure can accommodate the loading.

We will examine the structural behaviour of the components and a major common sub-component by subdividing the structure into smaller systems. These systems will be assumed to suffer as a result of particular types of loading, and the procedure for calculating the induced stresses and deformed shape is outlined below.

The assumptions with respect to loading and boundary conditions will be examined later using a simple finite element program.

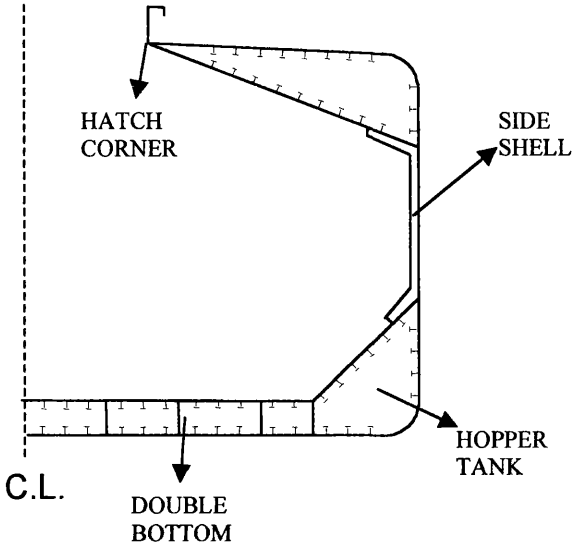

Figure 4.4.1.1 The midship section of the vessel

The above figure shows the structural components that are studied in the following sections.

4.4.2 Double Bottom

The double bottom will act as a beam with fixed ends. It consists of the keel plates, the inner bottom plates and the double bottom floors. The former two are assumed to be the flanges of the beam and the latter can be idealised as the web of the beam. The behaviour of the double bottom could, therefore, be simulated as an I-beam with, of course, the same structural properties.

The representation of the double bottom as an I-beam is inadequate for calculating stresses. Boundary conditions that represent reality need to be assumed. The double bottom is connected to the hopper tanks at each side. The behaviour of the hopper tanks is studied later. However, if we assume that they are rigid, they will try to rotate in-wards as their geometrical shape dictates. If we assume that the double bottom is simply supported, then its boundaries would rotate out-wards. We can conclude then that the hopper tank and the double bottom, within their boundaries, restrain each other by exhibiting rotations different in sign. The magnitude of these rotations and hence the determination of the dominant component is examined in the next section. The boundary conditions assumed for the double bottom, based on the above-mentioned behaviour in

the physical boundaries, are fixed ended. The figure below shows the assumed deformed shape and the fixed end bending moment distribution.

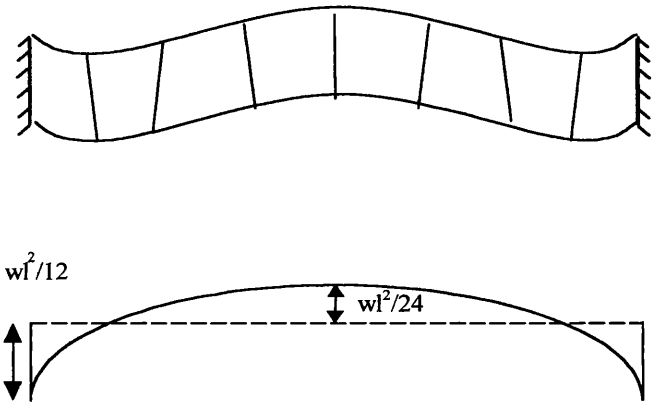

Figure 4.4.2.1 The double bottom assumed deformed shape and bending moment distribution.

4.4.3 Hopper Tank

A small finite element model was set up to establish the behaviour of the two boundaries between the hopper tanks and the double bottom. Half of the double bottom was considered as it interacted with one hopper tank, as shown in figure 4.4.3.1. The area on which the water pressure acts is subdivided into two regions. The first region is under the keel plate; the second region is around the hopper tank.

The stiffness matrix for the finite element model was created to comprise the torsion stiffness of the hopper and the bending stiffness of the double bottom. The effect of the transverse bulkheads was incorporated into the model by multiplying the moment matrix with reduction factors. At the bulkheads, the moment was zero, and reaching maximum value at one third of the distance between the two bulkheads, constant for one third then reducing to zero. Although this reduction of the applied moment does not fully simulate the stiffer structural components closer to the transverse bulkheads, it was thought to be adequate.

The matrix moment comprises the moment resulting from water pressure forces underneath the double bottom. The matrix was multiplied by the inverse of the total stiffness matrix to give us the rotations at the ends of the double bottom where it is connected to the hopper tanks to provide equilibrium at that point in the structure. The total moment used to calculate the stress from the water pressure was calculated by adding the moment to provide equilibrium, with the moment acting on the hopper

resulting from wave pressure and then subtracting the moment caused by the wave pressure underneath the double bottom.

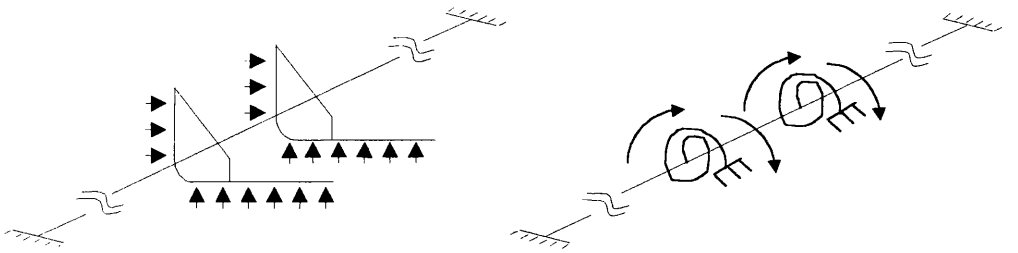

Figure 4.4.3.1- Graphic representation of the finite element model

M_P = the moment to cause rotation at the hopper 4.4.1

$$M_L = \frac{\omega \cdot B^2}{12}$$ F.E. moment caused by pressure underneath the double bottom 4.4.2

$$K_M = \begin{bmatrix} \frac{E \cdot I}{b} & 0 & \dots & 0 \\ 0 & \frac{E \cdot I}{b} & \dots & 0 \\ \dots & \dots & \dots & 0 \\ 0 & 0 & 0 & \frac{E \cdot I}{b} \end{bmatrix}$$ Stiffness matrix for double bottom 4.4.3

$$M = \begin{bmatrix} r_1 \cdot \frac{\omega \cdot B^2}{12} \\ r_2 \cdot \frac{\omega \cdot B^2}{12} \\ \dots \\ r_{30} \cdot \frac{\omega \cdot B^2}{12} \end{bmatrix}$$ Moment underneath the double bottom 4.4.5

$K = K_T + K_M$ Stiffness matrix for hopper structure 4.4.4

$$K_T = \begin{bmatrix} \frac{G \cdot J}{L} & -\frac{G \cdot J}{L} & \cdots & 0 \\ -\frac{G \cdot J}{L} & 2 \cdot \frac{G \cdot J}{L} & \cdots & 0 \\ \cdots & \cdots & \cdots & -\frac{G \cdot J}{L} \\ 0 & 0 & -\frac{G \cdot J}{L} & \frac{G \cdot J}{L} \end{bmatrix}$$ Total stiffness matrix 4.4.6

$$X = K^{-1} \cdot M$$ Rotation at the hopper corner 4.4.7

$$M_R = X \cdot \frac{E \cdot I}{B}$$ Moment to provide equilibrium 4.4.8

$$M = M_P + M_R - M_L$$ Total moment 4.4.9

$$\sigma_p = \frac{M}{z}$$ Stress at the hopper corner 4.4.10

4.4.4 Side Shell

The side bracket was modelled as a beam because an effective breadth was included in the calculations. The area that the bracket should be able to support was considered as having a height equalling the distance between the hopper tank and the upper wing tank and a breadth equalling the spacing of the brackets. The fixed end moments and the forces at the supports were calculated. Then the stresses were worked out by introducing a cut at the foot of the bracket and then calculating the properties (inertia, etc.) (Fig 4.4.4.1).

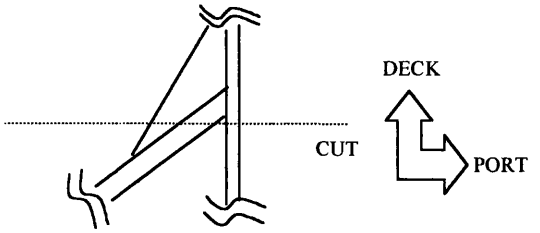

Figure 4.4.4.2 - The position of the 'cut' to calculate structural properties

The stresses calculated are parallel to the side shell plating and perpendicular to the bottom plating. The welding and hence the possible cracks have an angle of 47 degrees to the side shell plating. The stresses calculated were transformed into a direction perpendicular to the welding.

$$\sigma = \frac{M}{z} \qquad 4.4.4.1$$

$$\tau = \frac{ShearForce}{SectionArea} \qquad 4.4.4.2$$

4.4.5 Hatch Corner

The hatch corner is a part in which the maximum vertical bending moment stresses are combined with high compressive stresses as a result of wave pressure at the side plates. Also, the large openings of the hatch introduce high stress concentration factors.

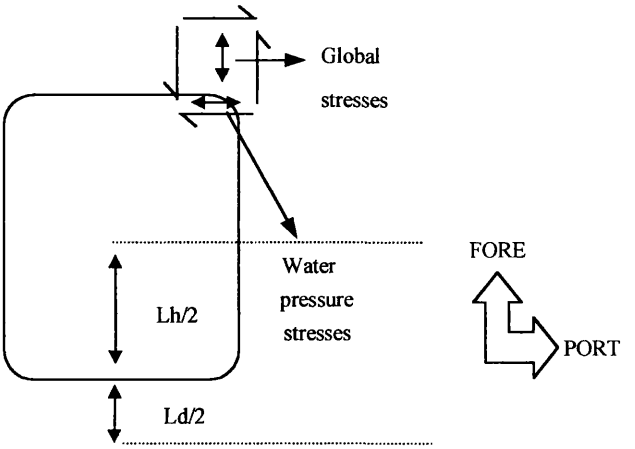

Figure 4.4.5.1 - The direction of stresses at the hatch corner.

The assumption made here for the load distribution is that the deck structure carries the load, which acts above two-thirds of the length of the side shell. The global bending and local compressive stresses were combined using the stress transformation equations.

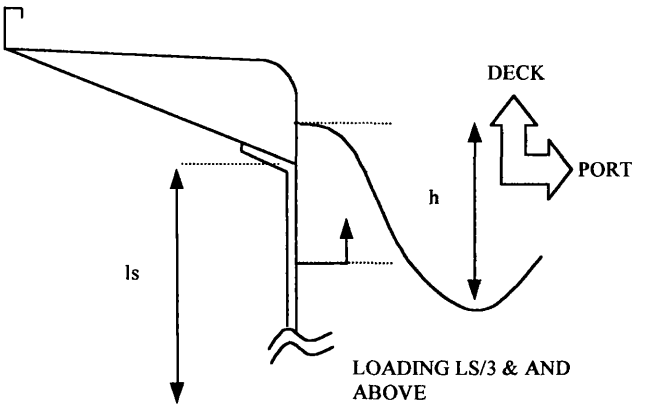

Figure 4.4.5.2 - The hydrodynamic loading model used to calculate the water pressure stresses affecting the hatch corner.

$$\sigma_{\varphi} = SCF_1 \cdot \sigma_x \cdot \cos^2\theta + SCF_2 \cdot \sigma_p \cdot \sin^2\vartheta + \tau \cdot \sin 2\theta \qquad 4.4.5.2$$

Where σ_x : is the global bending stress

σ_p : is the stress due to water pressure

τ : is the global shear stress

$$\sigma_p = \frac{(\frac{Ld}{2} + \frac{Lh}{2})}{\frac{Ld}{2} \cdot t} \cdot \int Pdh \qquad 4.4.5.2$$

The stress concentration factors SCF_1 and SCF_2 are a function of the geometry of the hatch opening, and were calculated according to Brock [16]. The graph can be found in appendix 10. The results are shown below:

SCF_1 =3.62

SCF_2 =3.8

4.4.6 Moments and forces in the plate between stiffeners

The calculations of the forces and moments acting on the plates between stiffeners were performed by assuming that the longitudinal/transverse stiffeners provide fixed

boundaries to the plates. This assumption is conservative, as illustrated in the figure below.

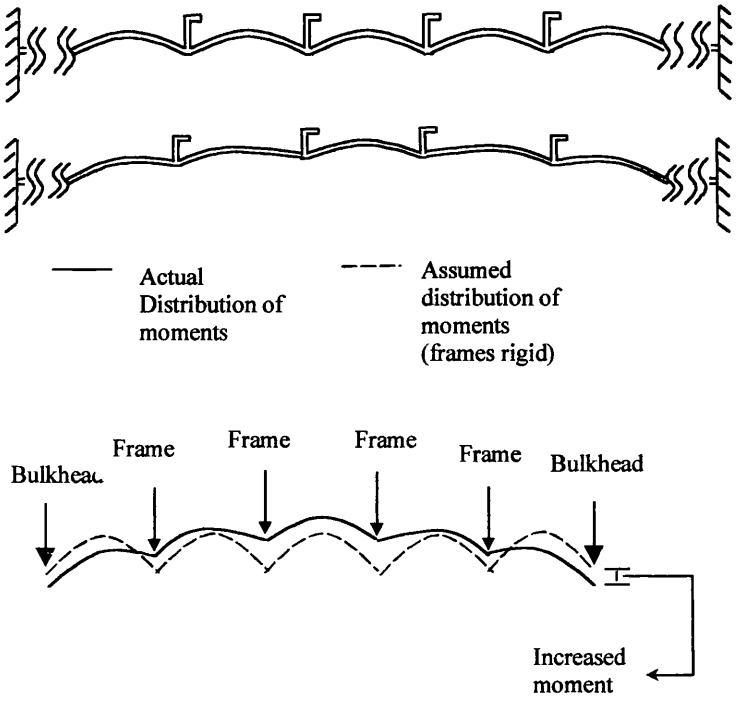

Figure 4.4.6.1 Actual and assumed distribution of moments

This methodology was used to calculate the stresses for the following details:

- Bottom longitudinal when water pressure is considered.
- Inner bottom longitudinal when water pressure is considered.
- Hopper longitudinal when water pressure is considered.
- Side shell transverse when water pressure is considered.

4.5 Stress Combination and Transformation

Assuming that stress and shear stress are known in a plane, the stresses and shear stresses in any plane inclined in ϕ degrees will be:

$$\sigma_{\varphi} = \sigma_y \cdot \sin^2\theta + \sigma_x \cdot \cos^2\theta + \tau \cdot \sin 2\theta \qquad 4.5.1$$

$$\tau_\phi = \frac{1}{2} \cdot (\sigma_x - \sigma_y) \cdot \sin 2\phi - \tau_{xy} \cdot \cos 2\phi \qquad 4.5.2$$

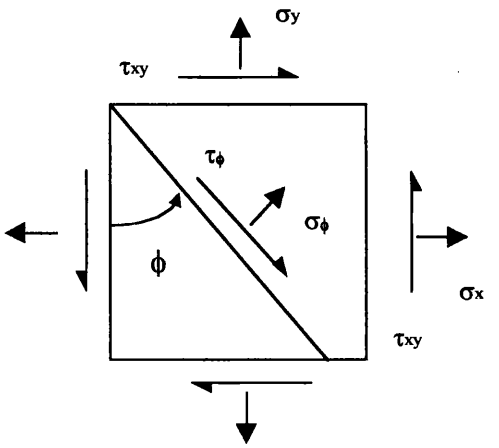

Figure 4.4.6.1 Stress and shear stress transformation

The above equations are valid when we are combining and transforming stresses and shear stresses in the same plane and in the same material (e.g. in a plate). In the following chapters, this project has to consider stresses that arise from the plates towards the welding material. An empirical formula was used:

$$\sigma_\theta = \sqrt{(\sigma_{wp})^2 + (\tau_{wp})^2} \qquad 4.5.3$$

Where

$$\tau_{wp} = \tau_p \cdot \frac{t_{foot}}{2 \cdot t_{weld}} \qquad 4.5.4$$

$$\sigma_{wp} = \sigma_p \cdot \frac{t_{foot}}{2 \cdot t_{weld}} \qquad 4.5.5$$

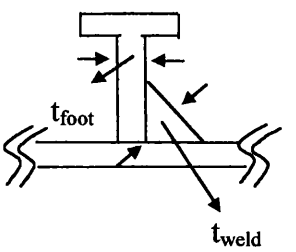

Figure 4.4.6.2 The stiffener and plate with the relevant thickness

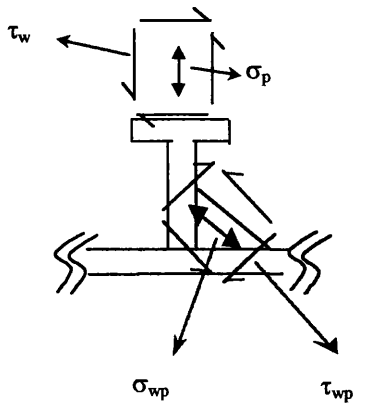

Figure 4.4.6.3 The stiffener and plate with the relevant stresses

Where σ_θ is considered to be the maximum resultant stress from the combination of induced stress and shear stress.

4.6 Discussion

This chapter concentrated in describing a methodology of assessing the structure with respect to global and local loading. The first section evaluated the ultimate hull girder capacity based on a simplified methodology. The capacity can be considered adequate when the section is as built. However when the effects of corrosion were included in the calculations the capacity reduced, reaching a value lower than the evaluated applied load with probability of occurrence approximately once in twenty years. It should be noted however that the methodology for the calculation of vertical bending moment capacity assumes that the maximum capacity is reached when the first stiffener fails either in compression or tension. In reality the capacity is usually higher since the rest of the panels are able to carry some more load.

The assumptions used to determine the boundary conditions of the structural components and sub-components can be considered conservative since in the ship structure there are essentially no components with fixed ends. The assumptions regarding the proportion of loading carried by the structural components and the boundary conditions are assessed for their validity in the next chapter. A finite element model was created so that we can compare the stresses evaluated with the ones obtained by the first principle methodology outlined above.

References

1. Coates, R. C., Coutie, M. G., Kong, F. K. , "Structural Analysis" , Nelson, London, 1980, 2nd edition

2. Meriam, J. L., Kraige, L. G. "Engineering Mechanics, Statics", John Wiley & Sons, New York, 1993, 3rd edition

3. Benham, P. P., Crawford, R. J., "Mechanics of engineering material", Longman Scientific and Technical, Harlow, 1987.

4. Cook, R. D., Young, W. C., "Advanced mechanics of materials", Macmillan Publishing company, New York, 1985

5. Rees, W. A., " The mechanics of solids and structures ", McGraw –Hill , London, 1990

6. Young C.W., "Roark's Formulas for Stress & Strain", New York, McGraw-Hill, 6th edition, 1989

7. Hughes, O., "Ship structural design: a rationally based, computer-aided, optimization approach.", John Willey & Sons, New York, 1983

8. Kollbrunner, C. F., Basler, K. ,"Torsion in Structures", Springer-Verlag, New York, 1969

9. Pedersen, T., "Beam theories for torsional–bending response of ship hulls", Journal of Ship Research, vol. 35, pp254, 1991

10. Senjanovic, I., Fan, Y., "Pontoon Torsional strength analysis related to ships with large openings", Journal of Ship Research, Vol. 35, pp 339, 1991

11. Rutherford S. E., "Ultimate Longitudinal strength of Ships: A case study", SNAME, Annual meeting 1990

12. Paik J.K, Doe K. H., Bong H. S., Kim S. M., Han S. K., "Deterministic and probabilistic safety evaluation for a new double-hull tanker with transverless system" trans. SNAME, Vol. 100, 1992, pp173-198

13. Damonte R., Figari M., Porcari R., "Ultimate bending moment of the ship hull girder", Int. Shipbuild. Progr. 44, no. 440 (1997), pp299-319

14. Smith, C. S. Dow, R. S., Hugill, J. D., Clark, J. D., "Evaluation of ultimate ship hull strength", Extreme loads response symposium , SNAME, 1981

15. Gordo J.M, Guedes Soares C., "Approximate method to evaluate the hull girder

collapse strength", Unit of Marine Technology and Engineering, Instituto Superior Tecnico, Universidade Tecnica de Lisboa

16. Brock J. S., "The Stresses Around Square Holes with Rounded Corners", Journal of Ship Research, vol. 2, pp37,1958

Appendix 9
APROXIMATE ULTIMATE STRENGHT CALCULATION
Methodology based on Hughes [7]

Material characteristics

$E := 0.207 \cdot 10^{12} \cdot kg \cdot m^{-1} \cdot sec^{-2}$

$\sigma op := 245 \cdot 10^{6} \cdot kg \cdot m^{-1} \cdot sec^{-2}$

$\nu := 0.3$

Plate characteristics

$t := 25 \cdot mm$

$b := 0.8 \cdot m$

$l := 0.8 \cdot m$

Stiffener characteristics

Breadth and thickness of flange

$bf := 41 \cdot mm$

$tf := 20 \cdot mm$

Height and thickness of web

$hw := 210 \cdot mm$

$tw := 11 \cdot mm$

Depth and hydrostatic pressure

$depth := 12.3 \cdot m$

$g = 9.807 \cdot m \cdot sec^{-2}$

$\rho := 1025 \cdot kg \cdot m^{-3}$

$q := \rho \cdot g \cdot depth$

$q = 1.236 \cdot 10^{5} \cdot kg \cdot m^{-1} \cdot sec^{-2}$

Mode 1 Compression failure of stiffener

Calculation of tripping stress for stiffener

$Af := bf \cdot tf$

$Aw := hw \cdot tw$

$Ax := Af + Aw$

$f := \frac{Af}{Ax}$

$Isp := hw^{2} \cdot \left(Af + \frac{Aw}{3} \right)$

$Isz := \frac{bf^{2} \cdot Af \cdot \left(\frac{Ax}{3} - \frac{Af}{4} \right)}{Ax}$

$\sigma at := \frac{\pi^{2} \cdot E \cdot f \cdot (1 - f)}{1 + 2 \cdot f} \cdot \left(\frac{bf}{l} \right)^{2}$

Calculation of critical applied stress

$$A := hw \cdot tw + bf \cdot tf + b \cdot t$$

$$ynao := \frac{\left(hw \cdot tw \cdot \frac{hw}{2}\right) + \left[bf \cdot tf \cdot \left(hw + \frac{tf}{2}\right)\right] - b \cdot t \cdot \frac{t}{2}}{(hw \cdot tw + bf \cdot tf + b \cdot t)}$$

$$I := \frac{1}{12} \cdot bf \cdot tf^3 + \frac{1}{12} \cdot tw \cdot hw^3 + \frac{1}{12} \cdot b \cdot t^3 + hw \cdot tw \cdot \left(\frac{hw}{2} - ynao\right)^2 + bf \cdot tf \cdot \left(hw + \frac{tf}{2} - ynao\right)^2 + b \cdot t \cdot \left(\frac{t}{2} + ynao\right)^2$$

$$\lambda := \frac{l}{\pi \cdot \sqrt{\frac{I}{A}}} \cdot \sqrt{\frac{\sigma op}{E}}$$

$$\Delta o := \frac{l}{750}$$

$$Mq := q \cdot b \cdot \frac{l^2}{24}$$

$$\delta o := \frac{q \cdot b^4}{32 \cdot E \cdot t^3}$$

$$ys := hw + tf - ynao$$

$$\eta := \frac{(\delta o + \Delta o) \cdot ys}{\left(\frac{I}{A}\right)}$$

$$\mu := Mq \cdot \frac{ys}{I \cdot \sigma op}$$

$$\zeta := 1 - \mu + \frac{1 + \eta}{\lambda^2}$$

$$R := \frac{\zeta}{2} - \sqrt{\frac{\zeta^2}{4} - \frac{1 - \mu}{\lambda^2}}$$

$R = 0.875$

$$\sigma c1 := \begin{cases} (R \cdot \sigma op) & \text{if } \sigma op < \sigma at \\ (R \cdot \sigma at) & \text{if } \sigma op > \sigma at \neq 0 \end{cases}$$

$\sigma c1 = 2.144 \cdot 10^{8} \cdot kg \cdot m^{-1} \cdot sec^{-2}$

Mode 2 Compression failure of plate

$$\sigma cr := \frac{\pi^2 \cdot E}{\left[12 \cdot \left(1 - \nu^2\right) \cdot \left(\frac{b}{t}\right)^2\right]}$$

$$\delta o := \frac{b}{200}$$

Calculation of m magnification factor (the first value is guess value)

$m1 = 1$

$$\text{root}\left[0.7 \cdot \left(\frac{\delta o}{t}\right)^2 \cdot m1^2 - \frac{1}{m1} - \frac{\sigma op}{\sigma cr} - 0.7 \cdot \left(\frac{\delta o}{t}\right)^2 + 1, m1\right] = 5.494$$

$m1 = 5.49$

Residual stress and the corrections applied

$$\alpha := \frac{b}{t} \cdot \left(\frac{\sigma op}{E}\right)^{0.5}$$

$\alpha = 1.101$

$\sigma ri := 0.1 \cdot \sigma op$

$$\sigma r = \begin{cases} 0 & \text{if } \alpha < 1 \\ \left(\sigma ri \cdot \frac{\alpha - 1}{0.6}\right) & \text{if } 1 \leq \alpha \leq 1.6 \\ \sigma ri & \text{if } \alpha > 1.6 \end{cases}$$

$\sigma r = 4.12 \cdot 10^{6} \cdot kg \cdot m^{-1} \cdot sec^{-2}$

Calculation of n magnification factor (the first value is guess value) with assumed residual stress equal to 10% of yield stress

$n := 0.5$

$$\text{root}\left[0.7\cdot\left(\frac{\delta o}{t}\right)^2\cdot n^2 - \frac{1}{n} - \frac{\sigma r}{\sigma cr} - 0.7\cdot\left(\frac{\delta o}{t}\right)^2 + 1, n\right] = 1.022$$

$n := 1.022$

$$\sigma := \sigma cr\cdot\left(1 - \frac{1}{m1}\right) + 0.375\left(1 - \nu^2\right)\cdot\sigma cr\cdot\left(\frac{\delta o}{t}\right)^2\cdot\left(m1^2 - 1\right)$$

$\sigma = 1.96\cdot 10^8 \cdot kg\cdot m^{-1}\cdot sec^{-2}$

$$\varepsilon := \frac{\sigma cr\cdot\left(1 - \frac{1}{m1}\right) + 0.375\left(1 - \nu^2\right)\cdot\sigma cr\cdot\left(\frac{\delta o}{t}\right)^2\cdot\left(2\cdot m1^2 - n^2 - 1\right)}{E}$$

$\varepsilon = 1.172\cdot 10^{-3}$

$$K := \frac{\sigma}{E\cdot\varepsilon}$$

$K = 0.808$

$be := K\cdot b$

Position of Neutral axis taking into account the effective breadth

$$yna := \frac{\left(hw\cdot tw\cdot\frac{hw}{2}\right) + \left[bf\cdot tf\cdot\left(hw + \frac{tf}{2}\right)\right] - be\cdot t\cdot\frac{t}{2}}{(hw\cdot tw + bf\cdot tf + be\cdot t)}$$

Moment of Inertia and area of the stiffener and plate with effective breadth

$$Ie := \frac{1}{12}\cdot bf\cdot tf^3 + \frac{1}{12}\cdot tw\cdot hw^3 + \frac{1}{12}\cdot be\cdot t^3 + hw\cdot tw\cdot\left(\frac{hw}{2} - yna\right)^2 + bf\cdot tf\cdot\left(hw + \frac{tf}{2} - yna\right)^2 + be\cdot t\cdot\left(\frac{t}{2} + yna\right)^2$$

$Ae := hw\cdot tw + bf\cdot tf + be\cdot t$

$ys := t + ynao$

$$\lambda := \frac{l}{\pi\cdot\sqrt{\frac{Ie}{Ae}}}\cdot\sqrt{\frac{\sigma op}{E}}$$

$$\Delta o := -\frac{l}{750}$$

$$Mq := q \cdot b \cdot \frac{l^2}{24}$$

$$\delta o := \frac{q \cdot b^4}{32 \cdot E \cdot t^3}$$

$$ys := hw + tf - ynao$$

$$\eta := \frac{(\delta o + \Delta o) \cdot ys}{\left(\frac{I}{A}\right)}$$

$$\mu := Mq \cdot \frac{ys}{Ie \cdot \sigma op}$$

$$\zeta := 1 - \mu + \frac{1 + \eta}{\lambda^2}$$

$$R := \frac{\zeta}{2} - \sqrt{\frac{\zeta^2}{4} - \frac{1 - \mu}{\lambda^2}}$$

$$R = 0.875$$

$$\sigma c2 := R \cdot \sigma op$$

$$\sigma c2 = 2.143 \cdot 10^8 \cdot kg \cdot m^{-1} \cdot sec^{-2}$$

$$\sigma c1 = 2.144 \cdot 10^8 \cdot kg \cdot m^{-1} \cdot sec^{-2}$$

$$\varepsilon ult := \begin{cases} \frac{\sigma c2}{E} & \text{if } \sigma c2 < \sigma c1 \\ \frac{\sigma c1}{E} & \text{if } \sigma c1 < \sigma c2 \end{cases}$$

$$\varepsilon ult = 1.035 \cdot 10^{-3}$$

Ultimate Strength Calculation

$$Itot := 1.857 \cdot 10^{14} \cdot mm^4$$

$ytot := 7504mm$

$\varepsilon y := \frac{\sigma op}{E}$

$yy := (17.2 - 7.504) \cdot m$

$yult := 7304mm$

$\phi ult := \left| \frac{\varepsilon ult}{yult} \right|$

$M := E \cdot Itot \cdot \phi ult$

$M = 5.451 \cdot 10^{9} \cdot kg \cdot m^{2} \cdot sec^{-2}$

Appendix 10 Stress concentration factor calculation for the hatch corner

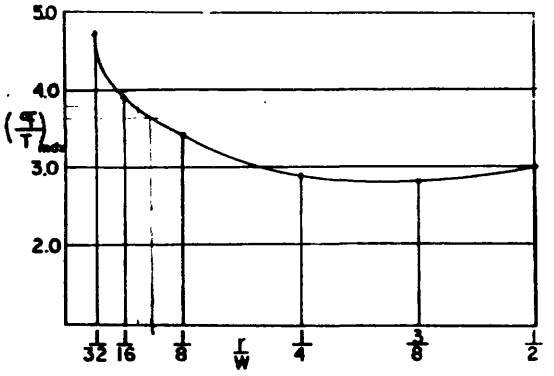

Fig. 4 Maximum stress as a function of r/W for Case 1. Tension parallel to side of square

Stress concentration factor calculation from Brock[16]

Chapter 5

Finite Element Model

5.1 Introduction to the finite elements

In the previous chapter we discussed the structural behaviour of the major components and sub-components that comprise the vessel by applying simple beam theory and assuming various boundary conditions. The actual structural behaviour is more complicated and the only engineering tool available that can provide a better approximation of the real behaviour is finite element analysis. Finite element analysis might be defined simply as a procedure in which the structure is broken down into a number of elements for which predefined equations exist to describe their behaviour. These elements are connected at certain points (nodes). The introduction of loading and supports allows a number of simultaneous algebraic equations to be written and solved.

5.2 Literature survey

The combination of structural analysis, matrices and the development of the digital computer led, in the early 1950s, to the first application regarding frameworks pioneered by Livesley [1]. The needs of the aircraft industry with respect to safety and weight led to the refinement and expansion of the capabilities of the analysis. Finite element analysis became widely used by engineers in other fields, as computers became faster and cheaper and as the method was continuously improved and enhanced. In the last fifty years thousands of papers and books have been written regarding the mathematical formulation of solution procedures and elements, structural applications and overall discussions of methodologies, modelling and result appraisal. The literature survey focuses on documents that provide useful information with respect to finite element idealisation and guidelines for the overall procedure of pre- and post-processing.

NAFEMS is a public organisation charged with maintaining standards and quality assurance in finite element technology in the U.K. The book "A finite element primer" [2], published by the above-mentioned organisation, describes the fundamental concepts of finite element analysis by including a limited portion of mathematical formulations. Static problems are discussed and the most common elements, including their applicability and limitations, are presented. Other problems, such as dynamic, non-linear elasto-plastic, buckling and heat transfer problems, are also discussed, with examples and

general remarks. The last part presents a considerable amount of information regarding the modelling of the structure, including its supports, loading and constraint equations. "Guidelines to finite element analysis" [3] published by NAFEMS offers recommendations, strategies and advice that can help the analyst organise the problem and perform the analysis in a systematic way. Both of these books are very instructive and helpful since they provide information that is normally possessed by experienced users.

Cook [4] presents his experience and thoughts regarding the finite element method. Beam and bar elements are discussed in the context of specific problems, using the stiffness method. Element formulation and linear static analysis are presented in an accessible fashion that enables the reader to acquire the knowledge needed for the book's very thorough discussion of the planning of the model, the detection of errors and the verification of results. It continues by discussing more complicated elements, as well as dynamic, buckling and non-linear problems.

The American society of civil engineers published a book [5] with similar aims to NAFEMS. It consists of a collection of papers by experienced users that discuss different components of linear and non-linear analysis. The discussions concentrate on the understanding of the limitations and possible errors rather than on the mathematical tools used to provide us with solutions. The paper that provided the most useful information is that of Ridlon, entitled " Modelling guidelines". It presents a guide to planning the analysis and discusses the various different aspects. It also provides modelling advice with specific examples, and explains through these the limitations of the various elements.

"Finite element analysis for thin-walled structures" [6] is a collection of papers regarding the application of finite element analysis to engineering problems. The first group of papers contains a significant amount of information regarding elements, modelling and possible errors. The second describes the application of the method to structures and discusses the results, approximations and limitations. The paper related to our study is written by Andrews. It considers the application of finite element analysis to a ship's structural design and discusses that of an aircraft carrier named *Invincible* in detail. Some features of the idealisation of the structure presented have been incorporated

into our model. The paper also discusses the uncertainties of loading in both global and local terms and its incorporation into the finite element model.

"Finite element methods in stress analysis" [7] is a collection of papers presenting the subject from theoretical and practical points of view. Emphasis is provided in element formulation and its application to engineering problems with a comparison of exact and finite element solutions. The most interesting paper with respect to our analysis is that of Moe, which describes the various types of elements and discusses their applicability. Also, it demonstrates the sub-structuring technique for analysing big and complex structures such as a complete ship hull.

Irons and Ahmad [8] present the finite element analysis with prominence upon educational and mathematical aspects. They cover the subject from the programmer's point of view, and attempt to associate the mathematical and physical meanings of the method and provide good guidance and explanations for anyone that would like to become involved in programming methodology with respect to the subject. It is a particularly well-written book with a characteristic style and it provides the background formulation of the finite element programs. Irons and Shrive [9] present the finite element method from the educational point of view with the same characteristic accessible style as Irons and Ahmad. The book essentially describes a course in finite element analysis with simple examples and clear explanations for when and how elements may provide an unreliable solution to problems. Although neither of the two previously mentioned books directly contributed to the formulation of the model and the processing of the results, they helped us acquire basic knowledge and understanding by virtue of an accessible and well-researched text.

There is a large number of other text books that describe the basic principles and mathematical formulation of the finite element method. Laursen [10] describes the application of matrices to structural analysis and demonstrates their uses with various examples and problems with respect to linear static analysis. Hall and Woodhead [11] and Rubinstein [12] offer a more advanced text than the one mentioned above. Both books assume limited mathematical knowledge of matrix analysis and unfold their structural analysis technique in an easy-to-understand fashion.

5.3 Finite element idealisation

Simple linear elastic analysis was selected as appropriate for our problem, since the geometry of the vessel under loading does not change significantly. Moreover, we assume that the material's (steel) stress will be proportional to strain irrespective of loading. This type of analysis provides a reasonable idealisation of the structural behaviour and reduces computational time. The computer package used was Lusas by FEA.

Computational time for any engineering problem introduces direct and indirect costs to the analysis. The required results essentially define the complexity of the finite element model. Barltrop [13] discusses the subject for ship and offshore structures and subdivides the models into three categories of complexity. The first involves very simple skeletal/beam models in which the properties of the cross section of the ship are modelled by a single beam attached to other beams to represent the varying geometric properties of the hull girder. It can be used to examine global behaviour under conditions of wave slamming and other hydrodynamic loads. The second is a composite model comprising beam, membrane, shell and bar elements with each element assigned to serve one or two particular roles and, therefore, combining to simulate the structural behaviour. This type of modelling is suitable for overall local and global forces induced upon the structure by a particular loading. The third is the most complicated and involves more accurate representation of the structure. It is time-consuming with respect to modelling and solving and most appropriate for fatigue calculation and the detail distribution of local loads. Most books mentioned in the previous section recommend a "ladder" analysis, wherein a relatively simple model is first created and then, according to the results, the mesh is refined in areas of stress concentration or of particular concern. Since the aim of our analysis is to determine the structural behaviour of the major sub-components of the structure and examine the assumptions of the previous chapter, the second category of modelling was deemed to be most appropriate. Due to time constraints, it was necessary that the first step of the "ladder" be completed.

A three dimensional model is needed in order to study the overall transverse and longitudinal structural behaviour. The model extends over three cargo holds in the parallel mid-body so that the boundary conditions effects are minimised. The length is

equal to two cargo holds as recommended by Lloyds [14] and ABS [15], although it was decided to represent both sides of the ship rather than impose symmetry conditions at the centreline. Symmetry conditions are usually imposed to decrease the computational requirements of the analysis. However, in our case, the elements used and the degree of detail in our model, combined with the computational power available, allow us to analyse the structure with its full breadth.

The structure was represented by beam elements that have axial, torsional and bi-directional shear and bending stiffness, and with constant properties along the length of the member. Two major difficulties had to be overcome. The first was the idealisation of the stiffeners and the second was the inclusion of the shear stiffness of the structural components. Barltrop [13] discusses the possible ways of including the bending effects of the stiffener, not only for the case of a beam model, but also for when plate elements are included in the model. With respect to our model, two possible methods are discussed. The first way to represent the stiffener is the "offset", in which the known inertia and area of the stiffener are assigned at a distance (offset) equal to half the plate thickness and the neutral axis of the stiffener. The second way to represent the stiffener is the "coplanar", in which the combined structural properties of the stiffener and the plate are calculated using an effective width for the plate. Although the second method requires more computation, it was considered more appropriate, since the first requires twice the number of elements. Moreover, the eccentricity should be assigned to the correct side of the plate. The effective width of the plates was calculated according to a table in Young's book [16]. The stiffeners and their effective plating were built into groups of four or five and their structural properties simulated by a beam element.

Shear effects are thoroughly discussed by Hughes [17] and Andrews [6]. There are two possible ways of representing the shear stiffness. The first involves the introduction into the structure of diagonally positioned bar elements. Bar elements are also referred to as rod or truss elements, and possess only axial stiffness and a constant cross-sectional area along their length. Andrews [6] presents a formula to calculate the area of the bar element so that it has equivalent behaviour in shear with the plate which it substitutes in the model. The second involves the introduction of membrane elements with the same

thickness designed only to resist shear in the transverse direction and not bending. The first method was used and the equation used to calculate the cross sectional area [6] is:

$$A_{fb} = 0.2 \cdot t \cdot \frac{a^2 + b^2}{b} \qquad 5.3.1$$

Where:

A_{fb}: Fictitious area of bar

a: Frame spacing

b: Longitudinal spacing

t: Plate thickness

The use of the second method was prohibited by computer related restrictions that where experienced when the finite element model shown in figure A11.8 was completed. The automatic meshing program produced a mesh, which exceeded the capabilities of the computer hardware available. The complex irregular mesh occurred because the beam elements, which for example modelled the hopper top, had different geometrical properties for the simulation of the different stiffness at the ends. It is interesting to note that the first method is usually the most common and was extensively used in the past when the abilities of the digital computers were more restricted. The finite element model used with distinction with respect to their element is shown in figure A11.2. Higher order element types exist. However, the above-mentioned simple elements according to ABS [15] are sufficient for the representation of the hull girder.

Material properties are considered to be elastic and isotropic. The Young modulus used is E = 207000 N/mm^2 and the Poisson's ratio ν = 0.3 typical for steel.

5.4 Supports and loading applied to the finite element model

The supports or boundary conditions prevent the appearance of mechanisms in the model when load is applied. Their presence, if adequate, will restrain the structure from producing infinite displacements in any axis of freedom. The number and positioning of the supports depends essentially on the problem studied. However, if we assign supports to inappropriate nodes or over-restrain the structure, forces and moments will be induced in the modelled structure that do not exist. The reason is that when loading is applied, and

the structure deforms inappropriate supports will hinder the deformation and change load paths producing stresses and strains that do not reflect reality. The nodes where supports should be applied are those that in reality are fixed (e.g. the foundations of a building). However, we are analysing a floating structure that in reality is supported by buoyancy forces and there are no fixed points/nodes. We need to assign supports at nodes that are distant from the part of structure studied and relatively stiff with respect to the rest of the structure. The section under consideration is in the middle of the central cargo hold, for both local and global loading. The above, in combination with the fact that the transverse bulkheads are the stiffest parts of the structure, lead us to the conclusion that supports should be assigned to nodes on the transverse bulkheads. The number of supports should be adequate to prevent the structure from moving in the six degrees of freedom. The supports assigned to the model for both loading conditions are shown in figure 5.4.1. Rotational restraints have not been used since they induce forces and moments that do not appear in the actual structure. The structure is prevented from rotating by two axial restraints for each rotational degree of freedom.

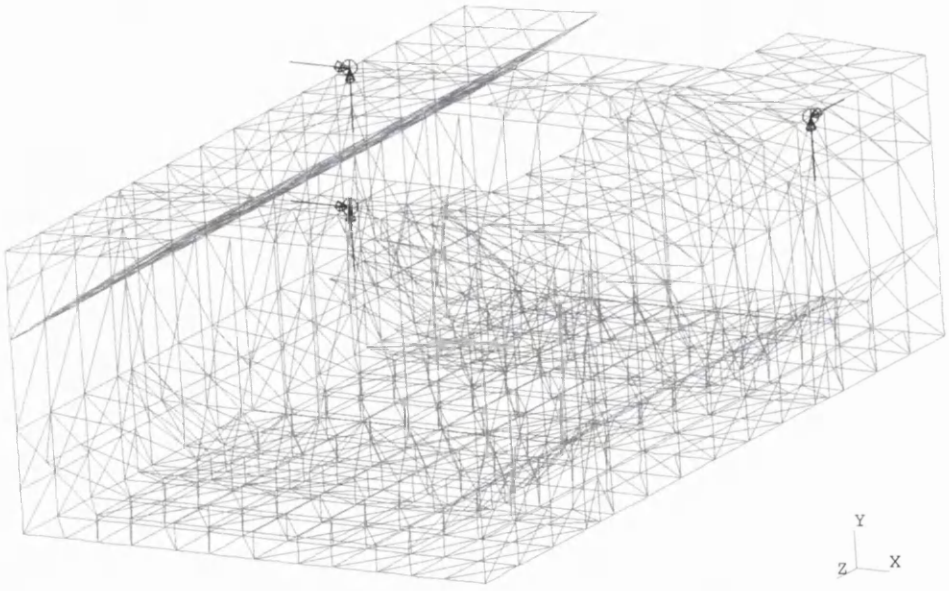

Figure 5.4.1 Restraints assigned to the structure

It should also be mentioned that supports can be used to model symmetry (the rest of the structure). In our case, with respect to local loading, we assume that the transverse interaction of the structure is limited to the extent of the transverse bulkheads. This

assumption should reflect reality, since that part of the structure is reinforced by the lower stool, upper stool and transverse ring webs in the tanks, if not by full transverse bulkheads. In the case of global loading, the rest of the structure was modelled by assigning the constraints to the fore and aft ends of the model. The constraints are defined for each end so that it can displace or rotate in any direction with the restriction that all the transverse elements at the ends remain straight. The constraints can be viewed in figure A11.2 (note that the different colour represents the fact that the constraints are independent to each other but are not different).

The heavy water ballast condition was selected as a basis for the analysis of the transverse structural behaviour. The hydrostatic load on the side of the structure, for reasons of simplicity, was assumed to be linear and to reach the upper end of the side shell transverse stiffener. The aim of the local analysis is to examine the boundary condition discussed in the previous chapter. An attempt to represent the actual loading for this would necessitate spending precious time on modelling the loading and calculating the assumed first-principles structural behaviour. Figure 5.4.2 shows the load applied to the cross section in the middle of the central hold. Figure A11.1 shows the three dimensional distribution of load and the distributed loading is shown in appendix 12.

Global loading was represented by inducing the vertical bending moment with probability of occurrence being 10^{-8} (around twenty years). The constraints discussed previously were included. The moments were applied at one node at each end positioned at the centre line with a vertical distance equal to the neutral axis and connected to the structure with elements included in the constraint (figure A11.3). Figure 5.4.3 shows the profile of the model with the applied load, and in figure A11.3 the three-dimensional equivalent, including the constraint planes, is shown.

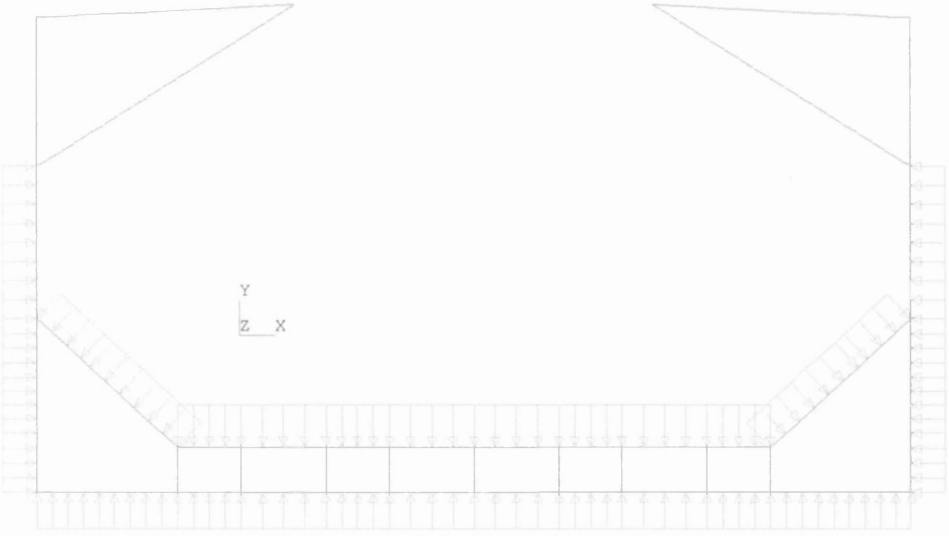

Figure 5.4.2 Local loading on the cross section in the middle of the central hold.

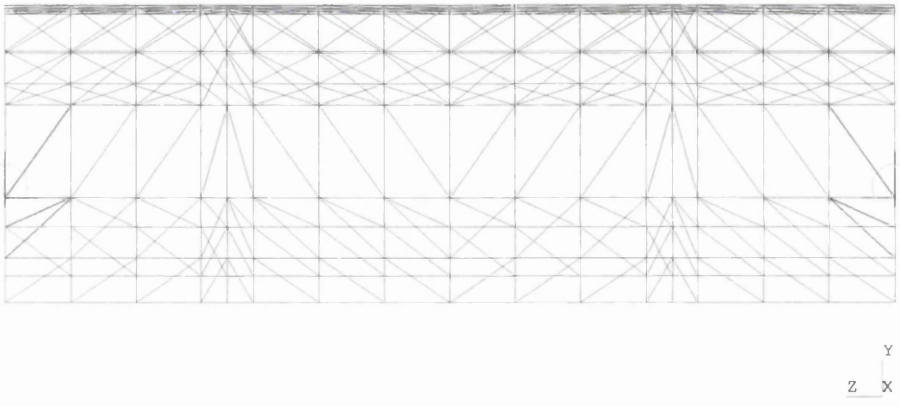

Figure 5.4.3 Global loading.

5.5 Hull structure local behaviour

The deformed shape of the section in the middle of our model can be seen in figure 5.5.1(additionally the superimposed deformed and undeformed shape can be viewed in figure A11.4). The loading applied to the model deforms the double bottom in a fixed end beam-like fashion. The hopper tanks tend to rotate inwards imposing the boundaries upon the double bottom and the side shell, which deforms as predicted in the previous chapter. However, the boundary conditions are, of course, not fixed-ended, since the rest of the structure also deforms.

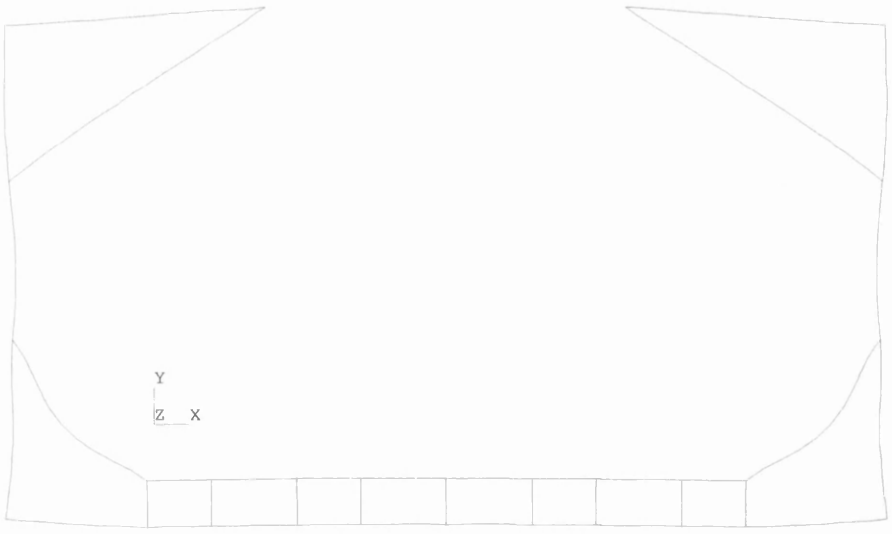

Figure 5.5.1Deformed shape of the section in the middle of the model

In figure 5.5.2, the local and global planes are shown, and in figure 5.5.3 the distribution of moment in local z direction is shown. The distribution shows us three points on the structure at which concentrations of fixed-end moments occur: the side shell connection with the hopper tank and the two connections of the hopper with the double bottom. A numerical comparison of the stresses for each component separately follows and in appendix 12 the first principles calculations are shown.

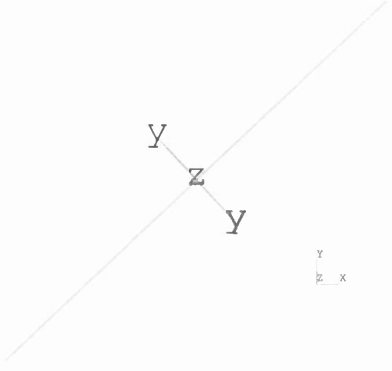

Figure 5.5.2 Local and global co-ordinate system (planes)

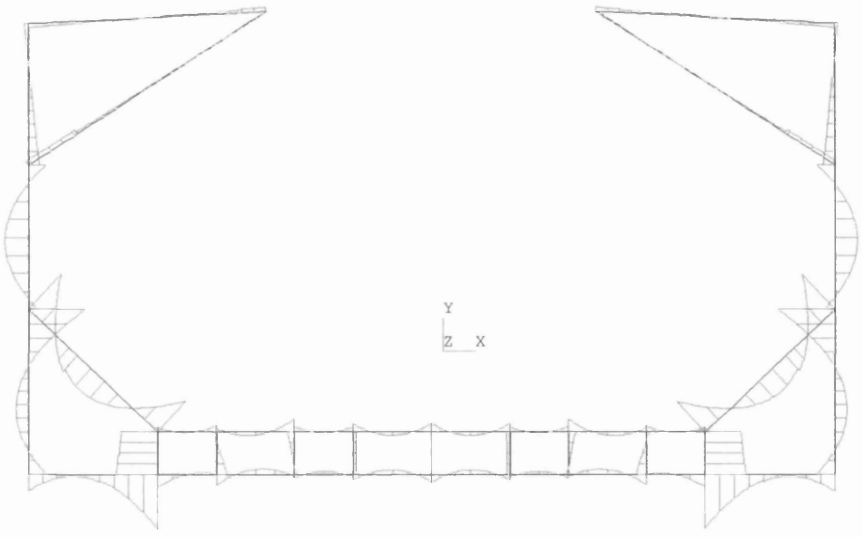

Figure 5.5.3 Distribution of local bending moment in the z direction

Section 1 Transverse behaviour of the double bottom

The double bottom deforms in two distinct ways (figure 5.5.4). The first is the overall local shape and the second is the local deformation between the double bottom girders. The interesting deformation is the global bending of the double bottom. The double bottom bends towards the deck rather than the sea, but since the loading inside the hold is higher than the water pressure outside, we would expect the opposite. This is probably the result of poor modelling of the transverse webs in the double bottom. In a numerical comparison, the global axial, local bending and global bending induced stresses were calculated and are shown in the table below.

Type of Loading	Finite Elements	First Principles
Global transverse axial force	16.52 N/mm^2	15.59N/mm^2
Local Bending	2.65 N/mm^2	2.755 N/mm^2
Global bending of double bottom	3.89 N/mm^2	5.229 N/mm^2

Table 5.5-1 Stress in double bottom

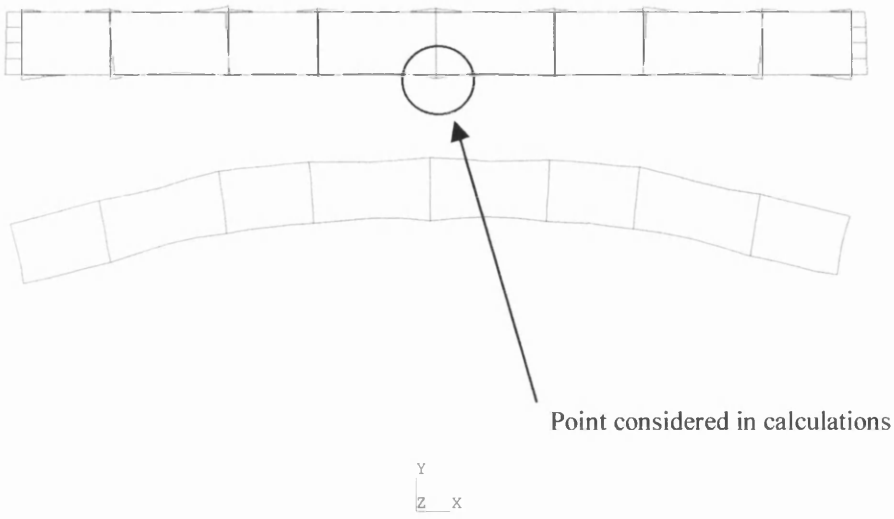

Figure 5.5.4 Bending moment distribution and deformed shape of the double bottom.

The bottom and keel plates are compressed. The global axial and global bending stresses were found by considering the axial forces midway the double bottom at the keel and bottom elements. The axial forces were subtracted one from the other and divided by two so providing us with the force induced by global bending. The first principles calculations can be found in section 1 of appendix 12.

Section 2 The hopper tank behaviour

The hopper tanks deform as expected by an overall rotation towards the hold and a bending of the beams representing the sides of the hopper tanks. The distribution of local moments in the z direction can be seen in figure 5.5.5, and it is interesting to note the high values of the local moment at the three connections with the rest of the structure. In table 5.5-2 the results produced from the two different methods are shown. The stresses from the finite element model are from the beam element connecting the double bottom with the upper hopper corner w and the first principles calculations can be found in section 2 of appendix 12. Again the axial, global bending and local bending stresses were considered. The global bending stress was calculated as in the previous section. Overall agreement is again achieved between the two methods. The axial stress from the first principles is different from the axial stress in the middle because the cross sectional area is different.

Type of Loading	Finite Elements	First Principles
Global transverse axial force	19.259 N/mm^2	17.102 N/mm^2
Local Bending	1.38 N/mm^2	2.046 N/mm^2
Global bending	1.94 N/mm^2	2.725 N/mm^2

Table 5.5-2 Stress at hopper tank corner

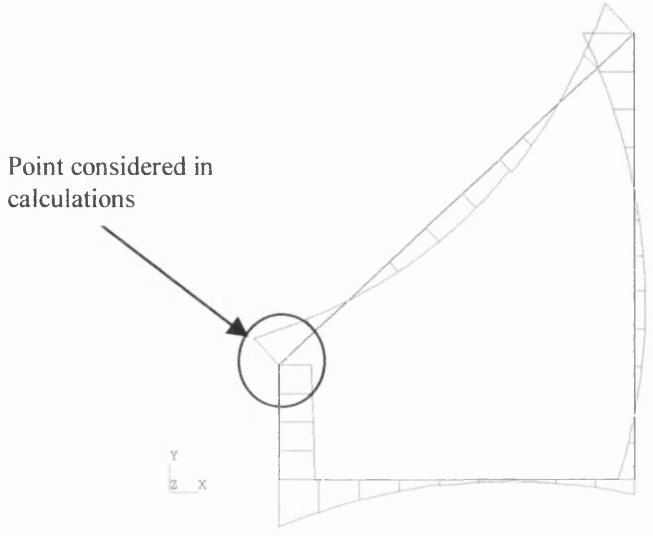

Figure 5.5.5 Bending moment distribution in local z direction and point for which calculations were performed (in the f.e. analysis from the element from the double bottom) at the hopper tank corner.

Section 3 Side shell bending

The side shell deforms as predicted by the first principle calculations and, therefore, the extent to which the boundary conditions are fixed-ended needed to be examined. The distribution of bending moment (figure 5.5.6) is altered by the deformation of the hopper and upper wing tank, decreasing the bending moment in the ends and increasing it in the middle. In the table below the hand calculation results are shown in comparison with the finite element results showing us that they are conservative for the ends and underestimating the stresses for the middle.

Position	Finite Elements	First Principles
Lower end	144.243 N/mm^2	204.272 N/mm^2
Middle	193.142 N/mm^2	102.136 N/mm^2

Table 5.5-3 Stress at side shell

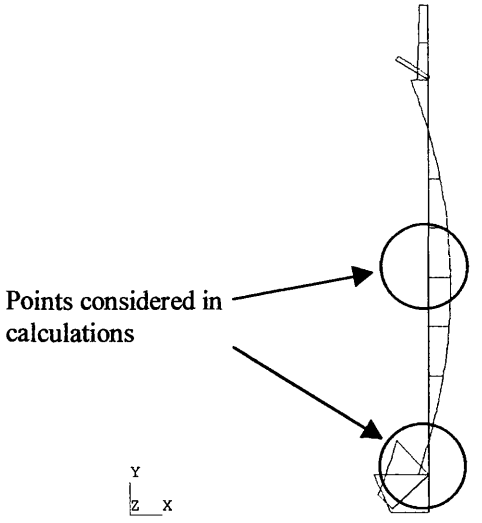

Figure 5.5.6 Bending moment distribution in local z direction at the side shell and points considered in the calculations.

Section 4 Deck

The deformation of the deck is more complex than that of the side shell. The deck deforms as a result of the transverse loading carried by the hoppers and the side shell. Essentially, it is compressed at both port and starboard ends. The deformation of the deck was restricted by the position of the supports (figure 5.5.9), so the supports were redistributed in the double bottom (figure A11.5 in appendix 11) for the calculation of the stresses at the hatch corner. Although this provided us with almost the same numerical results, it showed us the deformation of the deck without the interference of the supports (figure 5.5.8 also figuresA11.7 and A11.8). The existence of the large hatch opening alters the distribution of the forces and causes stress concentration in the corners of the hatch. The strips between the hatch and the edge of the deck tend to bend outwards and the strips that connect the port and starboard sides tend to bend inwards. The first bending is due to the rotation of the upper wing tanks, which reduces in the hold ends because of the support provided by the transverse bulkhead. The second inward bending is caused by the transverse bulkheads, which translate towards the double bottom (figure A11.9). The deformations are of the order of two to seven millimetres and the translation in global y direction of representative nodes at the deck is shown in figure 5.5.8. There are two main uncertainties, one regarding the loading and the other regarding the stress concentration factor. The assumption in chapter 4 is that the loading applied to the upper one-third length of the side shell is carried by the deck (method 1). The force acting on the deck

calculated for equilibrium in section 1 provides a higher value (method 2). The finite element model provided a number close to the second assumption. The stress concentration factor at the hatch corner is approximately 4 for the transverse loading (chapter 4), to verify this a refined mesh is needed at the hatch corners. The first principles calculations can be found in section 4 of appendix 12. Good agreement is found between the finite elements and method 2.

Position	Finite Elements	First Principles (m1)	First Principles (m2)
Deck strip	100.943 N/mm^2	43.975 N/mm^2	96.75 N/mm^2

Table 5.5-4 m1 and m2 imply methods 1 and 2 also the f.e. stress shown is the average of the three points shown in figure 5.5.9

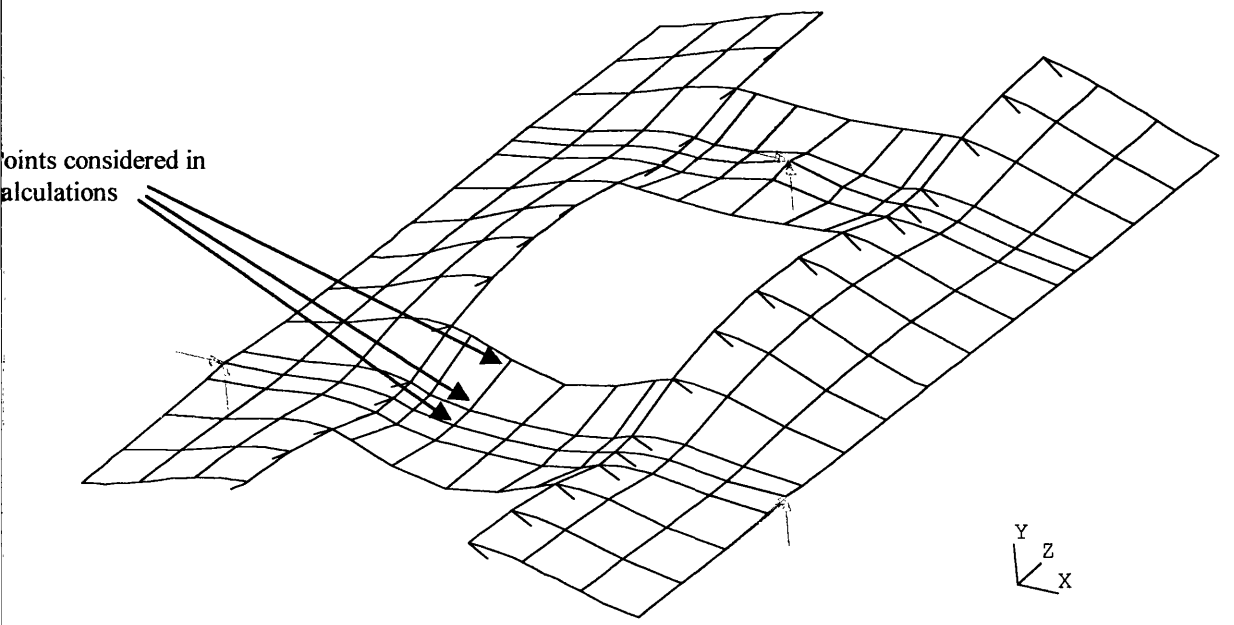

Figure 5.5.7 Deformed shape of the deck with initial supports.

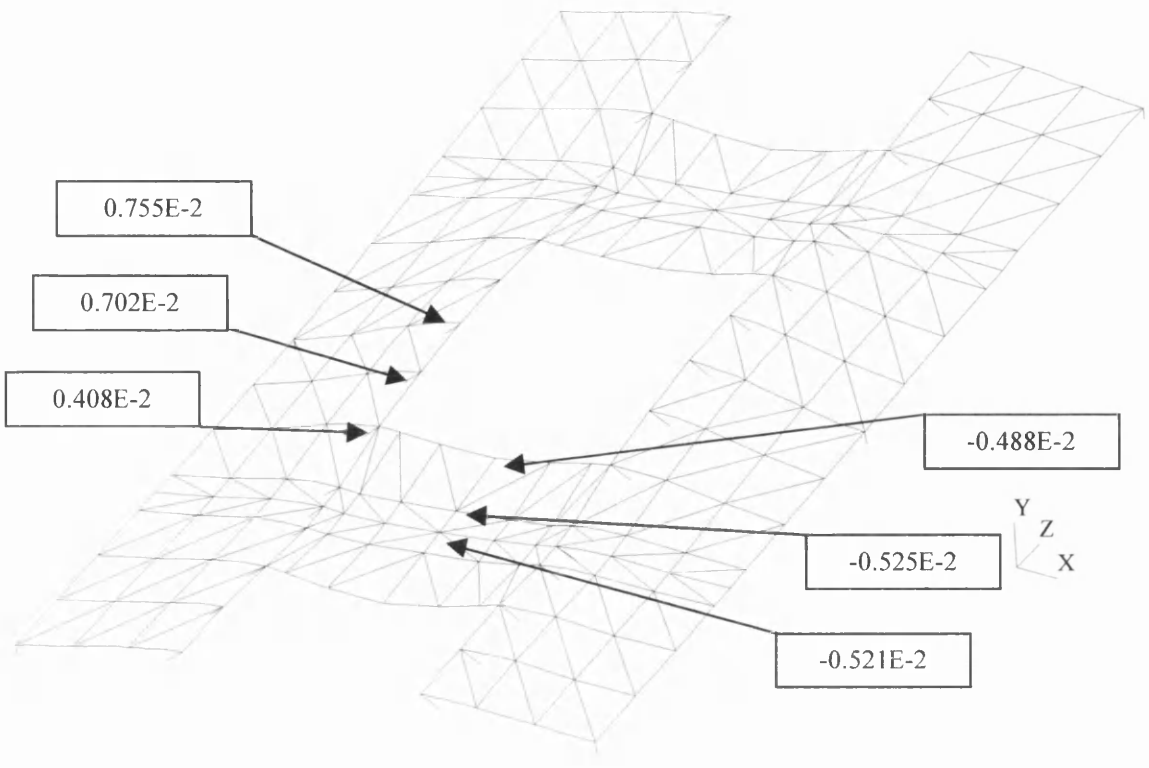

Figure 5.5.8 Deformed shape of the deck with the alternative supports and the translation of the nodes in the y direction (units in meters)

5.6 Hull structure global behaviour

Simple beam theory was used to compare the results obtained by the finite element model. ABS [14] recommends its use for checking, if appropriate modelling, boundary conditions and loading are used. This is because it argues that both bending stresses and deflections are usually in good agreement with beam theory irrespective of the open deck configuration. Stresses were calculated for the centre section of our model at the side (table 5.6-1). The distance (y) shown in the table is measured from the neutral axis with positive towards the deck and negative towards the bottom. The sine is not carried to the stresses. The stresses from the bottom to the neutral axis are compressive and the stresses from the neutral axis to the deck are tensile

y values (m)	Beam Theory(N/mm^2)	F. E. (N/mm^2)
10.294	252.4	257.9
7.874	193.0	214.7
4.694	115.1	117.3
-1.006	24.7	20.1
-4.746	116.4	105.3
-7.506	184.0	174.5

Table 5.6-1 Comparison of finite element and beam theory results

Comparison of the results shows good overall agreement except for the position near the neutral axis. The maximum stress is on the deck where high tensile steel is used with a yield strength of 326 N/mm^2.

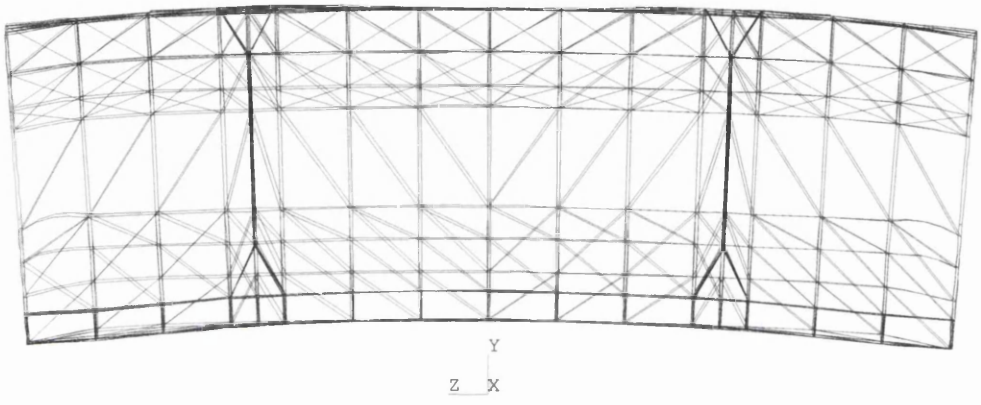

Figure 5.6.1 Deformed shape under global loading

5.7 Discussion

The methodology presented in the previous chapter for stress calculations for various parts of the structure was assessed using a beam/bar finite element model both for local and global loading. The assessment revealed good agreement with respect to global results but some weaknesses with respect to the first principles local methodology assumed in the previous chapter. Overall, this chapter provided us with a better understanding of the behaviour of the structure under loading.

The comparison of the hand calculations with the finite element would have been more informative if we included more loading conditions and the transverse loading was more realistic. Also a better meshed model with plate elements was intended to be used (figure A10.8). However time constraints interacting with computer hardware constraints did not allow us to perform these calculations. The four points that the induced stresses

were calculated are discussed below.

- The stress in the double bottom results from axial, local bending and global bending of the double bottom. The dominant stress is the axial stress, which is induced by transverse loading. The two different methods provided similar results (f.e.: 16.5 N/mm^2, f.p.: 15.59 N/mm^2) although the first principle method depended on the load carried by the lower stools. The local bending stress is in full agreement (f.e.: 2.65 N/mm^2, f.p.: 2.755 N/mm^2) with the first principles higher due to the fixed end boundary assumption. The global bending has a difference (f.e.: 3.89 N/mm^2,f.p.: 5.229 N/mm^2) due to the modelling error of the transverse webs in the double bottom.
- The hopper tank rotates inwards and as for the previous calculations three types of stresses were calculated the axial, the local bending and the global bending. The dominant stress is the axial (f.e.: 19.259 N/mm^2, f.p.: 17.102 N/mm^2). The local and global bending stresses are reasonably close with the first principles methodology on the conservative side. (local bend. f.e.: 1.38 N/mm^2, f.p.: 2.046 N/mm^2, global bend, f.e.: 1.94 N/mm^2, f.p.: 2.725 N/mm^2)
- The side shell is induced to bending moments due to the transverse loading. Two points were considered one in the end and one in the middle. The first principle methodology was on the conservative side at the ends (f.e.: 144.243 N/mm^2, f.p.: 204.272 N/mm^2) and non conservative in the middle (f.e.: 193.142 N/mm^2, f.p.: 102.136 N/mm^2). The reason is that the rotation of the hopper tank releases the moment from the end and induces higher moment in the middle.
- The average transverse stress on the deck structure was calculated with two first principle methods and the finite element method. The second first principle method provided us almost the same result as the finite element method. (f.e.: 100.94 N/mm^2, f.p.: 96.7 N/mm^2). Unfortunately the stress concentration factor at the hatch corner could not be evaluated due to the insufficient mesh and computer problems faced when more complicated plated meshes were created.

The unexpected behaviour of the double bottom can be justified by the poor modelling of the transverse webs in the double bottom and the hopper tanks. This conclusion was reached after comparing the results of the finite element model with the

hand calculations. Being in a position to verify results generated from computer programs is important and useful as proven by the above case

Overall the first principle methodology presented in appendix 12 produces realistic results and the method can be easily applied for the calculation of the stresses on the bulk carrier structure.

References

1. Crisfield M. A., "Finite elements and solution procedures for structural analysis", Pineridge Press Ltd, Swansea, 1986

2. "A finite element primer", Nafems,1986

3. "Guidelines to finite element analysis", Nafems, 1984

4. Cook R. D., "Finite element modelling for stress analysis", John Wiley and Sons, New York, 1995

5. "Finite element idealization", ASCE, New York, 1987, edited by C. Meyer

6. "Finite element analysis of thin walled structures", Elsevier Applied Science, London, 1983, edited by J. W. Bull

7. "Finite element methods in stress analysis", Tapir, Trondheim, 1970

8. Irons B., Ahmad S., "Techniques of finite elements", Ellis Horwood Ltd., Chichester , 1986

9. Irons B., Shrive N.., "Finite element primer", Ellis Horwood Ltd., Chichester, 1983

10. Laursen H., "Matrix analysis of structures", McGraw-Hill., New York, 1966

11. Hall A. S., Woodhead R. W., "Frame analysis", John Wiley and Sons, London, 1961

12. Rubinstein M. F., "Matrix computer analysis of structures", Prentice Hall International, London, 1966

13. Barltrop N.D.P., "Floating Structures a Guide for Design and Analysis", BMT/OPL, 1998

14. "Structural Design Assessment procedure : Direct calculations – guidance notes", Lloyd's Register, April 1996

15. "Guidance for the finite element analysis of bulk carrier structures", The ABS Safehull system, ABS, August 1994

16. Young C.W, "Roark's Formulas for Stress & Strain", New York, McGraw-Hill, 6th edition., 1989

17. Hughes, O. "Ship Structural Design: A rationally based computer aided approach", John Wiley & Sons, New York,1983

Appendix 11 Explanatory figures regarding the finite element analysis

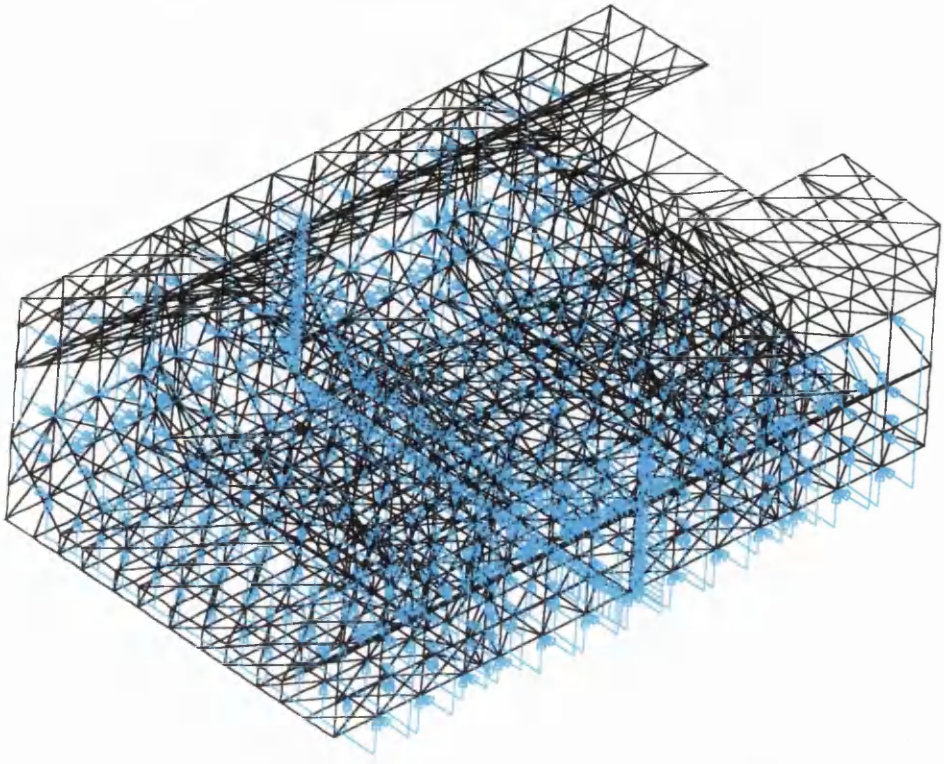

Figure A11 1 Loading applied to the model

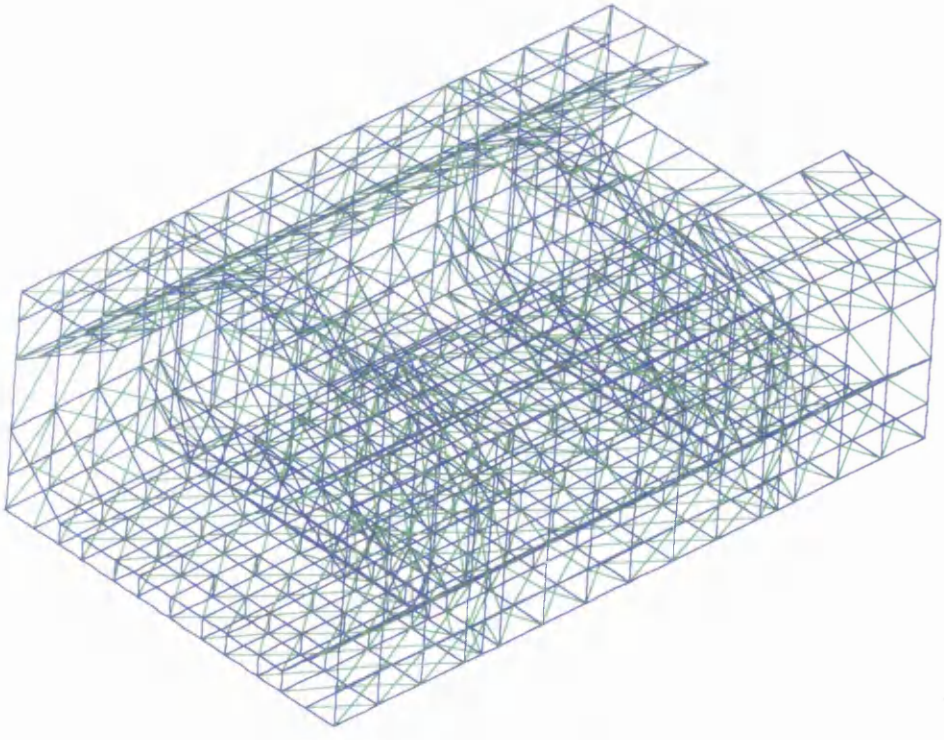

Figure A11 2 The two different types of elements used (blue beam elements – green bar elements

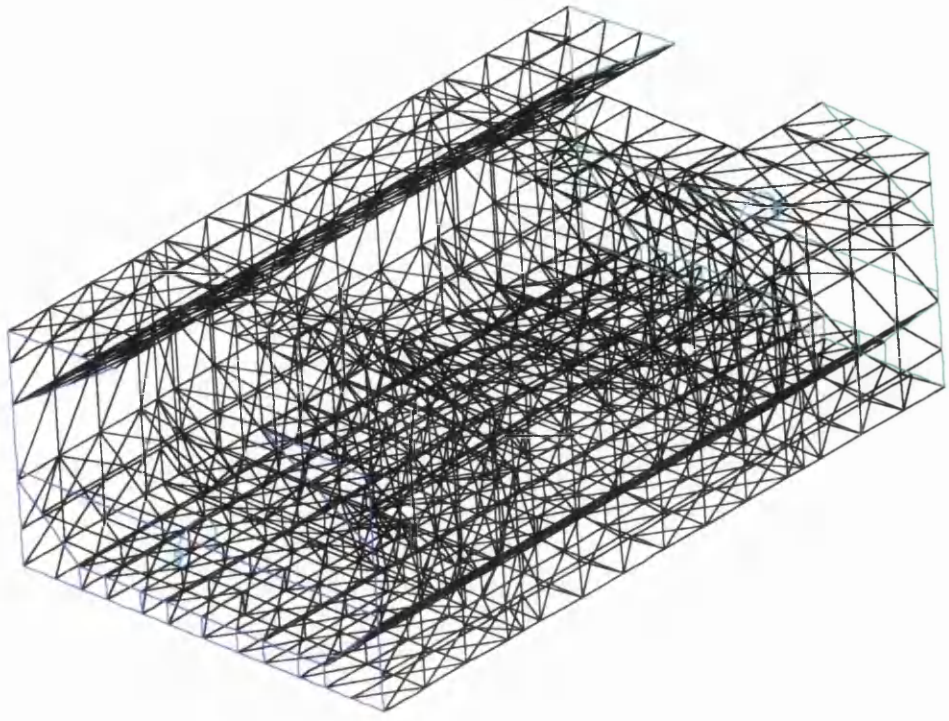

Figure A11 3 Constraint equation and loading applied to the ends for global loading (note different color of the region where the constraint equation was applied means that the two regions are independent of each other)

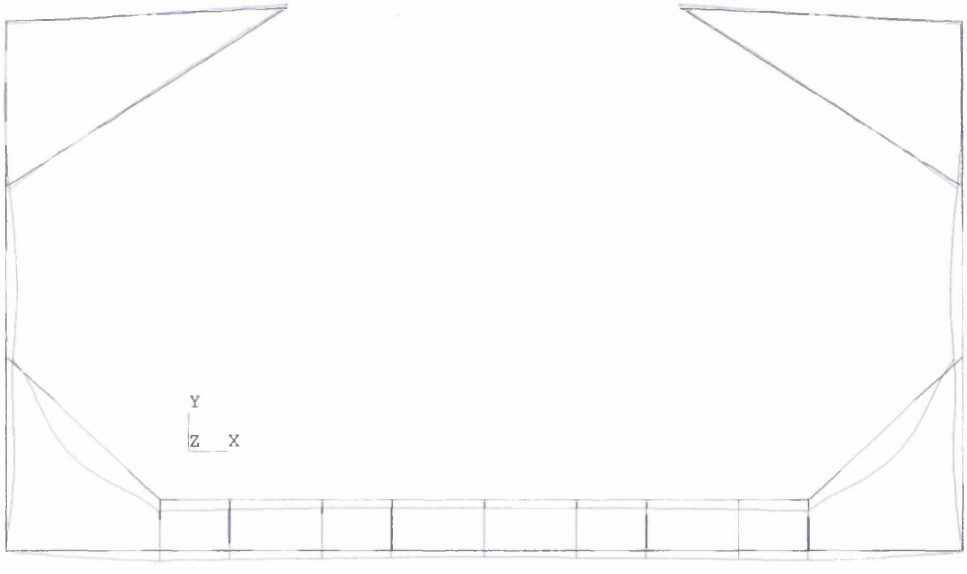

Figure A11 4 Undeformed shape of the midship section (black) and the superimposed deformed shape (blue).

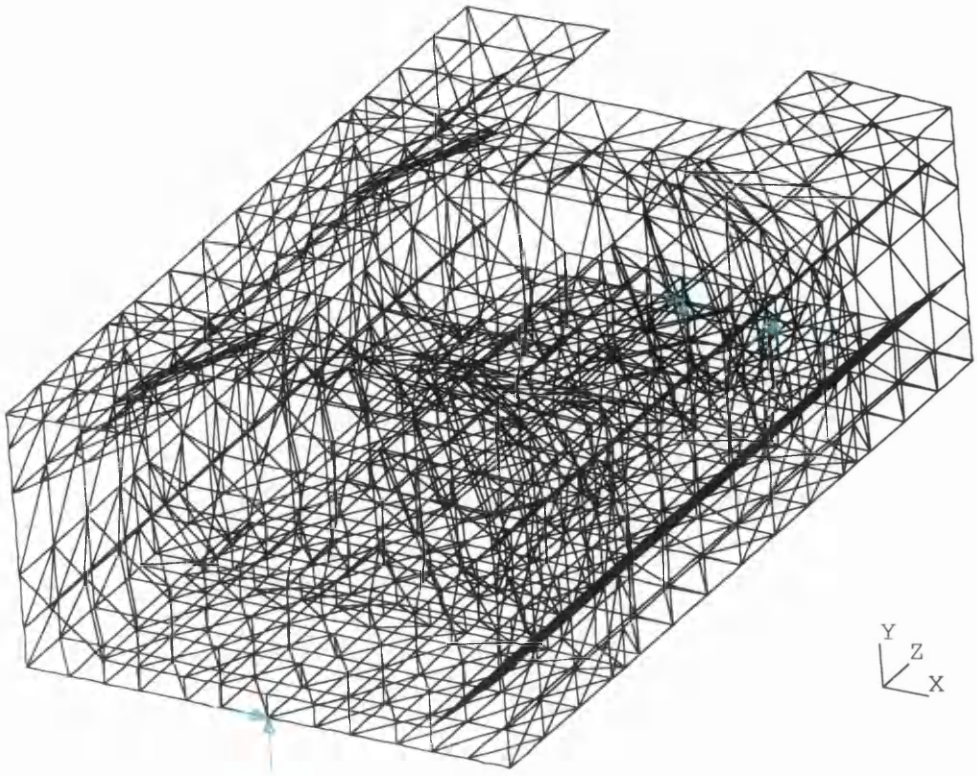

Figure A11 5 Boundary conditions positions for better deformed shape of deck

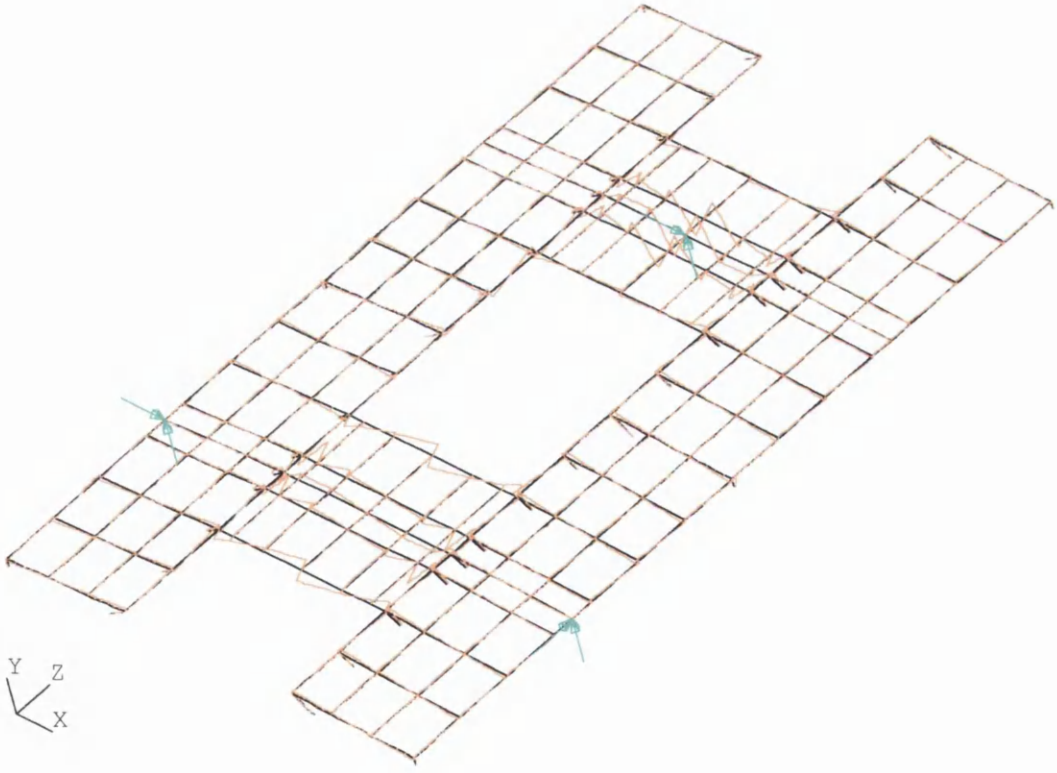

Figure A11 6 Local bending moment distribution on deck under initial supports in local z direction

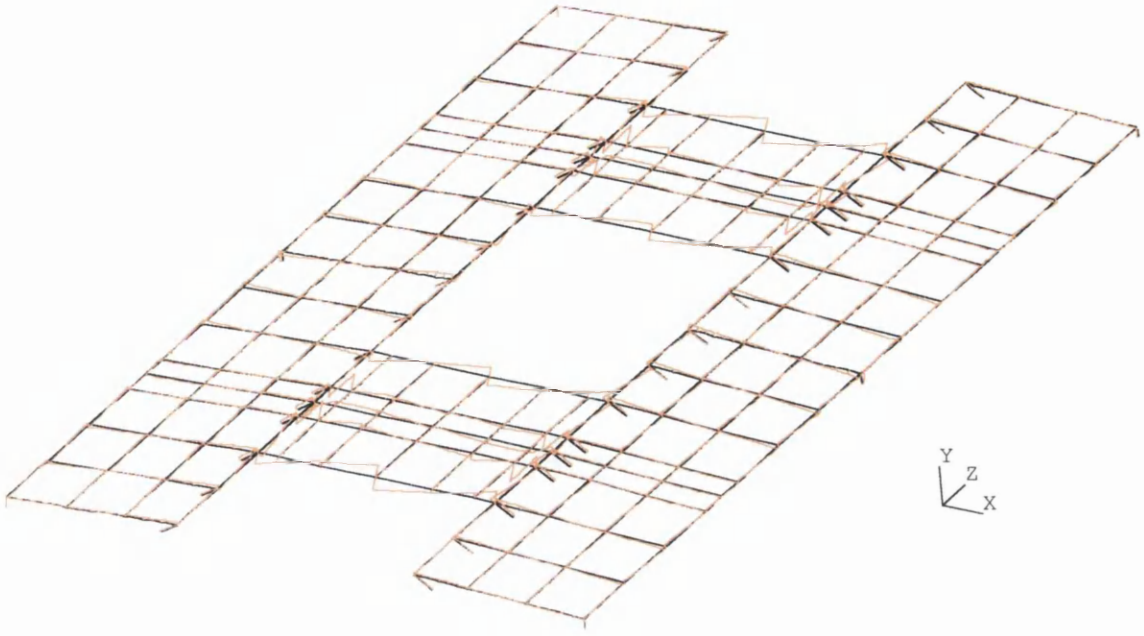

Figure A11 7 Local bending moment distribution on deck under the second position of supports in local z direction

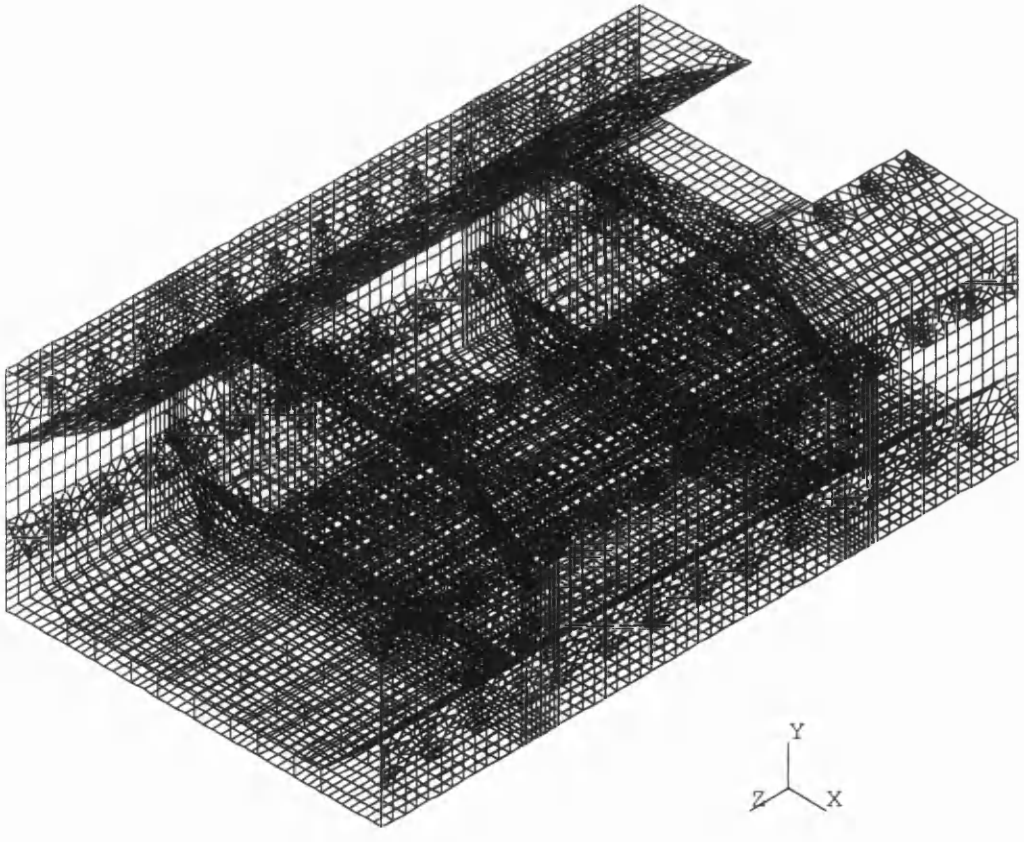

Figure A11 8 Plate element model

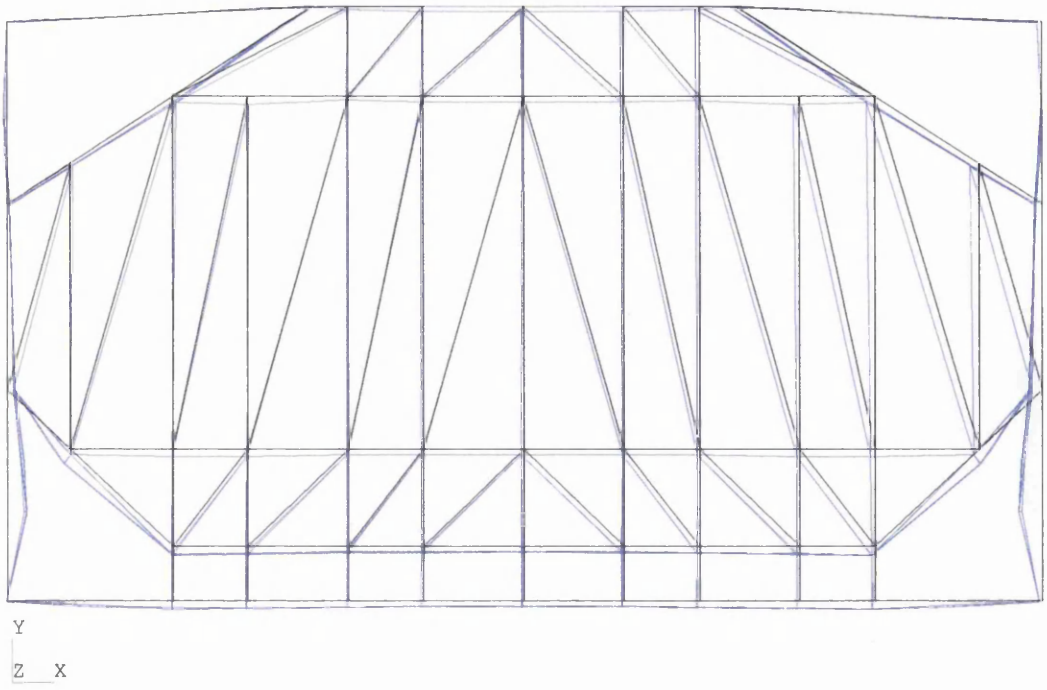

Figure A11 9 Undeformed shape of the transverse bulkhead section (black) and the superimposed deformed shape (blue).

Appendix 12 Hand Calculations of the loading and the resulting stresses for comparative purposes with the finite element model.

Calculations of the Distributed Loading

N = newton

Spacing of sections

$d = 4 \cdot m$

$\rho = 1.025 \frac{tonne}{m^3}$

$g = 9.807 m \cdot sec^{-2}$

$h1 = 16.12 m$

$h2 = 13.71 m$

$l = 2 \cdot (2 \cdot 3.12 + 2 \cdot 2.34) \cdot m$

$a = 5.18 m$

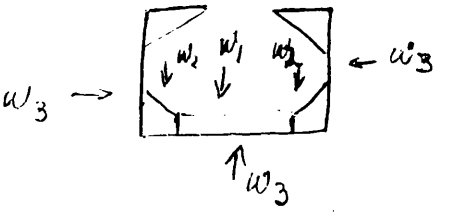

$\omega 1 = \rho \cdot g \cdot h1 \cdot d$

$\omega 1 = 6.48141 10^5 \cdot N \cdot m^{-1}$

$\omega 2 = \rho \cdot g \cdot h2 \cdot d$

$\omega 2 = 5.512421 0^5 \cdot N \cdot m^{-1}$

$h3 = \frac{(\rho \cdot g \cdot h1 \cdot l + \rho \cdot g \cdot h2 \cdot 2 \cdot a) \cdot d}{\rho \cdot g \cdot (2 \cdot a + l) \cdot d}$

$h3 = 15.345 m$

$\omega 3 = \rho \cdot g \cdot h3 \cdot d$

$\omega 3 = 6.169651 0^5 \cdot N \cdot m^{-1}$

Loading applied perpendicular to the hopper top plates

Length of hopper top plate

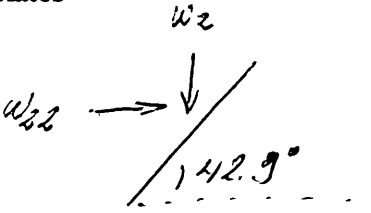

$lh = 7.0713 m$

$\omega 22 = \frac{\omega 2 \cdot a}{\cos(42.9)} \cdot \frac{1}{lh}$

$\omega 22 = 8.60441 10^5 \cdot N \cdot m^{-1}$

Methodology used to calculate the stresses using first principals.

Section 1 Transverse behaviour of double bottom

Calculation of stresses at double bottom center

N = newton

Sectional properties of double bottom

Mean Dimensions of the plates and the transverse frame cross section

t1 = 23·mm

b1 = 1·m

t2 = 15·mm

d = 1.680 m

t3 = 20·mm

b2 = 1·m

b1e = 0.7931·m

b2e = 0.7931·m

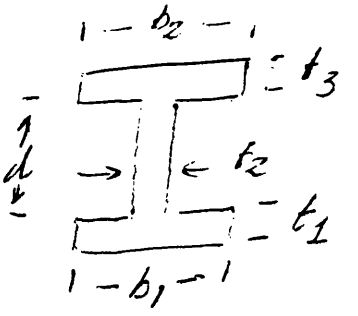

Neutral axis calculation of the cross section

We have four such double bottom strips so

$$y = \frac{t1 \cdot b1 \cdot \frac{t1}{2} + t2 \cdot d \cdot \left(\frac{d}{2} + t1\right) + t3 \cdot b2 \cdot \left(\frac{t3}{2} + d + t1\right)}{t1 \cdot b1 + t2 \cdot d + t3 \cdot b2}$$

y = 0.825 m

Inertia of the cross section

$$I = \frac{t1^3 \cdot b1e}{12} \cdot 4 + \frac{d^3 \cdot t2}{12} \cdot 4 + d \cdot t2 \cdot \left(\frac{d}{2} + t1 - y\right)^2 + \frac{t3^3 \cdot b2e}{12} + b2e \cdot t3 \cdot \left(\frac{t3}{2} + t1 + d - y\right)^2 + t1 \cdot b1e \cdot \left(y - \frac{t1}{2}\right)^2$$

$I = 0.048\,m^4$

I = 4·I

$I = 0.193\,m^4$

l = 2·(2·3.12 + 2·2.34)·m

Global axial compressive stress

Distributed loading on the side of the vessel

$\omega 3 = 616965\,N \cdot m^{-1}$

$\lambda = 17.8\,m$

$a = 12.2\,m$

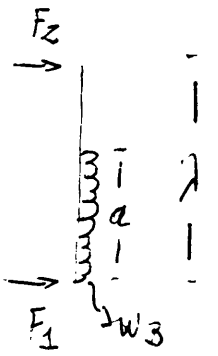

Force at double bottom

$$F1 = \omega 3 \cdot a \cdot \left(\lambda - \frac{a}{2}\right) \cdot \frac{1}{\lambda}$$

$F1 = 4.948\,10^{6}\ \cdot N$

$F2 = \omega 3 \cdot a - F1$

$F2 = 2.579\,10^{6}\ \cdot N$

Compressive axial stress

In order to have a better estimate we need to include the cross sectional area of the lower stool

$Als = (3.104 0.016 + 1.6 0.022 + 0.8 0.016)\cdot m^2$

Cross sectional area of the double bottom at the centerline

$Adb = 4\cdot(0.024 1 + 0.015 1.68 + 0.022 1)\cdot m^2$

We have six four meter sections so the force acting on half the hold length is three times F1

$$\sigma ca = \frac{3 \cdot F1}{3 \cdot Adb + Als}$$

$\sigma ca = 15.59\cdot N\cdot mm^{-2}$

Local bending stress

$\omega 2 = 616965\,N\cdot m^{-1}$

$le = 3.12\,m$

$ye = 0.013\,m$

$Ie = 0.00236124\,m^4$

$$Me = \frac{\omega 2 \cdot le^2}{12}$$

$$\sigma e = Me \cdot \frac{ye}{Ie}$$

$\sigma e = 2.755\cdot N\cdot mm^{-2}$

Distributed loading per meter due to water pressure and cargo

$\omega 3 = (648141 - 616965)\cdot N\cdot m^{-1}$

$$Mfe = \frac{\omega 3 \cdot l^2}{24}$$

The bending moment from the rotation of the end rotation of the hopper tank is calculated in section 2

$Mr = X_3 \cdot Kb$

$M = Mfe + Mr$

$$\sigma = \frac{M}{I} \cdot y$$

$\sigma = 5.229 \cdot N \cdot mm^{-2}$

Section 2 the hopper tank behaviour

Calculation of the stress due to water pressure at the corner joint of the hopper tank with the plate of the double bottom.

$N = newton$

Axial Global stress

$F1 = 4.948 \cdot 10^6 \cdot N$

In order to have a better estimate we need to include the cross sectional area of the lower stool

$Als = (3.104 \cdot 0.016 + 1.6 \cdot 0.022 + 0.8 \cdot 0.016) \cdot m^2$

Cross sectional area of the double bottom at the hopper corner

$Adb = 4 \cdot (0.021 \cdot 1 + 0.015 \cdot 1.68 + 0.018 \cdot 1) \cdot m^2$

We have six four meter sections so the force acting on half the hold length is three times F1

$$\sigma ca = \frac{3 \cdot F1}{3 \cdot Adb + Als}$$

$\sigma ca = 17.1 \cdot N \cdot mm^{-2}$

Local bending stress

$\omega 1 = 6.48141 \cdot 10^5 \cdot N \cdot m^{-1}$

$lh = 3.12 \cdot m$

$$yh := \frac{20}{2}\cdot mm$$

$$Ih = 2.57\cdot 10^{-3}\cdot m^4$$

$$Mfe := \frac{\omega 1\cdot lh^2}{12}$$

$$\sigma bl := \frac{Mfe}{Ih}\cdot yh$$

$$\sigma bl = 2.046\cdot N\cdot mm^{-2}$$

Young modulus

$$E = 207000\cdot newton\cdot mm^{-2}$$

Poisson ratio

$$v = 0.3$$

Shear modulus

$$G := \frac{E}{2\cdot(1+v)}$$

$$G = 7.962\cdot 10^{10}\cdot N\cdot m^{-2}$$

Neutral axis of the double bottom

$$y = 0.825\cdot m$$

Inertia of the double bottom

$$I = 0.193\cdot m^4$$

Torsional constant of the hopper tank

$$J = 954785862\cdot mm^4$$

Half breadth of the double bottom

$$B = 10.92\cdot m$$

Length of the section

$$L := \frac{24}{6}\cdot m$$

$$L = 4\cdot m$$

Stiffness due torsion

$$Kt = \frac{G \cdot J}{L}$$

Stiffness due to rotation

$$Kb = \frac{E \cdot I}{B}$$

The torsion stiffness matrix

$$KT = \begin{bmatrix} 2Kt & -Kt & 0 & 0 & 0 & 0 & 0 \\ -Kt & 4Kt & -Kt & 0 & 0 & 0 & 0 \\ 0 & -Kt & 4Kt & -Kt & 0 & 0 & 0 \\ 0 & 0 & -Kt & 4Kt & -Kt & 0 & 0 \\ 0 & 0 & 0 & -Kt & 4Kt & -Kt & 0 \\ 0 & 0 & 0 & 0 & -Kt & 4Kt & -Kt \\ 0 & 0 & 0 & 0 & 0 & -Kt & 2Kt \end{bmatrix}$$

The rotation stiffness matrix

$$KB = \begin{bmatrix} Kb & 0 & 0 & 0 & 0 & 0 & 0 \\ 0 & Kb & 0 & 0 & 0 & 0 & 0 \\ 0 & 0 & Kb & 0 & 0 & 0 & 0 \\ 0 & 0 & 0 & Kb & 0 & 0 & 0 \\ 0 & 0 & 0 & 0 & Kb & 0 & 0 \\ 0 & 0 & 0 & 0 & 0 & Kb & 0 \\ 0 & 0 & 0 & 0 & 0 & 0 & Kb \end{bmatrix}$$

The stiffness matrix

$$K = KB + KT$$

Density of sea water

$$\rho = 1025 \cdot kg \cdot m^{-3}$$

$$h1in = 16.12 \cdot m$$

$$hex = 15.345 \cdot m$$

Internal pressure at mid double bottom

$$pin1 = \rho \cdot g \cdot h1in$$

External pressure underneath the vessel

$$pex = \rho \cdot g \cdot hex$$

Loading of the double bottom

$$Lo = \frac{(pinl - pex)\cdot B^2 \cdot L}{12}$$

Height of the double bottom

$dbh = 1.68\cdot m$

The moment matrix due to the bending of the double bottom

$$M = \begin{bmatrix} 0Lo \\ \frac{Lo}{3} \\ \frac{2Lo}{3} \\ Lo \\ \frac{2Lo}{3} \\ \frac{Lo}{3} \\ 0Lo \end{bmatrix}$$

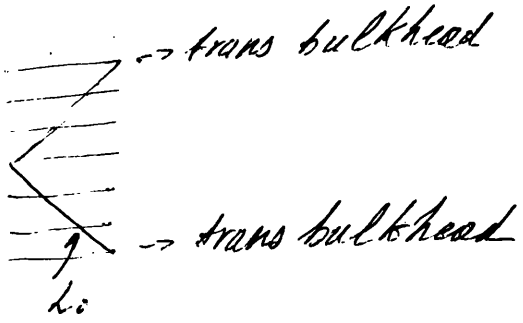

It is a seven-section model, which at each end a transverse bulkhead exists so the reduction factors shown are assumed to model the stiffer behaviour of the structure near the transverse bulkheads.

The transformation to find rotations

$X = K^{-1}\cdot M$

The rotation at the middle of the hold

$X_3 = 8.348\cdot 10^{-5}$

The stress at the hopper corner

$$\sigma = \frac{\left[\left(X_3\cdot Kb\right) + Lo\right]\cdot(dbh - y)}{I}$$

$\sigma = 2.725\cdot N\cdot mm^{-2}$

Section 3 Side shell bending

Calculation of stress at side shell due to wave pressure

$N = newton$

Sectional properties of side frame

$I = 0.00168363m^4$

$l = 5.67\,m$

$y = 0.208\,m$

Distributed loading per meter due to water pressure

$\omega = 616965\,N \cdot m^{-1}$

Fixed ended moment

$$Mfe = \frac{\omega \cdot l^2}{12}$$

$Mfe = 1.653 \cdot 10^{9}\ N \cdot mm$

Stress at the end

$$\sigma a = \frac{Mfe}{I} \cdot y$$

$\sigma a = 204.203\,N \cdot mm^{-2}$

Stress at the middle

$$\sigma m = \frac{Mfe}{2 \cdot I} \cdot y$$

$\sigma m = 102.101\,N \cdot mm^{-2}$

Section 4 Deck

Calculation of the stress due to water pressure at the corner joint of hatch

N = newton

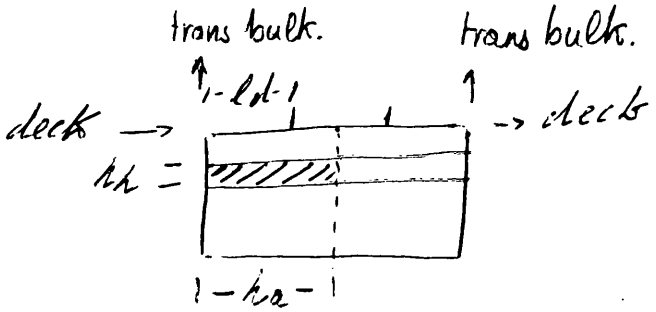

Half length of hatch area

$ha = 12\,m$

Height of area

$hh = 1.9\,m$

$\omega = 1.543 \cdot 10^{5} \cdot kg \cdot m^{-1} \cdot sec^{-2}$

Loading per meter squared

Applied force to the structure

$F = \omega \cdot ha \cdot hh$

$F = 3.518 \cdot 10^{6}\ N$

Thickness of deck plate

$td = 25 \cdot mm$

Length of hatch element

$ld = 3.2 \cdot m$

Applied stress to the deck plate

$$\sigma = \frac{F}{ld \cdot td}$$

$\sigma = 43.975 \cdot N \cdot mm^{-2}$

Alternative method

$F2 = 2.58 10^{6} \cdot N$ from Section 1

F2 is calculated in section 1 based on section length of 4m. The length of hold is 24 but only half is considered for calculations.

$$F = \frac{6}{2} \cdot F2$$

$$\sigma = \frac{F}{ld \cdot td}$$

$\sigma = 96.75 \cdot N \cdot mm^{-2}$

Chapter 6

Midship Section Fatigue Study

6.1 Review of factors contributing to fatigue of the hull structure

The need for fast, reliable and safe transportation demands new ships, which can combine higher speed than that of the past with high payload and low operating cost, all at commercially acceptable levels. Because these requirements can only be achieved by lightweight structures, the structures have become prone to fatigue damage. The presence of discontinuities and cutouts in the structural components adds to the problem. In bulk carriers, which are relatively complicated structures, fatigue is a very important aspect, and needs special attention in order for the structure to maintain its operational efficiency and safety.

Throughout its service life a ship experiences environmental loading, which causes cyclic stress variations in structural members. If these details are inadequately designed, the variations can cause fatigue cracking, which, although rarely leading to catastrophic failure, can necessitate costly and lengthy repairs.

Fatigue damage evaluations are beginning to be carried out by the designers and/or classification societies, to investigate the fatigue behavior of certain structural connections, which are important for the ship's integrity. If the fatigue life of these details is not acceptable then the details are redesigned until satisfactory fatigue life is achieved. Fatigue analysis is a useful means of making sure that the ship will be operational, at least, throughout its designed life.

The calculations for fatigue-life prediction presented in this chapter assume the fluctuating loading presented in chapter 3 and determine stress ranges according to the methodology of chapter 4.

6.2 Literature survey

Fatigue lives under multiaxial loading may differ significantly from those observed under equivalent uniaxial loading conditions. Radhakrihnan [1] and Bong-Ryul and Soon-Bok [2] present the multiaxial stress-based approach developed by Sines, combined with the improvements of Findley, Kakuno, Kawada and McDiarmid. They also consider the strain-based approach with main procedures, the maximum principal strain amplitude, maximum shear-strain amplitude, von Mise's effective shear-strain amplitude, the Brown-Miller approach, the Lohr-Ellison approach and the energy-based approach. Stress-based

approaches can be applied to high-cycle fatigue where gross yielding does not occur, whereas the strain-based approach is more suitable for low cycle fatigue where the energy method appears more promising.

In this study, the fatigue behaviour of certain structural details is investigated. The most important aspect in any fatigue analysis is the determination of fatigue loading and, consequently, of stress distribution. DnV [3] provides a method of calculating stress distribution, and methods of performing fatigue analysis, mainly concentrating on mobile offshore units. Barltrop [4] provides very useful information on fatigue-analysis methods and methods for predicting wave loads. Sections 4 and 6 of his book, which deal with wave loading and structural response analysis, are particularly useful.

Certain connections of a ship's structure, i.e. frame stiffeners, are dominated by loading caused by wave-pressure distribution at the side of the vessel. This pressure does not vary linearly with wave height, and, therefore, spectral analysis is not sufficiently accurate to predict the response to this loading. Barltrop [5] describes several methods for calculating the response to this wave pressure by considering a) the pressure profile within four regions, and b) the cubic weighted wave pressure.

The method of spectral analysis is also well presented by Cronin [6]. He describes the full spectral analysis together with the useful example of a steel jacket. The fatigue behaviour of the longitudinal stiffeners of an oil tanker and a containership that have been subjected to dynamic loads is analysed by Xue, Pittaluga, and Cervetto [7], again by applying spectral analysis, and including the pressure distribution at the sides of the ships. Chen and Mavrakis [8] discuss the modelling errors of spectral fatigue analysis for compliant offshore structures and propose a methodology for their elimination.

Xu [9] summarises the work of a five-year research program on fatigue and fracture reliability that was conducted at the University of California. His paper presents an example of fatigue-damage calculation and the recommendation of a better design for fatigue strength. Radaj [10] considers the fatigue strength of welded structures. His book presents various knowledge requirements, components and development methods for fatigue-resistant welded structures. Maddox [11] discusses the subject of fatigue in his book by subdividing it into two major parts; the first being academically oriented

regarding basic knowledge and the second descriptive with respect to design rules and their applicability.

The presence of corrosion in ballast and cargo tanks results in a reduction of fatigue life. SSC - 326.[12] contains useful corrosion data for welded marine steels and their details. It is also a very useful reference guide for fatigue and fracture methodologies. Ebara [13] discusses long-term corrosion-fatigue strength, corrosion-fatigue variables and corrosion-fatigue crack initiation and propagation. Akid [14] presents results from studies where corrosive and non-corrosive enviroments were simulated and concludes that simple damage-accumulation fatigue models are insufficient to satisfactorily predict fatigue life. Tokaji [15] studied the corrosion-fatigue strength of coated and uncoated steel specimens in a corrosive enviroment and concludes that the various types of coating increased the fatigue life of the specimens, but also notes the poor resistance to cracking of the coatings when subjected to cyclic loading.

Last, but certainly not least, Fricke [16] discusses the basic principles of fatigue with respect to ships' structures. The text is an excellent review, which deals with all aspects of fatigue cracking, and shows how important it is considered to be by the classification societies. Unfortunately it was published after the calculations were performed.

6.3 Corrosion model

6.3.1 Review of hull corrosion causes and protection applicable

The steel hull will inevitably suffer from corrosion in the marine environment. The most common causes and mechanisms of hull corrosion are [17]:

- Galvanic corrosion, which occurs when two metals of different electrochemical potential are in metallic contact in an electrolyte such as salt water.
- Direct chemical attack, wherein certain chemicals containing elements such as chlorine and sulphur attack the steel without the presence of an electrolyte.
- Anaerobic corrosion, which is caused by sulphate-reducing bacteria present in many harbours.

It is interesting to note that for galvanic corrosion the metals need not be different, as in the case of a flanged plate, where the locked-in stress at the flange makes that portion anodic to the rest of the plate [17]. Overall, we can comment that mechanisms usually interact with each other.

Usually the plate/stiffener is allowed to corrode down to 80%-90% of the original thickness [18]. However, it should be noted that for a 20mm-thick plate the corrosion allowance is 4mm-2mm. The thickness of the welding material is usually around 6mm-4mm, so the corrosion allowance leads to 50%-100% loss of thickness.

Methods of prevention /protection/retardation [19]:

- Cathodic protection: where the electrolytic corrosion is controlled by the introduction of a sacrificial anode. An impressed current is an alternative way of applying the same principle, in which, by means of current, the areas requiring protection have their potential value depressed lower than any naturally occurring anodic areas.
- Coatings are a passive way of protecting the structure. Various paints exist which can provide a protection from 3 to 20 years. However, if the paint has any imperfections, pitting corrosion will progress rapidly, since the process will concentrate in the area of the defect.

Soft coatings based on oil or waxes may fail prematurely when used with cathodic protection [17]

6.3.2 Corrosion Equation

It is generally accepted that a corrosive environment leads to an increase in the stress-range level due to the decrease in steel thickness. Including the equation 4.2.1 [20], which is multiplied to the stress range, enhanced the fatigue model with respect to corrosion:

$$S_{cor}(t) = \frac{t}{t - k_{cor} \cdot T} \qquad 6.3.2.1$$

Where:

t : Thickness of steel

k_{cor} : Corrosion rate

T: Time

$S_{cor}(t)$: Corrosion factor

Corrosion rates at particular points in ships' hulls vary greatly from ship to ship due to the combined effect of different routes and cargoes. A thorough statistical study conducted by DNV [9] shows the complexity and the peculiarity of the problem; results of the fact that in most of the points studied the standard deviation is almost the same as the corrosion rate, if not greater. Indicative values for corrosion rates have been published [17]. In this project the rates for unprotected steel [21] are considered. Although conservative, these rates do not in fact vary a great deal from those published by DNV, taking into consideration the standard deviation.

Condition	Corrosion rate
Immersed in still water	0.15 mm/year
Splash zone	0.5 mm/year
Immersed in fast flowing water	0.8 mm/year
Ballast tanks	0.2-0.4 mm/year

Table 6.3-1 - Indicative values for corrosion rates

6.4 Review of fatigue damage parameters

Fatigue cracks within structural details as a result of cyclic loading have been an important parameter in the operation of ships. This is a common problem for ships subjected to wave loads that induce fatigue damage, especially in structural details with high stress concentrations. Although this damage does not lead to loss of ships, it is often the cause of costly repairs and replacements of hull structures, which greatly influence serviceability and operational economy.

Since higher tensile steels have been used extensively for reducing ship-steel weight, ship classification societies, designers, and builders have devoted greater consideration to fatigue behaviour. This is due to the fact that high tensile steel structures have higher operational stress levels but show no improvement in fatigue properties compared with those of mild steel structures.

One problem for ships' structures when performing a fatigue analysis is the number and variability of structural elements to be considered. Another difficulty is the determination of stress ranges considering the complexity of the load components acting on these locations.

6.5 Environmental model

The surface of the sea is subdivided into regions called Marsden zones [22] (appendix 4). Each of these zones covers a geographical area over which wave statistics have been estimated from ships' observations, these being significant wave height, wave period, and frequency of occurrence. For this report, 4 different zones, (6, 7, 10 and 11) have been selected, and the corresponding scatter diagram was calculated and is shown in appendix 14.

The calculation of the ship's response to different sea states was performed by spectral analysis. Spectral analysis assumes that the ship's response to wave excitation is linear, so that the total response in a seaway is described by a superposition of the response to all regular wave components that constitute the irregular sea, leading to a frequency domain analysis. Spectral analysis requires the responses of the ship to unit wave amplitude. For this reason all the results from the strip theory program are for unit wave amplitude.

Spectral analysis combines transfer functions with wave spectrum and results in the response spectrum, from which all the response statistics can be calculated. This has to be done for all wave heights and all wave periods, and also needs to take into account the probability of occurrence of each sea state.

The transfer function, modeling the response to a sinusoidal wave with unit amplitude for different frequencies, is usually arrived at from calculations based on the theory of ship motions in potential flow. The estimated transfer function is, however, only valid for a particular ship speed, wave-heading angle, and loading condition. For this study, ship speed has been kept constant at the service speed (15 knots). The wave headings that have been used for the analysis are 0,30,60,90,120,150,180 degrees. In addition, three different loading conditions were selected: a ballast, an ore and a grain condition. The

fatigue-damage calculations are, therefore, performed for three different cases, i.e. for the three loading conditions.

In those cases where the response of the ship is non-linear with wave amplitude, then a different analysis needs to be adopted. Non-linear effects in the response analysis come from dynamic wave pressure forces acting on the ship. If the assumption is made that stresses due to water pressure vary linearly with wave height, then the area affected by these stresses will be under-estimated. The procedure adopted in this project performs the dimensionalisation of the global stresses and calculates them with respect to water pressure. The calculation is performed using the transformation relationship, followed by non-dimensionalisation with respect to wave amplitude; the transfer function calculated then becomes the input to the spectral analysis.

After this operation, we can combine each transfer function with the sea spectrum, to arrive at the response spectrum. This should be done for every wave height and wave period, these being the input parameters in the I.S.S.C. sea spectrum.

6.5.1 Wave spectrum used for the fatigue model

The wave spectrum defines the distribution of energy among the different hypothetical regular wave components, having various frequencies and directions. The wave spectrum that was chosen for this study is the I.S.S.C. (Special case to Pierson-Moskowitz) wave spectrum, which permits wave period and significant wave height to be assigned separately. It has the form:

$$S(\omega)=\frac{0.11\cdot Hs^2}{\omega_1}\cdot\left(\frac{\omega}{\omega_1}\right)^{-5}\cdot e^{\left\{-0.44\cdot\left(\frac{\omega}{\omega_1}\right)^{-4}\right\}} \qquad 6.5.1.1$$

Where:

$$\omega_1=\frac{2\cdot\pi}{T} \qquad 6.5.1.2$$

ω: Wave frequency

H_s: Significant wave height

T: Average wave period

6.5.2 Hull structure response spectrum

The response spectrum is a combination of the transfer function and the wave spectrum. The response spectrum is equal to:

$$\text{RS} = \text{Wave spectrum} \cdot \text{Transfer function}^2 \qquad 6.5.2.1$$

From the response spectrum we are able to calculate the response statistics, such as the area under the response spectrum curve which is denoted by 'm_o' and defines the standard deviation of the response. The response statistics are used to calculate the fatigue damage of the structural details concerned.

6.6 Calculation of fatigue damage using Miner-Palmgren rule

Fatigue damage is usually determined by the 'Miner-Palmgren' [23] accumulated damage rule which is also more often found in codes of practice. In the Miner hypothesis, it is assumed that one cycle of randomly varying stress, having amplitude 's_i', causes the following degree of fatigue damage:

$$\delta D_i = \frac{1}{N_i} \qquad 6.6.1$$

Here, 'N_I' is the number of cycles of a sinusoidal varying stress of amplitude 's_i' that is required to cause failure. The cumulative damage due to fatigue during exposure to the random stress environment will then be given by:

$$\delta D_i = \sum_i \frac{n_i}{N_i} \qquad 6.6.2$$

Here, 'n_i' is the number of stress cycles of level 's_i', during the period of exposure and the summation is taken over all levels of stress experienced during the period of time

under consideration. Failure of the structure is then presumed to occur when the length of exposure is sufficient for this sum to equal unity, i.e. when D = 1.

Assuming that the basic fatigue design curve has the form:

$$N \cdot \sigma^m = K \qquad 6.6.3$$

Then the fatigue damage becomes:

$$D = \frac{n}{K} \cdot \overline{\sigma}^m \qquad 6.6.4$$

where 'n' is the total number of cycles, '$\overline{\sigma}^m$' is the mean value of 'σ^m' and 'σ' is a random variable denoting fatigue stress occurring for 'n' cycles, 'K' is a constant which depends on the welding classification.

Equation 6.6..4 is valid for a non-stationary as well as a stationary process. If the is assumed to be a stationary narrow band Gaussian process, it follows a Rayleigh distribution and equation 6.6.4 can be expressed as:

$$D = \left(\frac{n}{K}\right) \cdot \left(2 \cdot \sqrt{2} \cdot \sigma\right)^m \cdot \Gamma\left(\frac{m}{2} + 1\right) \qquad 6.6.5$$

where σ is the root mean square, (rms) of the process and '$\Gamma(...)$', is the gamma function.

The long-term process with 'n_i' sea-states can usually be described as 'n_i' stationery processes, for each one assuming 'f_i' is the zero-crossing rate:

$$f_i = 2 \cdot \pi \cdot \sqrt{\frac{m_2}{m_0}} \qquad 6.6.6$$

Or

$$f_i = \frac{1}{Tz} \qquad 6.6.7$$

Where 'Tz' is the average response period.

If we assume that 'T' is the time over which the fatigue damage is calculated, the damage in the 'i-th' sea-state is written as:

$$D_i = \left(\frac{n_i}{K}\right) \cdot \left(2 \cdot \sqrt{2} \cdot \sigma_i\right)^m \cdot \Gamma\left(\frac{m}{2} + 1\right) \qquad 6.6.8$$

Where 'σ_i' is the rms stress in the 'i-th' sea-state and

$$n_i = \gamma_i \cdot f_i \cdot T \qquad 6.6.9$$

Where

γ_i : is the percentage of time in the 'i-th' sea-state. This is the frequency of occurrence of each sea-state

f_i : is the zero-crossing rate as defined in equation 6.6.6

The total fatigue damage then becomes:

$$D = \left(\frac{\left(2 \cdot \sqrt{2}\right)}{K}\right) \cdot \Gamma\left(\frac{m}{2} + 1\right) \cdot T \cdot \sum_{i=1}^{x} \left\{\gamma_i \cdot f_i \cdot \sigma_i^m\right\} \qquad 6.6.10$$

Equation (6.6.10) is the basic equation used in this study to calculate the fatigue damage.

In the special case where corrosion is included in the fatigue damage the equation becomes:

$$D = \left(\frac{\left(2 \cdot \sqrt{2}\right)}{K}\right) \cdot \Gamma\left(\frac{m}{2} + 1\right) \cdot T \cdot \sum_{i=1}^{x} \left\{\gamma_i \cdot f_i \cdot (\sigma_i \cdot S_{cor}(t))^m\right\} \qquad 6.6.11$$

If we calculate fatigue damage for a year we can predict the fatigue life of the detail by inverting this value. Another useful way of assessing the results is the usage factor.

$$UF = \sqrt[m]{Y_b \cdot D} \qquad 6.6.12$$

The usage factor shows us that the reserves of fatigue strength are calculated for a certain number of years (Y_b). The calculations were performed using Fortran so that one program was created for each combination of crack and loading condition. Two different flowcharts can be seen in appendix 13 one for the calculation of stress and the other for fatigue life calculations.

6.7 Stress Range Calculation

6.7.1 Details Considered for fatigue analysis

In a ship's structure there may be many hundreds of different structural details that make up a particular section. The same applies to the bulk carrier structure. For the purpose of a fatigue analysis it is almost impossible to consider all these details. Current practice suggests that only the most important details need to be considered in a fatigue analysis. Selection of these details depends mainly on judgement guided by experience. Many classification societies provide design rules and guidance on their selection. Another complication arises from the fact that for every detail a separate stress analysis has to be performed in order to calculate the stresses from the loads acting on each detail. These loads need not be the same, as the location from detail to detail changes, and different factors and geometries have to be considered every time.

For the purpose of this study eight different details have been selected as can be seen in figure 6.7.1. These details are typical of the section under consideration, and are those that experience has shown to be the most prone to fatigue for various reasons as explained in the rest of the section. The more complicated details are shown in appendix 15 as they appear in the ship's plans. The loading considered for the analysis is presented in chapter 3 and appendix 6.

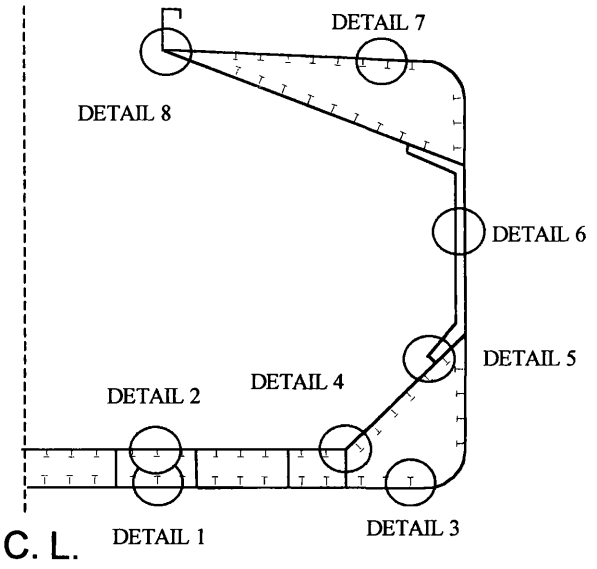

Figure 6.7.1 - The midship section of the vessel and the details considered.

6.7.2 Bottom longitudinal (detail 1)

The welding connection between the keel plating and the longitudinal stiffener (fig. 6.7.2.1) suffers with respect to fatigue from global stresses in the longitudinal direction and water pressure stresses in the transverse direction.

Two cracks were considered, each one affected by different stresses. The first crack propagates in a direction normal for the longitudinal axis of the ship. The stresses that cause this crack to propagate are caused by global bending moments and shear forces (fig. 6.7.2.2). The second crack undergoes stresses due to water pressure at the bottom shell plating. The crack initiates at the edge of the weld and propagates through the thickness of the plating (fig. 6.7.2.3).

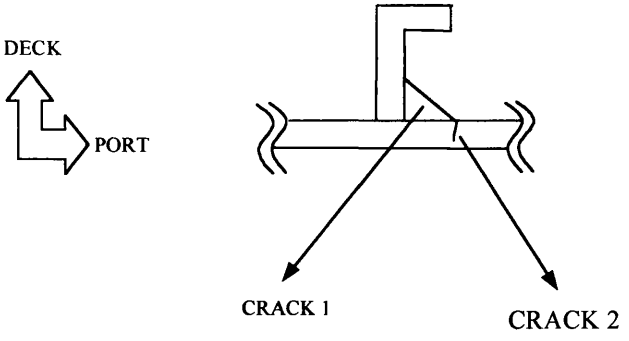

Figure 6.7.2.1 Most probable cracks at the keel plating/stiffener connection

Crack1

The equation used to determine the stress range for crack 1 is:

$$\sigma_{\varphi} = \sigma_x \cdot \cos^2 \theta + \tau \cdot \sin 2\theta \qquad 6.7.2.1$$

Where σ_x : is the global bending stress
τ : is the global shear stress

The S-N curve used is class E

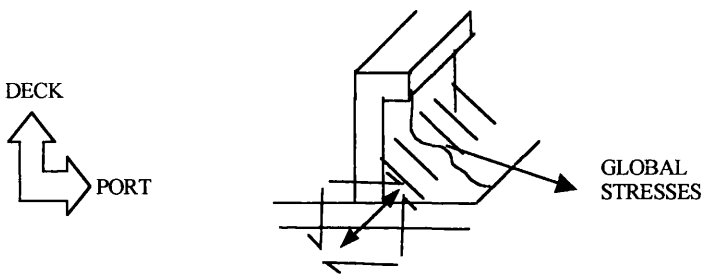

Figure 6.7.2.2 Direction of global stresses acting on the weld

Crack 2

The equations used to determine the stress range for crack 2 are:

$$M = \frac{wl^2}{12} \qquad 6.7.2.2$$

$$\sigma_p = \frac{M}{z} \qquad 6.7.2.3$$

The S-N curve used is class F

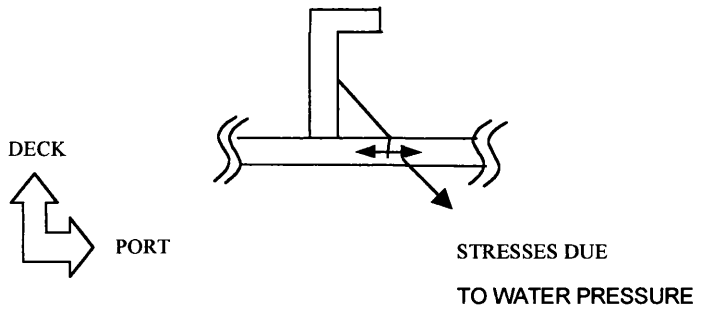

Figure 6.7.2.3 Direction of stresses due to water pressure acting on the weld

6.7.3 Inner bottom longitudinal (detail 2)

The double bottom longitudinal stiffeners are likely to suffer fatigue damage from global or local loading (fig. 6.7.3.1). The local loading that causes fatigue damage is due to cargo accelerations in the hold.

The first crack considered suffers from global loading (fig. 6.7.3.2). The second crack is influenced by the acceleration of the cargo stored in the hold (fig. 6.7.3.3). The procedure to calculate the stresses acting on the crack begins with by calculating the acceleration of a strip of the cargo and, therefore, the distributed loading on the plate. The plate is considered as fixed ended.

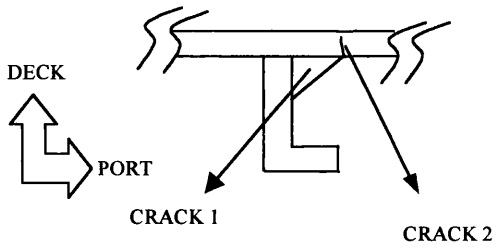

Figure 6.7.3.1– Most likely cracks at the bottom plating/stiffener connection.

Crack1

The equation used to determine the stress range for crack 1 is:

$$\sigma_{\varphi} = \sigma_x \cdot \cos^2\theta + \tau \cdot \sin 2\theta \qquad 6.7.3.1$$

Were σ_x : is the global bending stress

τ : is the global shear stress

The S-N curve used is class E

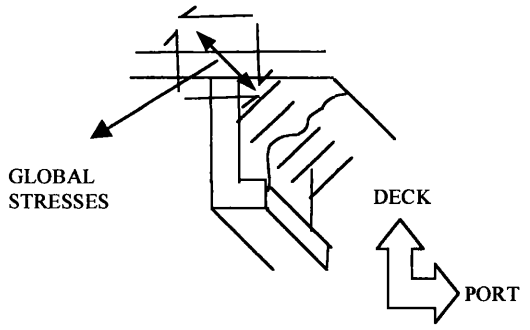

Figure 6.7.3.2 Direction of global stresses affecting the weld.

Crack 2

The equations used to determine the stress range for crack 2 are:

$$M = \frac{wl^2}{12} \qquad 6.7.3.1$$

$$\sigma_p = \frac{M}{z} \qquad 6.7.3.2$$

Where z : section modulus of the local section

The S-N curve used is class F

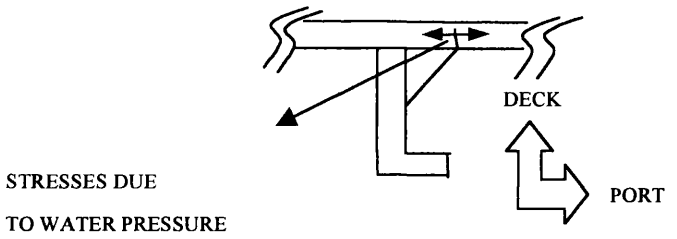

Figure 6.7.3.3 - Direction of stresses due to water pressure affecting the weld.

6.7.4 Hopper tank longitudinal (detail 3)

The third detail is a longitudinal stiffener inside the hopper tank welded to the bottom plating. The weld is a butt weld and the main stresses arise from global as well as local bending. The global stresses due to global bending moments and shear forces cause crack 1 to propagate in a direction normal for the longitudinal axis of the ship and normal for the weld, (fig. 6.7.4.2). The local bending stresses arise from the local bending between the two adjacent stiffeners, caused by the water pressure at the bottom of the plating. These stresses cause crack two to propagate through the thickness of the bottom plate, (fig. 6.7.4.3).

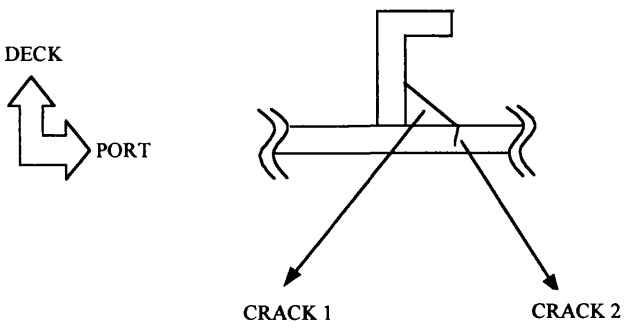

Figure 6.7.4.1 - Most probable cracks at the keel plating/stiffener connection.

Crack1

The equation used to determine the stress range for crack 1 is:

$$\sigma_{\varphi} = \sigma_x \cdot \cos^2 \theta + \tau \cdot \sin 2\theta \qquad 6.7.4.1$$

Were σ_x : is the global bending stress

τ : is the global shear stress

The S-N curve used is class E

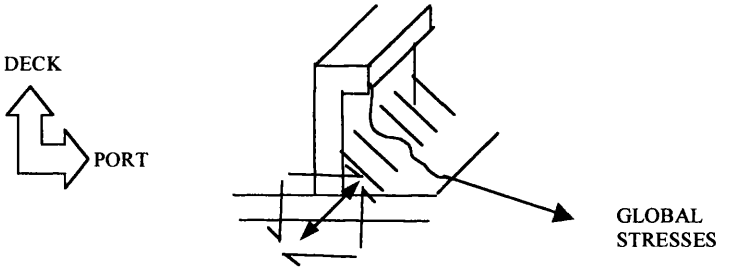

Figure 6.7.4.2 Direction of global stresses acting on the weld.

Crack 2

The equations used to determine the stress range for crack 2 are:

$$M = \frac{wl^2}{12} \qquad 6.7.4.2$$

$$\sigma_p = \frac{M}{z} \qquad 6.7.4.3$$

Where z : section modulus of the local section

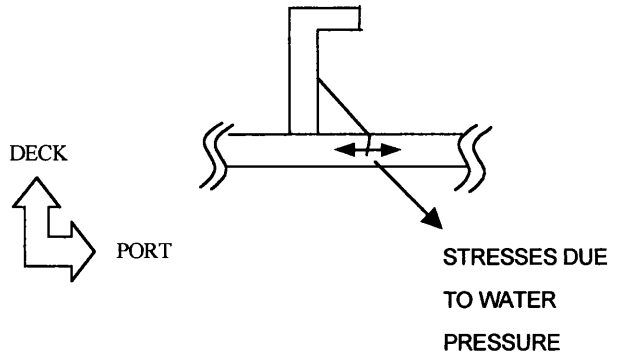

Figure 6.7.4.3- Direction of stresses due to water pressure acting on the weld.

6.7.5 Hopper tank corner (detail 4)

The fourth detail describes the connection between the hopper tank and the double bottom. This detail is prone to fatigue damage and was therefore selected for the fatigue analysis calculations. Perhaps the most accurate method would be to perform a finite element analysis however for this study a simpler analysis, based on first principles, was adopted. The main stresses present at this location come from the water pressure forces below and around the hopper tank.

Two cracks are significant at this location, (fig. 6.7.5.1). The first crack is propagating because of the global bending and shear stresses, and the second crack because of the local bending caused by water pressure and cargo acceleration forces.

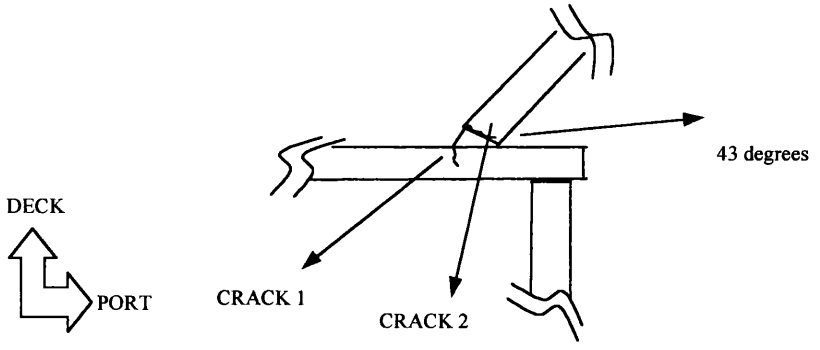

Figure 6.7.5.1 Most probable cracks at the hopper corner.

Crack 1

The equation used to determine the stress range for crack 1 is:

$$\sigma_\varphi = \varpi_{\alpha\tau} \cdot \sigma_x \cdot \cos^2\theta + \sigma_p \cdot \sin^2\vartheta + \varpi_{\alpha\tau} \cdot \tau \cdot \sin 2\theta \qquad 6.7.5.1$$

Where, σ_x : is the global stress

σ_p : is the stress due to water pressure

τ : is the global shear stress

$\varpi_{\alpha\tau}$: denotes the factor to account the effect of welding class change

The calculation of $\varpi_{\alpha\tau}$ is based on equation 6.6.4 ,where the same number of cycles and damage are assumed and the equivalent stress is calculated:

$$\bar{\sigma}_1 = \frac{\sqrt[m]{K_1}}{\sqrt[m]{K_2}} \cdot \bar{\sigma}_2 \qquad 6.7.5.2$$

$$\varpi_{\alpha\tau} = \frac{\sqrt[m]{K_1}}{\sqrt[m]{K_2}} \qquad 6.7.5.3$$

Initial w. class	Used w. class	$\varpi_{\alpha\tau}$
E	F	0.846
E	F2	0.745

Table 6.7-1 Values of the change of welding class factor

The S-N curve used is class F and F2

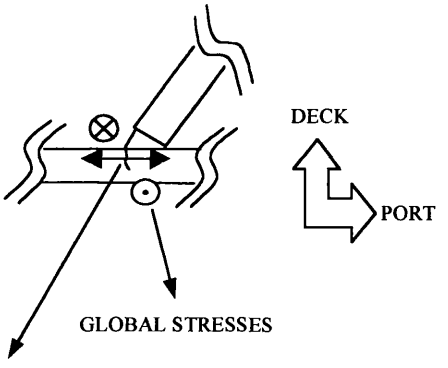

Figure 6.7.5.2 Stresses affecting crack 1 at hopper corner

Crack 2

The equation used to determine the stress range for crack 2 is:

$$\sigma_{\varphi} = \varpi_{\alpha\tau} \cdot \sigma_x \cdot \cos^2\theta + \sigma_p \cdot \sin^2\vartheta + \varpi_{\alpha\tau} \cdot \tau \cdot \sin 2\theta \qquad 6.7.5.4$$

$$\sigma_{pl} = \sigma_p \cdot \frac{t_h}{t_d} \cdot \frac{1}{\cos 43} \qquad 6.7.5.5$$

The stress due to wave pressure was transformed to the plane that is perpendicular to the direction of the crack, and the difference in thickness between the plate of the double bottom and the hopper plate was taken into consideration.

The SN curve used is class F and F2

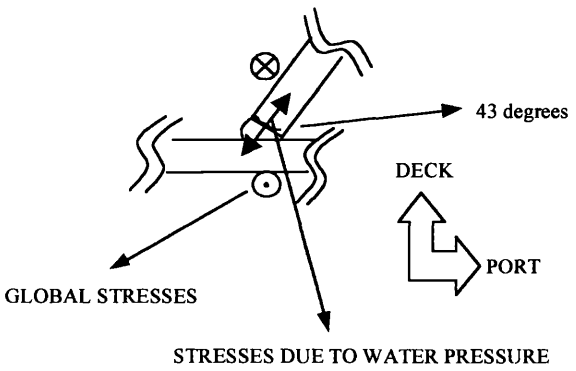

Figure 6.7.5.3 - Stresses affecting crack 2 at the hopper corner

6.7.6 Side shell stiffener connection with hopper upper plate (detail 5)

The weld connecting the side frame with the hopper tank top plate suffers throughout its life largely from stresses resulting from water pressure at the side of the ship and also from accidental loading during loading and unloading procedures that indirectly affect the fatigue life of the detail (fig. 6.7.6.1). Three possible cracks were considered. The first one starts from the weld and propagates through the frame thickness (fig. 6.7.6.2). The second one propagates inside the weld (fig. 6.7.6.3) and the third one starts from the weld and propagates in the hopper plating (fig. 6.7.6.4).

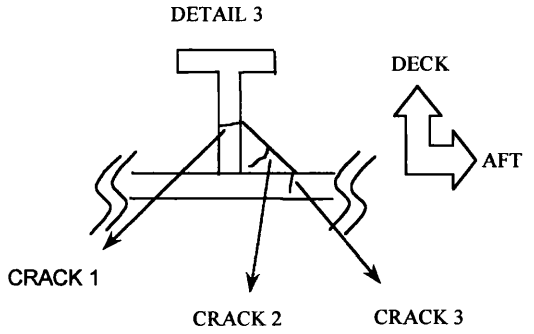

Figure 6.7.6.1 Most probable cracks at the connection of the side bracket with the upper hopper plating (The drawing is inclined by 47 degrees)

Crack 1

Stresses due to water pressure

S-N Curve is class F2

$$\sigma_\theta = \sigma_p \cdot \cos^2\theta + \tau_p \cdot \sin 2\theta \qquad 6.7.6.1$$

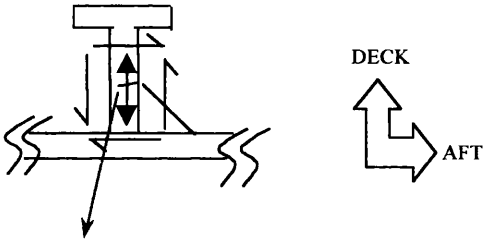

Figure 6.7.6.2 - Stresses affecting crack 1 at the upper hopper plate and side bracket connection.

Crack 2

Stresses due to water pressure two different S-N curves used for the two different planes

First plane due to water pressure S-N curves class W

$$\sigma_\theta = \sqrt{(\sigma_{wp})^2 + (\tau_{wp})^2} \qquad 6.7.6.2$$

Where

$$\tau_{wp} = \tau_p \cdot \frac{t_{foot}}{2 \cdot t_{weld}} \qquad 6.7.6.4$$

$$\sigma_{wp} = \sigma_p \cdot \frac{t_{foot}}{2 \cdot t_{weld}} \qquad 6.7.6.5$$

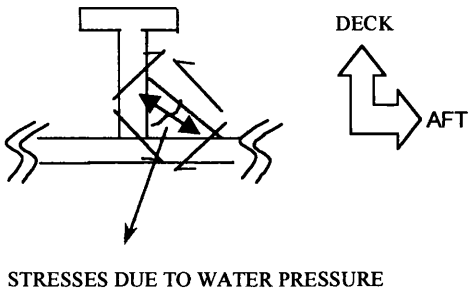

Figure 6.7.6.3 - Stresses affecting crack 2 at the upper hopper plate and side bracket connection.

Crack 3

Stresses due to global bending

S-N Curve used class F

$$\sigma_\theta = \sigma_x \cdot \cos^2\theta + \tau \cdot \sin 2\theta \qquad 6.7.6.6$$

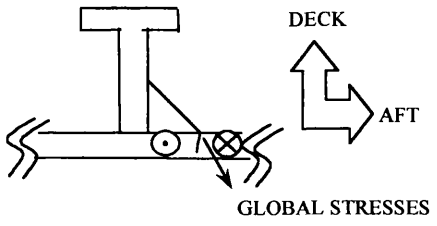

Figure 6.7.6.4 - Global stresses affecting crack 3 at the upper hopper plate and side bracket connection.

6.7.7 Transverse side shell stiffener (detail 6)

The welding connecting the side bracket with the side plate may suffer also from fatigue damage (fig. 6.7.7.1). The crack under consideration starts at the weld and propagates in the plate (fig. 6.7.7.2).

The weld suffers from mainly wave-induced stresses but there is also some contribution from global stresses. The wave-induced stresses were calculated using the

pressure profile as loading. The plate between the side brackets that is bent by the loading was considered. The bending will induce moments and forces at the supports and, therefore, stresses. The procedure included the calculation of a certain point at which the fatigue analysis would complete. The criterion for selecting the point was the dynamic water pressure.

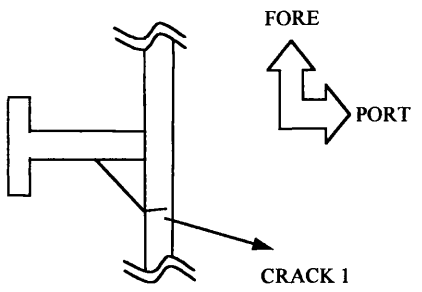

Figure 6.7.7.1 - Most probable crack at the side stiffener/side plate connection

$$\sigma_p = \frac{M}{z} \qquad 6.7.7.2$$

$$\tau_p = \frac{R}{A} \qquad 6.7.7.3$$

$$\sigma_\vartheta = (\sigma_x + \sigma_p)\cdot\cos^2\theta + (\tau + \tau_p)\cdot\sin 2\theta \qquad 6.7.7.4$$

Where, σ_x : is the global stress
σ_p : is the stress due to water pressure
τ : is the global shear stress
τ_p : is the shear stress due to water pressure

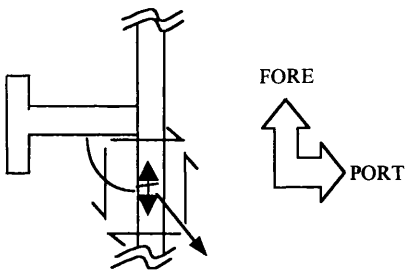

STRESSES DUE TO WATER PRESSURE AND GLOBAL

Figure 6.7.7.2 - The direction of global and water pressure stresses at the crack under consideration.

6.7.8 Upper wing tank longitudinal (detail 7)

Generally, all deck structural components suffer as a result of global stresses and especially those induced by global vertical bending moment because of the distance from the neutral axis. A welding detail inside the upper wing tank is considered where a longitudinal stiffener is connected to the deck plating (fig. 6.7.8.1).

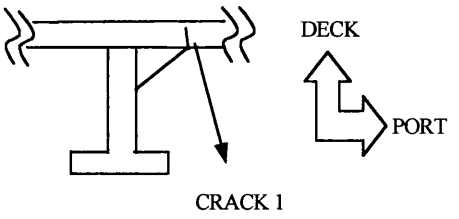

Figure 6.7.8.1 - Most probable crack at the deck plate/longitudinal stiffener connection

Global stresses were considered for a crack starting at the weld and propagating in the deck plating (fig 6.7.8.2). The global stresses and shear stresses were combined to calculate the overall stress in the area.

Crack 1

The stress equation combines the global stresses and shear stresses

$$\sigma_{\varphi} = \sigma_x \cdot \cos^2 \theta + \tau \cdot \sin 2\theta \qquad 6.7.8.1$$

The S-N curve used is class F

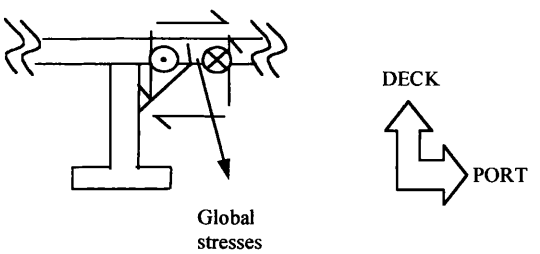

Figure 6.7.8.2 - The direction of the global stresses affecting the crack.

6.7.9 Hatch corner (detail 8)

The hatch corner is a crucial detail because the maximum vertical bending moment stresses are combined with high compressive stresses resulting from wave pressure at the side plates. There are also the large openings of the hatch that introduce high stress concentration factors.

$$\sigma_{\varphi} = SCF_1 \cdot \sigma_x \cdot \cos^2\theta + SCF_2 \cdot \sigma_p \cdot \sin^2\vartheta + \tau \cdot \sin 2\theta \qquad 6.7.9.1$$

where σ_x : is the global bending stress

σ_p : is the stress due to water pressure

τ : is the global shear stress

6.8 Discussion

One of the most important tasks in a fatigue calculation is determination of the stress ranges. Once the stress ranges are calculated for every detail in question, then the fatigue analysis is straightforward. An important parameter in every fatigue analysis is the selection of the appropriate S-N curve. In this section, the results of the fatigue analysis will be discussed.

As mentioned earlier in this chapter, eight different structural details have been selected for this fatigue analysis. Every possible crack path has been examined in detail, and fatigue calculations for each one has been performed. The summarised results for each detail and for each loading condition are presented in appendix 16.

The calculations are based on design SN curves with a mean life of about 2.5 years longer. The results are considered to be generally satisfactory and they give a good indication of those details that need special attention and frequent inspection. Rather than discussing the cracks of each detail in isolation, we will present a comparison of fatigue lives by subdividing the cracks into three major groups.

The first group will comprise the cracks affected only by global stresses and shear stresses. These are:

- Bottom longitudinal crack 1 (mean fatigue life: 48 years)
- Inner bottom longitudinal (mean fatigue life: 100 years)

- Hopper longitudinal crack1 (mean fatigue life: 49 years)
- Side frame and hopper connection crack 3 (mean fatigue life: 210 years)
- Deck longitudinal crack 1 (mean fatigue life: 29 years)

The main fatigue life was calculated by assuming equal probability of occurrence for each condition (Ore Load Arrival condition, Grain Load Arrival condition and Heavy ballast Arrival condition). We can conclude that the stresses induced by the vertical bending moment are dominant since the mean fatigue lives of the cracks reduce as their distance from the horizontal neutral axis increases. The crack that suffers the most fatigue damage is the deck longitudinal crack1. Table A16-19 presents the individual contribution to damage of the five different stresses and shear sresses. As mentioned above, the vertical bending moment stresses are proven to be dominant giving a lower fatigue life when considered separately. The contributions from vertical shear force stresses and horizontal bending moment stresses are equivalent but very low in comparison with those from the vertical bending moment stresses. Finally, those shear stresses caused by torque and horizontal shear forces contribute even less to the fatigue damage. We can draw the general conclusion that it is conservative if we consider only vertical bending moment stresses in the fatigue life calculations. The bottom longitudinal crack1 and hopper longitudinal crack 1 are two details having the same distance from the horizontal neutral axis but not from the vertical. The hopper longitudinal crack1 is further from the vertical neutral axis, and we would, therefore, expect that the mean fatigue life should be less than the fatigue life of the bottom longitudinal crack 1. The results reveal the opposite. This is due to the effect of the phases. Although the fatigue damage is higher when only horizontal bending stresses are considered (tables A16-16/17), the overall stress reduces when combined with the remaining stresses, including the dominant vertical bending moment stresses.

The second group comprises those cracks mainly influenced by local water pressure fluctuations and inertial loading. The group includes the following cracks:

- Bottom longitudinal crack 2 (mean fatigue life: 23 years)
- Inner bottom longitudinal crack 2 (mean fatigue life: 37 years)
- Hopper longitudinal crack 2 (mean fatigue life: 56 years)
- Hopper corner crack 1(mean fatigue life: 29 years)

- Hopper corner crack 2 (mean fatigue life: 12 years)
- Side frame and hopper connection crack 1 (mean fatigue life: 21 years)
- Side frame and hopper connection crack 2 (mean fatigue life: 10 years)
- Transverse frame stiffener connection crack 1 (mean fatigue life: 24 years)

The first three cracks mentioned above are influenced by inertial loading and for first and third crack both inertial and pressure fluctuations are considered. The difference with the latter two is that the overall bending of the double bottom and the local bending between stiffeners were included in the model for the bottom longitudinal crack, but only localized bending due to pressure fluctuations is included in that of the hopper longitudinal crack 2. In tables A16-17 and A16-18 it is shown that the fatigue damage is contributed to by the water pressure fluctuations for the hopper corner and transverse frame stiffener rather than by the global stresses. Hopper corner crack 2 and side frame and hopper connection crack 2 are the most likely to fail from the above-mentioned group as a result of fatigue.

Finally, the third group comprises only the hatch corner crack that has the shortest fatigue life amongst our results. This is contributed to by the stress concentration factors assumed. The mean fatigue life of the detail is 2.3 years. However the in-plane torsional distortion of the deck was not included in the calculations.

As expected, the effects of corrosion redue fatigue life by a proportional amount. Cracks with low fatigue life have their life reduced by a number of months and cracks with higher fatigue life by a number of years. The important aspects, mentioned earlier in the text, are the corrosion rates allowed by the classification societies that disregard the welding material and concentrate on the plates and stiffeners where their thicknesses are two or three times greater.

We can conclude this chapter by asserting that the hatch corner crack, the hopper corner crack 2 and the side frame and hopper connection crack 2 are the most probable cracks. It is important to mention that all lie on areas where a crack failure may result in flooding, initiating a chain of events that cannot be predicted by the designer, since the weather conditions, the cargo, the reactions of the crew and the structural condition of the vessel are uncertain.

References

1. Radhakrishnan V. M. "Multiaxial fatigue an overview", Sadhana, Vol. 20, Part 1, February 1995, pp. 103-122

2. Bong-Ryul Y., Soon –Bok L., "A critical review on multiaxial fatigue assessments of metals", Int. J. Fatigue, Vol. 18, No. 4, pp 235-244, 1996

3. "Fatigue Strength Analysis for Mobile Offshore Units", Classification notes #30.2, Det Norske Veritas, 1984

4. Barltrop N.D.P.,Adams A.J., "Dynamics of Fixed Marine Structures", London, BMT/Butterworth-Heinemann, 3rd Edition, 1991

5. Barltrop N.D.P., "Floating Structures a Guide for Design and Analysis", BMT/OPL, 1998

6. Cronin D. J., Godfey P.S., "Spectral Fatigue Analysis of Offshore Structures", Numerical methods in Offshore Engineering, 1975

7. Young C.W., "Roark's Formulas for Stress & Strain", New York, McGraw-Hill, 6th edition , 1989

8. Chen N., Mavrakis S. A., "Closed –form spectral fatigue analysis for compliant offshore structures", Journal of Ship Research, Vol. 32, No. 4, pp297-304, Dec. 1988

9. Valsgard, S., Andreassen E., Kim S.K, "Development of Ultimate Hull girder Capacity", Proceedings of the Conference Design and Operation of Bulk Carriers, London., 1998

10. Radaj D., "Design and Analysis of fatigue resistant welded structures", Abington publishing,, Cambridge, 1990

11. Maddox S. J., "Fatigue strength of welded structures", Abington publishing,, Cambridge, 1991

12. Burnside O.H., Hudak S. J., Oelkers E., Chan K., Dexter J, "Long –Term Corrosion Fatigue of Welded Marine Steels", (SSC-326) .,1984

13. Ebara R., "Corrosion fatigue in practical problems", Computational and experimental fracture mechanics developments in Japan, pp347-377, 1994

14. Akid R. "The influence of environment upon the accumulation of damage under corrosion fatigue conditions", Fatigue Fract. Engg. Mater. Struct. ,Vol. 19, No.2/3, pp 277-285, 1996

15. Tokaji K., Ogawa T., Hwang J.U., Kobayashi Y., Harada Y., "Corrosion fatigue behaviour of a steel with sprayed coatings", Journal of Thermal Spray Technology, Vol. 5, pp269- 276, September 1996

16. Fricke W., Petershagen H., Paetzold H., "Fatigue strength of ship structures" , GL- Technology, Hamburg, August, 1997

17. Parente J.,Daidola J.,Nedret S., Basar S., Rodi R.C., "Commercial Ship design for Corrosion Control", (SSC-397) 1997

18. Braidwood I.T. ,Zhu Z.Y. ,Buxton I. L.,Hills W.,Marshall P. W.,Stevens P. ,White N., "Bulk Carrier Structural Integrity: Predicting Fatigue Life with Influence Functions"., Proceedings of the Conference Design and Operation of Bulk Carriers, London, 1998

19. Rawson K. J.,Tupper E. C, "Basic Ship Theory" ,Essex, Longman Scientific & Technical, 4th Edition, Vol 1+2., 1994

20. Cramer E.H.,Shulte-Strauthaus R.,Bea R.G, "Ship Maintenance Project (Fatigue Damage Evaluation)" ,(SSC-386) .1995

21. "Guide For \Dynamic Based Design and Evaluation of Bulk Carrier Structures", March 1995., American Bureau of Shipping

22. Hobgen, H. and Lumb, "Ocean Wave Statistics", National Physics Laboratory, H.M. Stationery Office, London, 1967

23. Miner, M.A., " Cumulative Damage in Fatigue", Journal of Applied Mechanics, paper 12, Trans. Of ASME, vol 67, pp A159., 1945

Appendix 13 Flowcharts for FORTRAN program calculating and combining stresses for the fatigue study and calculating the fatigue life

Flowchart for stress calculation module

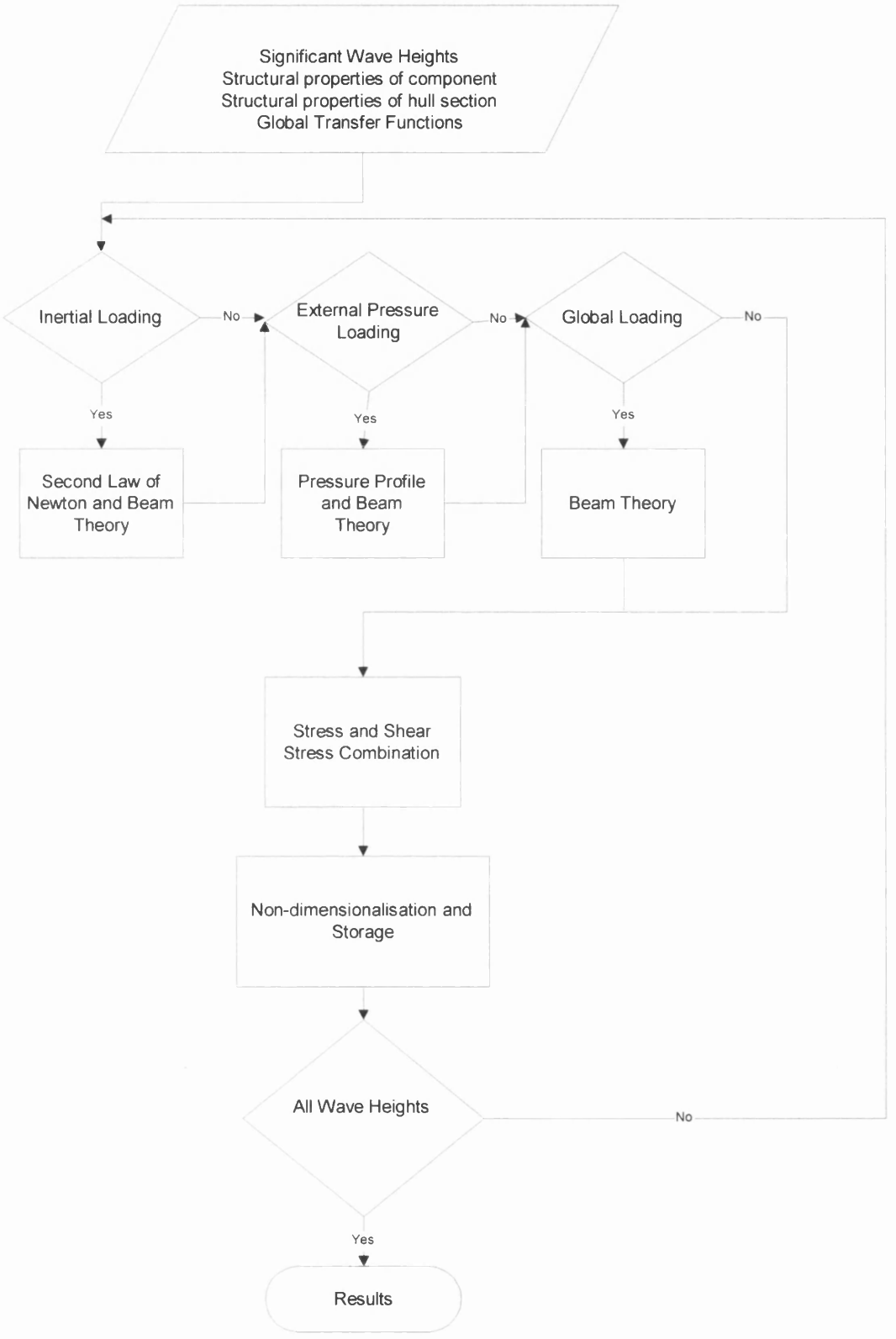

Flowchart for fatigue calculation module

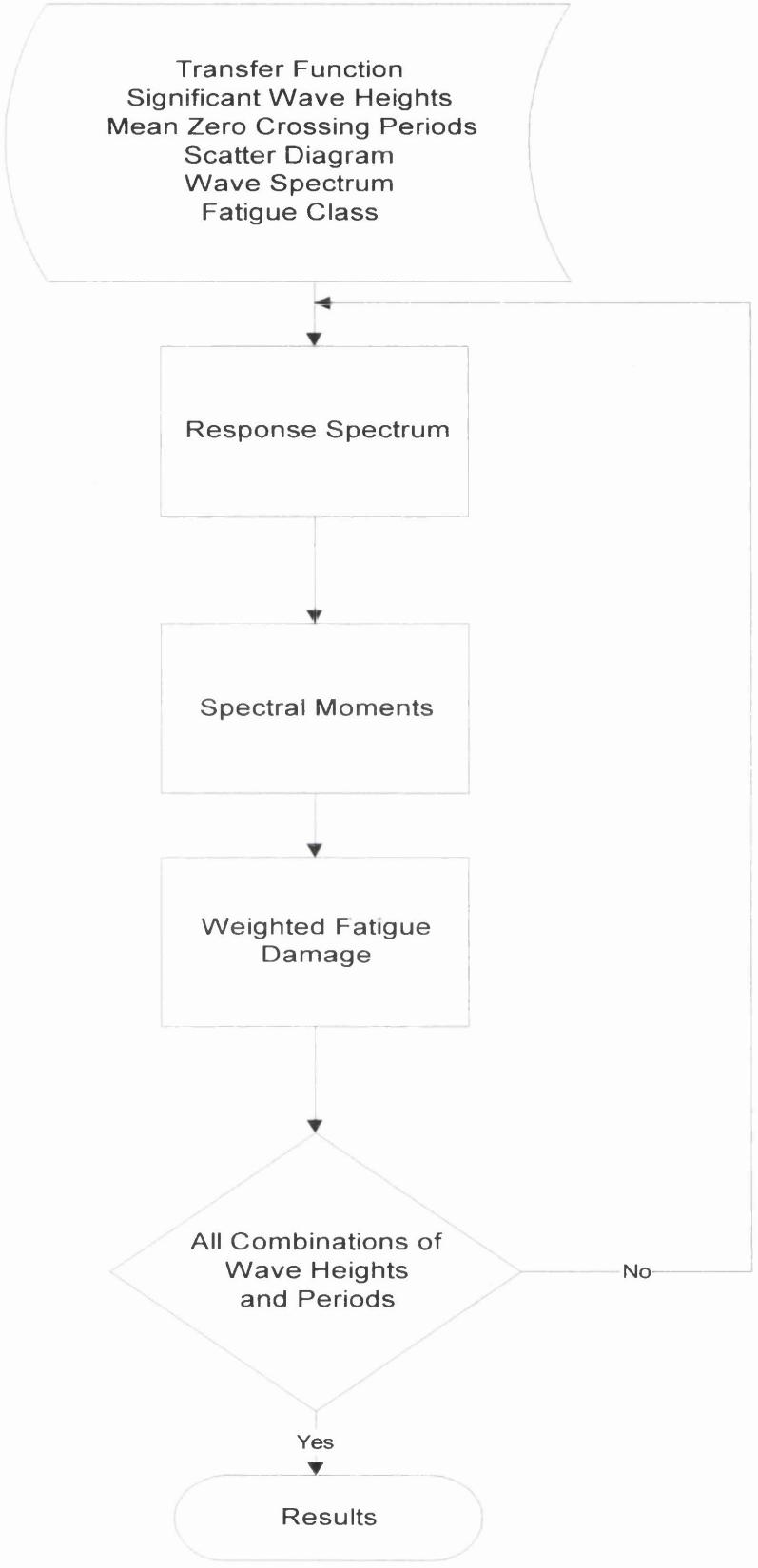

Appendix 14 Sea scatter diagram table combining areas 6,7,10 and 11

Scatter combining areas 6,7,10 and 11												
Hs/Tz	1	5	6.5	8.5	10.5	12.5	14.5	16.5	18.5	20.5	21	Totals
0.25	2.42E-02	2.77E-02	9.15E-04	4.18E-04	2.37E-04	9.70E-05	5.97E-05	8.15E-05	3.44E-05	6.60E-04	5.81E-04	5.50E-02
0.5	1.93E-03	6.79E-02	7.69E-03	1.92E-03	8.15E-04	3.45E-04	1.01E-04	9.59E-05	6.33E-05	1.61E-04	3.83E-03	8.49E-02
1	4.24E-03	1.21E-01	5.34E-02	1.21E-02	3.50E-03	1.35E-03	5.18E-04	3.14E-04	1.00E-04	2.69E-04	1.20E-03	1.98E-01
1.5	5.17E-03	5.86E-02	9.88E-02	3.32E-02	8.89E-03	2.73E-03	9.88E-04	3.03E-04	1.24E-04	2.08E-05	1.56E-04	2.09E-01
2	3.90E-03	1.55E-02	6.11E-02	4.44E-02	1.40E-02	3.61E-03	1.06E-03	3.28E-04	8.61E-05	3.80E-05	3.45E-05	1.44E-01
2.5	2.78E-03	5.96E-03	3.23E-02	3.60E-02	1.77E-02	5.24E-03	1.55E-03	4.51E-04	1.42E-04	5.08E-05	2.36E-05	1.02E-01
3	1.96E-03	2.05E-03	1.49E-02	2.36E-02	1.50E-02	5.77E-03	1.68E-03	5.19E-04	9.00E-05	1.72E-05	2.41E-05	6.56E-02
3.5	1.47E-03	1.32E-03	8.68E-03	1.60E-02	1.21E-02	5.67E-03	1.85E-03	5.64E-04	1.60E-04	2.71E-05	2.71E-05	4.78E-02
4	8.47E-04	5.98E-04	4.46E-03	9.26E-03	8.09E-03	4.42E-03	1.69E-03	6.22E-04	1.51E-04	3.28E-05	9.73E-06	3.02E-02
4.5	1.03E-03	4.90E-04	3.36E-03	7.55E-03	7.60E-03	3.92E-03	1.80E-03	7.51E-04	2.57E-04	5.63E-05	3.45E-05	2.69E-02
5	2.49E-04	1.05E-04	4.27E-04	1.48E-03	1.41E-03	8.38E-04	3.49E-04	9.96E-05	1.03E-05	1.68E-05	6.95E-06	4.99E-03
5.5	1.83E-04	1.16E-04	4.33E-04	1.13E-03	1.40E-03	7.63E-04	4.15E-04	1.28E-04	3.40E-05	6.95E-06	1.33E-05	4.62E-03
6	2.08E-04	1.16E-04	7.87E-04	1.78E-03	2.15E-03	1.40E-03	5.13E-04	1.66E-04	6.16E-05	3.47E-06	1.03E-05	7.18E-03
6.5	1.49E-04	1.40E-04	6.48E-04	1.53E-03	2.02E-03	1.14E-03	5.31E-04	1.85E-04	3.97E-05	1.60E-05	3.47E-06	6.40E-03
7	6.76E-05	2.37E-05	2.08E-04	7.37E-04	7.38E-04	4.94E-04	1.97E-04	7.45E-05	3.47E-06	0.00E+00	6.89E-06	2.55E-03
7.5	7.58E-05	2.02E-05	2.66E-04	6.85E-04	9.35E-04	5.73E-04	3.32E-04	1.25E-04	1.04E-05	9.78E-06	3.47E-06	3.04E-03
8	9.68E-05	2.36E-05	1.38E-04	5.50E-04	6.21E-04	5.26E-04	1.85E-04	1.10E-04	2.30E-05	0.00E+00	2.43E-05	2.30E-03
8.5	5.37E-05	1.96E-05	9.31E-05	2.63E-04	4.23E-04	2.97E-04	2.12E-04	9.81E-05	1.33E-05	3.47E-06	1.38E-05	1.49E-03
9	3.06E-05	3.47E-06	8.14E-05	1.88E-04	3.22E-04	3.01E-04	1.36E-04	9.66E-05	3.47E-06	9.73E-06	1.33E-05	1.18E-03
9.5	1.06E-04	2.09E-05	1.02E-04	3.36E-04	6.12E-04	4.16E-04	3.74E-04	1.82E-04	9.32E-05	6.47E-05	2.78E-05	2.33E-03
14	0.00E+00	0.00E+00	6.97E-06	1.74E-05	3.47E-06	3.82E-05	3.47E-06	0.00E+00	0.00E+00	3.47E-06	0.00E+00	7.30E-05
Totals	4.87E-02	3.02E-01	2.89E-01	1.93E-01	9.85E-02	3.99E-02	1.45E-02	5.29E-03	1.50E-03	1.47E-03	6.05E-03	1.00E+00

Appendix 15
Major details as shown in ship's plans

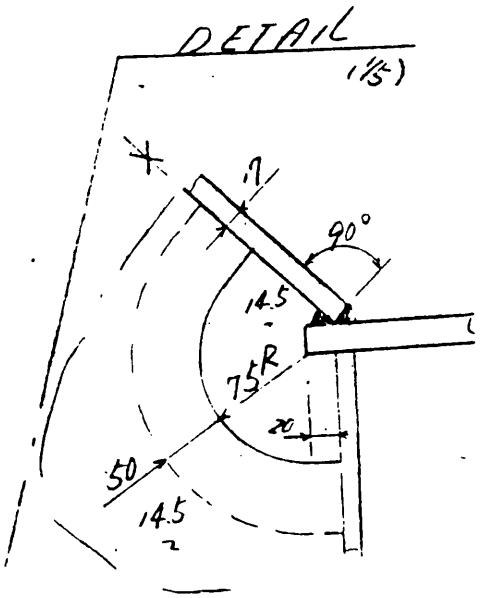

Figure A15 1 Hopper corner (detail 4)

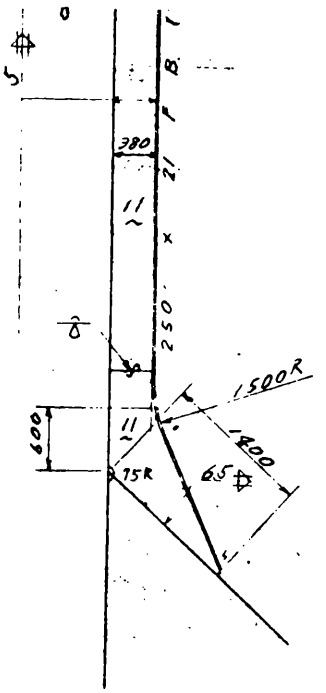

Figure A15 2 Side shell stiffener connection with hopper upper plate (detail 5)

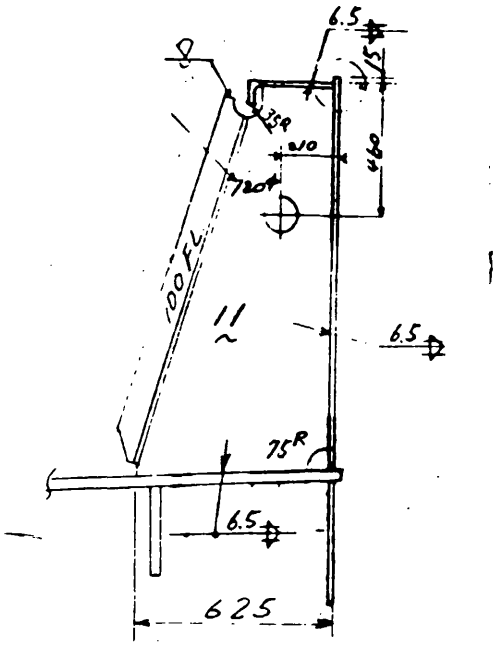

Figure A15 3 Hatch corner (detail 8)

Appendix 16 Fatigue life of details in years and usage factors

FATIGUE LIFE IN YEARS

DETAIL 1 BOTTOM LONGITUDINAL

CRACK 1

	SN Class E		
COR. RATE	0	0,15	0,5
ORE	52,0	51,1	48,7
GRAIN	51,0	50,2	47,9
BALLAST	41,4	40,7	38,8
COMBINED	48,1	47,4	45,1

Table A16-1

CRACK 2

	SN Class F		
COR. RATE	0	0,15	0,5
ORE	14,4	14,2	14,1
GRAIN	27,9	27,5	27,3
BALLAST	26,3	25,9	25,8
COMBINED	22,9	22,5	22,4

Table A16-2

DETAIL 2 INNER BOTTOM LONGITUDINAL

CRACK 1

	SN Class E		
COR. RATE	0	0,1	0,4
ORE	108,4	106,7	101,69
GRAIN	106,15	104,48	99,58
BALLAST	87,74	86,37	82,32
COMBINED	100,8	99,2	94,5

Table A16-3

CRACK 2

	SN Class F		
COR. RATE	0	0,1	0,4
ORE	39,61	38,99	38,68
GRAIN	44,57	43,87	43,52
BALLAST	27,81	27,37	27,16
COMBINED	37,3	36,7	36,5

Table A16-4

DETAIL 3 HOPPER LONGITUDINAL

CRACK 1

	SN Class F		
COR. RATE	0	0,15	0,5
ORE	53,87	53,03	50,54
GRAIN	51,11	50,31	47,95
BALLAST	42,18	41,52	39,58
COMBINED	49,1	48,3	46,0

Table A16-5

CRACK 2

	SN Class F		
COR. RATE	0	0,15	0,5
ORE	65,6	63,2	61,5
GRAIN	52,4	50,1	47,4
BALLAST	49,0	47,2	44,9
COMBINED	55,7	53,5	51,3

Table A16-6

DETAIL 4 HOPPER CORNER

CRACK 1

	SN Class F2		SN Class F	
COR. RATE	0	0,15	0	0,15
ORE	31,4	30,58	45,9	44,7
GRAIN	31,64	30,81	46,26	45,04
BALLAST	25,29	24,62	36,9	35,99
COMBINED	29,4	28,7	43,0	41,9

Table A16-7

CRACK 2

	SN Class F2		SN Class F	
COR. RATE	0	0,15	0	0,15
ORE	13,23	12,97	19,47	18,89
GRAIN	13,40	13,00	19,58	19,00
BALLAST	10,97	10,65	16,04	15,57
COMBINED	12,5	12,2	18,4	17,8

Table A16-8

DETAIL 5 SIDE FRAME AND HOPPER CONECTION

CRACK 1

	SN Class F2		SN Class F	
COR. RATE	0	0,15	0	0,15
ORE	26,64	25,57	39,04	37,46
GRAIN	35,72	34,28	52,34	50,23
BALLAST	1,4	1,34	2,02	1,97
COMBINED	21,3	20,4	31,1	29,9

Table A16-9

CRACK 2

	SN Class W	
COR. RATE	0	0,15
ORE	11,69	11,2
GRAIN	15,68	15,04
BALLAST	1,08	1,037
COMBINED	9,5	9,1

Table A16-10

CRACK 3

	SN Class E	
COR. RATE	0	0,15
ORE	300	292
GRAIN	190	187
BALLAST	141	139
COMBINED	210,3	206,0

Table A16-11

DETAIL 6 TRANSVERSE FRAME STIFFENER

CRACK 1

	SN Class F2		SN Class F	
COR. RATE	0	0,15	0	0,15
ORE	21,35	20,49	31,28	30,02
GRAIN	26,83	25,75	39,32	37,73
BALLAST	23,66	23,18	34,67	33,96
COMBINED	23,9	23,1	35,1	33,9

Table A16-12

DETAIL 7 DECK LONGITUDINAL

CRACK 1

	SN Class E		
COR. RATE	0	0,2	0,4
ORE	32,0	31,2	30,5
GRAIN	31,4	30,7	29,9
BALLAST	24,8	24,2	23,6
COMBINED	29,4	28,7	28,0

Table A16-13

DETAIL 8 HATCH CORNER

CRACK 1

	SN Class D			SN Class C		
COR. RATE	0	0,15	0,5	0	0,15	0,5
ORE	1,31	1,25	1,14	3,24	3,24	2,82
GRAIN	1,29	1,24	1,13	3,2	3,2	2,7
BALLAST	1,01	0,97	0,88	2,4	2,3	2,1
COMBINED	1,2	1,2	1,1	2,9	2,9	2,5

Table A16-14

USAGE FACTORS BASED ON 25 YEARS

DETAIL 1 KEEL LONGITUDINAL

CONDITION	BALLAST	CLASS	F2
STRESSES	ALL	VBM	HBM
UF	0,79	0,78	0,029
YEARS	51,04	52,04	-

Table A16-15

DETAIL 3 HOPPER LONGITUDINAL

CONDITION	BALLAST	CLASS	F2
STRESSES	ALL	VBM	HBM
UF	0,78	0,78	0,053
YEARS	51,11	52,04	169685

Table A16-16

DETAIL 4 HOPPER CORNER

CONDITION	BALLAST	CLASS	F2
STRESSES	ALL	W.P.	GLOBAL
UF	1,32	1,16	0,65
YEARS	10,97	16,1	87,74

Table A16-17

DETAIL 6 TRANSVERSE FRAME STIFFENER

CONDITION	BALLAST	CLASS	F2
STRESSES	ALL	W.P.	GLOBAL
UF	0,90	0,87	0,27
YEARS	34,67	37,97	1223

Table A16-18

DETAIL 7 DECK LONGITUDINAL

CONDITION	ORE	CLASS	E			
STRESSES	ALL	VBM	VSF	HBM	HSF	TM
UF	0,92	0,93	0,07	0,057	0,029	0,021
YEARS	31,98	30,81	-	-	-	-

Table A16-19

DETAIL 8 HATCH CORNER

CONDITION	GRAIN	CLASS	C
STRESSES	ALL	W.P.	GLOBAL
UF	1,98	0,63	1,33
YEARS	3,2	97,4	10,49

Table A16-20

Chapter 7

IACS Current Regulations for the Bulk Carrier Structure

7.1 Introduction

The destruction or loss of any ship structure results in direct and indirect cost to the parties involved and to the world community in general. When a significant number of losses occur action is requested and all the parties involved react to the situation with each contributing what considers necessary.

The most important reaction regarding the Bulk Carrier losses with respect to regulatory point of view was that of IACS in partnership with IMO. In December 1996 the organisation announced its decision to require certain conditions intended to reduce risk and enhance safety in existing Bulk Carriers. Four main structural components were recognised as critical with respect to Bulk Carrier survivability, the transverse bulkhead, the double bottom, the side shell and the hatch cover. Although individual classification societies have made their rules the main requirements are enshrined in the IACS Unified Requirements.

7.2 Regulations applicable

Regarding the transverse bulkhead for existing vessels the UR S19 [1] applies. Minimum scantling requirements for vertically corrugated transverse watertight bulkheads between cargo holds #1 and #2 are in concern. The thicknesses for evaluation are determined by gauging and a minimum corrosion margin of 0.5mm is subtracted. The most severe combinations of cargo induced and flooding loads are considered in the evaluation. The bulkhead strength is assessed for bending moment, shear force and local strength. Effective shedders or gussets need to be fitted if the section modulus is not adequate. The shear force is considered by a reduced shear area to account for non-perpendicularly. The shear stress should not exceed half the yield stress of the material and shear buckling is considered according to UR S11 [2]. Local strength requirements include minimum plate thickness and lower stool/floor requirements based on the flange thickness and yield stress. UR S18 [3] is addressed to new vessels and is similar to UR S19 except that there are dimensional requirements for lower and upper stools and the rule is applied to all the transverse bulkheads assuming a reduced flooding head for those aft of hold #2.

Grundy and Geiro [4] investigate the capacity of the corrugated transverse bulkheads. Among other conclusions regarding the structural modelling and the quality and alignment of the welds they consider that the assumption of a span equal to the height of corrugations [1,3] could be un-conservative. Also that the requirements do not seem to provide load and resistance factors in excess of unity to ensure acceptable structural reliability of the bulkheads. Rainy, Mellor and Hunt [5] in a similar investigation with a case study discuss the relationship between low cycle fatigue and dynamic loading and that cracking in corrugated transverse bulkheads is a result of buckling. Although they discuss the corrosion effects they conclude that corrosion may be absent and still failure may occur. Also they question the relation of corrosion to the Bulk Carrier losses. Paik [6] presents a theoretical prediction of ultimate strength of corrugated transverse bulkheads and discusses probabilistic corrosion models concluding that the interaction needs to be studied more thoroughly so that reliable results can be produced.

The double bottom requirements (UR S22 [7]) for existing vessels apply to the girders and floors of the hold #1 double bottom. Calculations are based on net scantlings obtained by deducting 2mm from as built thickness so gaugings are not required. Again the most severe combinations of cargo induced and flooding loads are used. The shear capacity of the double bottom is defined as the sum of the shear strength of all the double bottom girders and of all floors reduced by half the shear strength of those floors adjacent to each stool. The requirement is formed as a maximum allowable hold loading. It should be noted that a small number of examples [8] and calculations performed for the Bulk Carrier under consideration produced allowable hold loading in excess of those listed in the loading manuals. New vessels are required to conform to UR S20 [9] with the same requirements except that the regulation should be applied to the double bottoms underneath all the hold rather than just hold # 1with the flooding head reduced.

The side shell structure is referenced in UR S12 [10] regarding new vessels only. The requirements include, minimum thickness of frame webs with higher requirements for hold #1, minimum thickness for side shell plating, lower and upper bracket minimum thickness and a minimum section modulus of the frame, bracket and shell plating. The regulation contains other geometrical features such as the side frame should be curved not knuckled with a minimum radius. The weld connections of frames and end brackets

should have a weld throat of 40%- 44% of the thickness of the web or side shell plating whichever less. When the side frames are asymmetrical tripping brackets are required every two frames.

With respect to the last requirement Kozliakov [11] suggests at least one row of tripping brackets should be fitted to the side shell according to the findings of his study. He investigated damages of the cargo holds of Bulk Carriers built in the period of 73-76 under the rules of USSR Register of shipping. A DnV report [12] shows that a number of Bulk Carriers, which had already been extensively upgraded, experienced upper end detachment from the ship side and top wing tank resulting in the side plating being set inboard considerably, and partly cracked. The reasons stated are the concentration of the loading in the centreline (ore) and the repaired lower end, which made weaknesses on the upper end become more vulnerable. It is interesting to note that much older Bulk Carriers were designed with their upper wing tanks bottom partly flat and also their hopper tanks tops partly flat. The evolution of the Bulk Carrier design abolished this characteristic for cargo handling purposes.

The hatch covers of new vessels additionally to the ILLC 66 requirements should comply with UR S21 [13]. The requirements apply to the hatch covers located inside the fore quarter length of the ship. The pressure considered acting on the hatch cover is a function of ship's length, design speed, block coefficient, the vertical distance from the summer draft to the top of the hatch coaming and the longitudinal position of the hatch cover. Allowable stresses and shear stresses for secondary and primary supporting members and local net plate thickness requirements are set. Distinction is made for ships without forecastle or breakwater (M/V *Derbyshire*). Also corrosion allowance is considered and steel renewal or coating application are discussed as different options to overcome excessive corrosion problems.

Byrne and Evans [14] discuss weather conditions related to two case studies where hatch cover structural damage occurred. They evaluate the ILLC 66 design requirements with finite element models both for as new and allowing for a corrosion margin under the loading calculated for the case studies. The structural capabilities of the hatch cover under the ILLC 66 design are inadequate to sustain the loading that may occur in rough weather.

The UR S1/S1A [15/16] address the subject of loading and discharging sequences by including these in the loading manual with the resultant bending moments shear forces and torsional loads. A multi-point loading instrument is required for both new and existing Bulk Carriers, which provides the crew information regarding the stresses induced to the structure. The rules do not specify if the instrument should be in use during the voyage. A loading component, which was not included in our study, was slamming. The vibrations that smaller vessels experience due to slamming reach the superstructure so the crew acknowledges the loading and reacts accordingly. The Panamax or capesize Bulk Carrier structure absorbs the vibrations before these reach the superstructure so the crew is not aware of their existence especially in bad weather conditions when it is not safe to walk on the deck. Also the rules do not enforce an instruments which would indicate flooding in the holds and tanks.

The new SOLAS Chapter XII main features prevent existing and new single skin Bulk Carriers from carrying high-density cargo unless the vessel can sustain the flooding of hold #1 in all the loading conditions. Also the aft corrugated transverse bulkhead in hold # 1 and double bottom in hold # 1 should be able to with stand the flooding of the foremost hold (UR S19 – UR S22).

The UR Z10.2 [17] (1992) was created in response to the IMO Assembly resolution A713 (17) "Safety of ships carrying solid bulk cargoes". The enhanced survey program is mainly applicable to the special survey. The hull structure on the cargo regions is of prime concern. Extensive thickness measurements are needed and a close up examination of the scantlings of the vessel. The condition of coating is examined and recorded in the executive hull summary. The findings determine except the repairs if needed the planning of the next surveys and details that need special attention. Annual or intermediate surveys also are more intense involving close up examination of the details and thickness measurements. The survey program became mandatory in 1995 under chapter XI of SOLAS. It is probably the best and most effective measure taken up to now. However its effectiveness is dependent on the care of the surveyors performing the inspection.

7.3 Discussion

We may remark that two main categories of Bulk Carriers that have suffered structural damage. The first comprises of relatively new and well maintained ship where corrosion was not an issue but still suffered damage (M/V *Derbyshire* and others) so the problem may be design related (e.g. hatch cover). The second comprises of vessels rather old or not well maintained where the contribution of corrosion is inevitable. ESP has certainly proven to be successful with only two ships having suffered damage after they had undergone the survey, a number reasonable regarding other ship types. However we need to consider more thoroughly the first category.

Assuming an existing single side skin Bulk Carrier has undergone the structural reinforcements according to IACS requirements. If the hold # 1 is flooded and the transverse bulkhead does not collapse ([4] are sceptic) and the double bottom does not collapse in shear then we need to foresee what might happen to hold # 2. The side shell should not suffer damage (ESP should ensure no collapse) and the hatch cover should not fail under bad weather conditions ([14] prove the inadequacy of ILLC 66 even under no corrosion (ESP) recognised by IACS through the enforcement of UR S21). So essentially reinforcements, costing around $48,000 to $ 292,000 [18] for a Panamax Bulk Carrier depending on the design and state of the hull and where the repairs take place, rely on the weather conditions when the initial damage may occur. It is interesting to note that according to statistics presented in the first chapter show that the majority of accidents happen in bad weather conditions.

The implementation for existing Bulk Carriers of the UR S21 rather than UR S19 and S22 will protect the primary boundary. In conjunction with ESP, stress monitoring of the ship's structure and simple mechanisms indicating flooding of the holds and tanks will probably provide reasonable safety margins for existing Bulk Carriers. However the cost of such an implementation has not been considered.

References

1. IACS Unified Requirement S19, "Evaluation of scantlings of the transverse watertight corrugated bulkhead between cargo holds Nos. 1 and 2, with cargo hold 1 flooded, for existing single side skin Bulk Carriers", 1997

2. IACS Unified Requirement S11, "Longitudinal strength standard", 1993

3. IACS Unified Requirement S18, "Evaluation of scantlings of corrugated transverse watertight bulkheads for single side skin bulk carriers considering hold flooding", 1997

4. Grundy P., Geiro A., "Ultimate strength limit state assessment of transverse bulkheads", RINA Conference, Design and Operation Of Bulk Carriers, London, 1998

5. Rainey R. C. T., Mellor B. G., Hunt G. W., "Failure of bulk carrier bulkheads after flooding", RINA Conference, Design and Operation Of Bulk Carriers, London, 1998

6. Paik J. K., "The strength and reliability of transverse bulkheads and hull structure of bulk carriers", RINA Conference, Design and Operation Of Bulk Carriers, London, 1998

7. IACS Unified Requirement S22, "Evaluation of allowable hold loading of cargo hold no. 1 flooded, for existing single side skin bulk carriers", 1997

8. Baxter J.C., Scotto F.J., "IACS unified requirements S19 & S22", Presented to the New York Metropolitan Section of SNAME, November, 1997

9. IACS Unified Requirement S20, "Evaluation of allowable hold loading for single side skin bulk carriers considering hold flooding", 1997

10. IACS Unified Requirement S12, "Side structures in single skin bulk carriers", 1997

11. Kozliakov V. V., "An analysis of structural peculiarities and causes of severe hull damages of bulk carriers, tankers and obo ships", RINA Conference, Tankers and Bulk Carriers the way ahead, December, 1992, London

12. "Excessive corrosion and detachment of upper part of main frames from ship side", DnV, Casualty Information, no.10, 1994

13. IACS Unified Requirement S21, "Evaluation of scantlings of hatch covers of bulk carrier cargo holds", 1997

14. Byrne D., Evans J., "Hatch covers: failures on laden bulk carriers in heavy weather with reference to current design practice", RINA Conference, Design and Operation Of Bulk Carriers, London, 1998

15. IACS Unified Requirement S1, "Requirements for loading conditions, loading manuals and loading instruments", 1997

16. IACS Unified Requirement S1A, "Additional requirements for loading conditions, loading manuals and loading instruments for bulk carriers, ore carriers and combination", 1997

17. IACS Unified Requirement Z10.2, "Hull surveys of bulk carriers", 1992

18. Tustin R.D., "Existing bulk carrier safety- on the evaluation of corrugated water tight bulkhead and double bottom structure of existing single side skin bulk carriers with the foremost hold flooded", RINA Conference, Design and Operation of Bulk Carriers, May, 1998, London

Chapter 8

Overall Discussion & Conclusions

8.1 Overall Discussion & Conclusions

Assessing a ship's structure involves breaking it down into its various components. We made a simplified study of a bulk carrier structure by considering the various components of loading that it might suffer throughout its life. The majority of loading conditions was studied and still water bending moments and shear force diagrams were calculated. We also investigated possible structural failures resulting from global extreme loading and fatigue-related loading. Particular care was taken to perform the analysis in a manner that would allow us to understand the behaviour of the structure. It was considered necessary to sacrifice the accuracy of the results for the knowledge and understanding gained from performing a first principle analysis. Unfortunately the planned, plated finite element model was never able to be run because the mesh was too fine for the program as configured on the available workstation on which it was planned to be run. A simplified beam/bar finite element model was run, but only for a test load case. The methodology used was examined using more sophisticated tools such as finite elements. With all approximate methods and in both the finite element and first principle calculations, weaknesses and simplifications exist. However we are able to draw the following useful conclusions from the analysis.

1. Longitudinal Strength

- The assumption that the lightship weight distribution can be modelled as a modified Bilge Coffin diagram was a good approximation since the values calculated have small difference from those listed in the trim and stability booklet.
- The intact loading conditions listed in the trim and stability booklet do not induce still water vertical bending moments that exceed the rule (ABS) based value.
- The alternate loading conditions give rise to high shear stresses in the fore end of the structure, which were calculated based on the C.S.S.P. program and exceeded the permissible values. However the correction from the classification's society rule of local forces at the transverse bulkheads was not applied.
- The alternate conditions when hold # 1 is damaged induce to the structure still water vertical bending moments which exceed the rule based value that is required for the intact conditions.

- The intact ore load condition, for the vessel considered, results in a higher wave vertical bending moment than the equivalent damaged condition (hold #1 damaged).
- The extreme vertical bending moment predicted does not exceed the ultimate strength capacity of the structure. However the safety factor is low.

2. Simplified analysis in comparison with finite element analysis

- The stress in the double bottom results from axial, local bending and global bending of the double bottom. The dominant stress is the axial stress, which is induced by transverse loading. The two different methods provided similar results (f.e.: 16.5 N/mm^2, f.p.: 15.59 N/mm^2) but agreement did depend on the assumption made about the proportion of transverse load carried by the bulkhead stools. The local bending stress is in full agreement (f.e.: 2.65 N/mm^2, f.p.: 2.755 N/mm^2) with the first principles value higher due to the fixed end boundary assumption. The global bending stress has a large difference between the two methods (f.e.: 3.89 N/mm^2,f.p.: 5.229 N/mm^2). This is probably the result of poor modelling of the transverse webs in the double bottom in the finite element analysis.
- The hopper tank rotates inwards and as for the previous calculations three types of stresses were calculated the axial, the local bending and the global bending. The dominant stress is the axial (f.e.: 19.259 N/mm^2, f.p.: 17.102 N/mm^2). The local and global bending stresses are reasonably close with the first principle methodology on the conservative side. (local bend. f.e.: 1.38 N/mm^2, f.p.: 2.046 N/mm^2, global bend, f.e.: 1.94 N/mm^2, f.p.: 2.725 N/mm^2)
- The side shell is induced to bending moments due to the transverse loading. Two points were considered one in the end and one in the middle. The first principle methodology was on the conservative side at the ends (f.e.: 144.243 N/mm^2, f.p.: 204.272 N/mm^2) and non-conservative in the middle (f.e.: 193.142 N/mm^2, f.p.: 102.136 N/mm^2). The reason is that the rotation of the hopper tank releases the moment from the end and induces higher moment in the middle.
- The average transverse stress on the deck structure was calculated with two first

principle methods and the finite element method. The second first principle method with an improved method of calculating the transverse force taken by the deck provided almost the same result as the finite element method. (f.e.: 100.94 N/mm^2, f.p.: 96.7 N/mm^2). Unfortunately the stress concentration factor at the hatch corner could not be evaluated due to the insufficient mesh and computer problems faced when more complicated plated meshes were created.

- Hand calculations can be used to analyse the complicated behaviour of the structure. The methodology is presented in chapter 4 and various improvements in detail in appendix 11.

3. Fatigue analysis

- The weakest details in our fatigue analysis are the following:
  - The hatch corner which has mean fatigue life of 2.9 years. The stresses at the hatch corner are induced by global and pressure fluctuation loads.
  - The side shell stiffener and hopper top plate connection, which has mean fatigue life of 9.5 years. The crack is through the weld of the stiffener with the hopper plate and is caused by pressure fluctuation load on the sides of the vessel.
  - The hopper corner connection where the hopper tank top plate connects with the double bottom plate. The crack is through the welding material and the detail has a mean fatigue life of 12.3 years. The dominant load for the crack mentioned above is the pressure fluctuation however global loads contribute as well.
- The possible cracks in a ship structure can be subdivided in those affected by global loading, inertial, transverse and local wave loading and their combination.
- The global loading consists of vertical bending moment, vertical shear force, horizontal bending moment, horizontal shear force and torsion. The contribution, of vertical and horizontal shear forces, horizontal bending moment and torsion, to the fatigue damage for the details as studied is insignificant. The dominant global load is the vertical bending moment. Note however that no attempt was made to

calculate the in-plane torsional distortion of the deck, which could lead to large stresses around the hatch corners.

- The selection of the correct s-n curve in the fatigue life calculations is important since fatigue life changes when significantly different s-n curve are used.

The various first principles methods used do not produce accurate results and are to simple to represent the complicated nature of the problems. Sophisticated finite element tools exist which allow more accurate calculations to take place and with respect to the fatigue analysis they can produce results faster. The methods presented and used in this report allow a useful cross-checking of the results obtained from a sophisticated method and indeed the application of the first principles hand methods demonstrated some flaws in the finite element model used (e.g. the poor modelling of transverse structure in the double bottom). This ability to make rough checks on computer generated results may become even more important as nowadays sophisticated methods are incorporated into computer programs which allow limited access to the assumptions and the procedures used.

Summarising the above the present Study is considered so far complete in respect of evaluation of the factors under study as set upon commencing this project regarding a Panamax Bulk Carrier, the M/V Victor built 1976 with particulars as per Chapter 2.